Université d'Ottawa · University of Ottawa

Université d'Ottawa · University of Ottawa

FACULTÉ DES ÉTUDES SUPÉRIEURES ET POSTDOCTORALES

FACULTY OF GRADUATE AND POSTDOCTORAL STUDIES

Javad BORUJERDI

AUTEUR DE LA THÈSE - AUTHOR OF THESIS

M. A. Sc. (Civil Engineering)

GRADE - DEGREE

Department of Civil Engineering

FACULTÉ, ÉCOLE, DÉPARTEMENT - FACULTY, SCHOOL, DEPARTMENT

TITRE DE LA THÈSE - TITLE OF THE THESIS

Numerical Evaluation of Low-Slope Roofs for Klind Uplift Resistance

A. Baskaran

DIRECTEUR DE LA THÈSE - THESIS SUPERVISOR

CO-DIRECTEUR DE LA THÈSE - THESIS CO-SUPERVISOR

EXAMINATEURS DE LA THÈSE - THESIS EXAMINERS

J. Beaudoin

D.T. Lau

H. Tanaka

J.-M. De Koninck, Ph.D.

LE DOYEN DE LA FACULTÉ DES ÉTUDES SUPÉRIEURES ET POSTDOCTORALES

DEAN OF THE FACULTY OF GRADUATE AND POSTDOCTORAL STUDIES

NUMERICAL EVALUATION OF LOW SLOPE ROOFS FOR WIND UPLIFT

By
Javad Borujerdi

A thesis presented to the
University of Ottawa
in partial fulfillment of the requirements for

Master of Applied Science
in Civil Engineering

Department of Civil Engineering
University of Ottawa
Ottawa, Canada

February 2004

The M.A.Sc. in Civil Engineering is a joint program
with Carleton University administered by the
Ottawa-Carleton Institute for Civil Engineering

Your file Votre référence
ISBN: 0-494-01423-7
Our file Notre référence
ISBN: 0-494-01423-7

Acknowledgement

I would like to express my sincere appreciation to my supervisor Dr. Baskaran, who provided me with financial support and research advice. I greatly appreciate his assistance.

Special appreciation is expressed to my wife for her encouragement and patient support. I also appreciate my children who tolerated my absence for the study.

The present research was carried out part of an ongoing consortium at National Research Council of Canada, the Special Interest Group for Dynamic Evaluation of Roofing Systems (SIGDERS). SIGDERS consists of following members whose support and commitments are greatly appreciated.

- ***Manufacturers***: Canadian General Tower Ltd., Carlisle SynTec Inc, GAF Materials Cooperation, Firestone Building Products Co., IKO industries Canada, Stevens Roofing Systems, Soprema Canada, Vicwest Steel
- ***Building owners***: Canada Post Corporation, Department of National Defense, Public Works and Government Services Canada and
- ***Associations***: Canadian Roofing Contractors' Association, Industrial Risk Insurers, National Roofing Contractors' Association and Roof Consultants Institute

William Lei, Technical Officer, collected some of the experimental data reported in this study. Dr. Chen and Dr. Zahrai, visiting postdoctoral fellows, carried out the initial numerical model studies. Their assistance is greatly appreciated.

The knowledge-based wind design module is being carried out through a joint research program between 2001 (Mr. Tom Kelly) company and National Research Council Canada. Richardo Rodas, a co-operative student, for the preparing of the graphic files and help of Patrick Brunette, in client service, for Access program are appreciated.

Abstract

Keeping the roofs in place against high wind events is a challenging task for architects and roof designers. There are two deign processes involved for the successful completion of this task. First, a comprehensive understanding of the wind induced loads. Second, accurate estimation of the roofing system response to the calculated wind loads. Roof designers can quantify the former according to a national building code or fabricate and test models in wind tunnels. Analytical procedures to predict the dynamic response of the roofs are limited. Mostly, experimental procedures are used to quantify the system response by simulating the wind gusts of different magnitudes over a roof specimen that can represent typical field conditions.

This dissertation contributes to an ongoing research project at the National Research Council Canada in the evaluation of roofing systems for wind uplift design. Accomplishments are grouped in two tasks. Task one provides development of a knowledge-based design module for the estimation of wind load distribution on roofs. Task two, numerical modeling using finite element methods and experiments to investigate the performance of roofing systems subjected to wind uplift loads.

For the Task one, all the data of wind uplift pressure distribution on roof configurations from open literature, including studies using wind tunnel boundary layer and full-scale measurements, are reviewed. During the review process more emphasis is placed on research results that are dedicated to design data than on wind simulation techniques and fundamentals of wind tunnel testing. Only boundary layer wind tunnel studies carried out after 1970 are considered for data identification if the study contains either mean or peak pressure coefficients on roofs. Microsoft Access, a database management program, is used to store collected data in records. A graphical user interface has been developed to search the database and queries can be made based on either building height or author. By choosing the desired height range or entering a specified author, the relevant design data records can be displayed, graphically.

For the Task two, various mechanically attached single-ply roofing systems were numerically modeled based on the Finite Element program with the capability of non-linear analysis. Experiments were also carried out and data obtained from the Dynamic Roofing Facility was used for benchmarking the developed model. Numerical results for various system configurations compared well with those obtained from the experimental studies. Since, there is no consensus on table size for evaluation of roofing system in various test procedures, the validated model was further used to investigate the effect of table size. Attempts were made to

identify the required table width. It was found that an increase in the table width beyond required table width did not significantly change the system response and it depends mainly on two system parameters, namely, fastener row spacing and fastener spacing. Influences of these two parameters on the required table width were also investigated.

Attempts have been made to develop correction factor curves such that it can be applied by the roof designer irrespective of the investigated table size. During this investigation, a relationship of the correction factor has been found with the ratios of table width over fastener spacing as well with fastener row spacing over fastener spacing. Based on this finding, generalized correction factor curves are developed. These curves can be practically applied when roofing systems are tested on table widths narrower than the required table width for a variety of roof configurations.

Table of Contents

List of Tables

List of Figures

Glossary

Symbols:

C_a	geometrical factor, [0]
C_d	statistical factor, [0]
C_e	exposure factor, [0]
C_f	correction factor, [0]
C_g	gust factor, [0]
C_p	pressure coefficient, [0]
F	Fastener force, N
F_r	fastener row spacing, mm
F_s	fastener spacing, mm
G	gust factor, [0]
GC_p	product of external pressure coefficient and gust effect factor, [0]
GC_{pi}	product of internal pressure coefficient and gust effect factor, [0]
H	building eave height, m
H_0	roughness length
H_R	reference height
Hg	building gradient height, m
L	building length, m
m	fastener row spacing over fastener spacing (F_r/F_s), [0]
N	number of simulations, [0]
n	table width over fastener spacing (W/F_s), [0]
p	pressure, kPa
q	reference velocity pressure, kPa
q_h	Velocity pressure evaluated at height h, kPa
U	speed at eave height m/s
Ug	speed at gradient height, m/s
V	wind speed, m/s
W	building width, m
α	power law index [0]

Subscripts:

i	internal
g	gradient

Abbreviations:

APP	Atactic Polypropylene
ASCE	American Society of Civil Engineers
CPE	Chlorrinated Polyethylene
CR	Chloroprene Rubber
CSPE	Chlorosulfonated Polyethylene
DRF	Dynamic Roofing Facility
EPDM	Ethylene-Propylene-Diene-Monomer
EVA	Ethylene Vinyl Acetate
EXP	Experimental
FM	Factory Mutual
NBCC	National Building Code of Canada
NBI	Norwegian Building Research Institute
NM	Numerical Model
NRC	National Research Council of Canada
PIB	Polyisobutylene
PVC	Polyvinyl Chloride
RTW	Required Table Width
SBS	Styrene Butadiene Styrene
SIGDERS	Special Interest Group for the Dynamic Evaluation of Roofing Systems
TP	Thermoplastic
TPO	Thermoplastic Olefin
TS	Thermoset
UEAtc	European Union of Agreement
UL	Underwriters Laboratory
UV	Ultraviolet

1 Introduction

1.1 General

Damages due to natural wind hazard caused by typhoons and hurricanes have been dramatic in recent years, incurring losses of life and property around the world. The insurance amount that was paid for the loss caused by Typhoon 9119 reached 567.5 billion yen, which was the largest amount in the world for natural disaster loss until 1991. According to the wind damage investigation, the most wind damage to houses was restricted to the envelope of buildings, in particular to the roof sheathing (Uematsu and Isyumov, 1999). The wind damages caused by Hugo (1989) and Andrew (1992) hurricanes in the United States were quite similar features to Typhoon 9119. Therefore, it is quite important study to keep the roof in place in the face of high wind events. Figure 1.1 shows typical roof failure during high wind event (Baskaran and Dutt, 1995).

Figure 1.1 Roof failure during high wind event

Wind effect on roof is dynamic. It varies based on a number of factors such as time, building dimension, geometry, surroundings and terrain. This is due to turbulence in the flow, which causes the erratic motion of individual air particles . Also, the statistical distributions of the wind induced loads should be considered rather than the simple averages. For example, wind pressure distribution varies spatially over a roof and it can have high suction at the corner and perimeter due to flow vortex and separations.

1.2 Problem Definition

Roof designers quantify the wind loads according to national building code or wind standards. Code provisions are a collection of facts and knowledge based on the experimental results. Wind loads are measured by testing models in wind tunnels or full scale measurement data, which are obtained from instrumented structures. Wind load design can be different from one code to other standards due to specific requirements and limited data for each country.

The evaluation of roofing systems subjected to the wind load is based on the standardized experimental test methods. To evaluate roofing systems, components are placed in an apparatus and wind load are simulated. The roof components assembled on the test table should replicate the field installation. If the roof system can withstand the stated pressure level of the test criteria, the manufacturer would be presented a rating or approval by the test organization.

To investigate the effect of various parameters on the system performance, the experimental approach is costly or difficult to set up. The parameter variables such as fastener spacing, fastener row spacing, membrane properties and table size can affect roof system response. Currently, there is no consensus on the table size to be used by these testing protocols in spite of the fact that a table size plays significant role in evaluating the performance.

1.3 Present Contribution

The goal of this research is to take advantage of existing computer software and numerical techniques on both wind load calculation for roofs and the system resistance evaluation. A knowledge-based design module for the estimation of wind load on roofs can help roof designers to optimize the roof wind design. In order to accomplish this task, Chapter two documents the involved procedures as follows:

- Review the literature to extract the useful wind load data on roofs
- Develop a database for wind pressure distribution on roofs
- Create a user-friendly interface for the database such that practitioners can make use of the database

In Chapter Three, existing testing methods are systematically reviewed. In that process, one of the major drawback namely, effect of testing table size on the roofing system response have been identified. To address this issue, Chapter Four documents the numerical techniques and experimental procedures that are being used by the present study. Various mechanically attached single-ply roofing systems are numerically modeled based on the Finite Element program with the capability of non-linear analysis. Experimental data obtained from the Dynamic Roofing Facility is used for benchmarking the developed model. Numerical results for various system configurations are compared with those obtained from the experimental studies.

Chapter Five presents the application of the validated model, which is used to investigate the effect of table size on the roofing system performance. Attempts are made to identify the required table width. It is found that an increase in the table width beyond a certain level did not significantly change the system response. It was also found that the specific limit depends mainly on two system parameters, namely, fastener row spacing and fastener spacing. Influences of these two parameters on the required table width are also investigated. Also for practical application, correction factor curves are developed when the table sizes are not wide enough for the roof performance evaluation.

2 Wind Loads on Roof Assemblies

2.1 Background

Designers use national building codes or local wind standards to determine wind uplift loads on roofs. Wind load is treated as one of the live loads acting on roof claddings. It magnitude depends on a number of factors such as wind speed and direction, building geometry, roof slope, surrounding and the terrain in the area of a building location. There are several different codes and standards in use in North America and they can vary in their treatment and quantification of wind loads. These differences are not only owing to variations of the climate conditions, but also the way in which various coefficients are defined by different codes.

Regardless of the code or standard used the roof designer needs a comprehensive understanding of the wind-induced loads. This chapter explains a knowledge-based design module developed by taking advantage of information technology tools for the estimation of the wind load distribution on roofs. To accomplish this task, first, all the data of wind uplift pressure distribution on roof configurations from open literature are collected. This includes studies using wind tunnel boundary layer and full-scale measurements. The existing studies scrutinized to extract useful design data. Second, a database management software with a user-friendly interface has been developed.

2.2 Wind Load Calculation

2.2.1 National Building Code of Canada (NBCC)

The National Building Code of Canada (NBCC, 1995) calculates the specified external pressure or suction due to wind using the equation:

$$p = qC_eC_pC_g \tag{2.1}$$

where p = specified external pressure or suction, acting statistically and in a direction normal to the surface.

q = reference velocity pressure, a function of reference wind speed and provided in three different levels of probability.

C_e = exposure factor which represents the effects of variation in the surrounding terrain and topography.

C_g = gust factor, ratio of maximum effect of loading to the mean loading effect.

C_p = pressure coefficient, which is the ratio of wind induced pressures on a building to the dynamic pressure (velocity pressure) of the wind speed at the reference height. This can be derived based on wind tunnel and full scale experiments.

The specified internal pressure is calculated using:

$$p_i = qC_eC_{pi}C_g \tag{2.2}$$

The internal pressure coefficient, C_{pi}, represents the effect of wind on the air pressure inside the building. C_{pi} depends mainly on the distribution and size of leakage paths and openings in the building.

The design pressure is the algebraic difference of the external and the internal pressures or suctions. The coefficients for the preceding equations are selected from graphs and or tables. For example, Figure 2.1 shows the product of the C_p and C_g values for gable roof configurations from the NBCC. These $\{C_p . C_g\}$ values are appropriate for less than 10° roof slopes. In terms of wind pressure, the roof area is divided into three zones that reflect location specific entities [c-corner, s-perimeter, r- field). For each zone, the values are given with respect to the area of the roof covering/cladding. For a building with 10° slope, a corner roofing (c) element with an area of 1-m^2 has a suction coefficient of 5.4 and this value decreases as the roof area increases.

2.2.2 American Society of Civil Engineers (ASCE)

In the United States, wind loads are mostly determined using the American Society of Civil Engineers (ASCE) *Minimum Design Loads for Buildings and Other Structures, (SEI/*ASCE 7-02). The design pressure due to wind is calculated using the equation:

$$p = q_h \times \{(GCp) - (GCpi)\} \tag{2.3}$$

where p = design wind pressure

q_h = Velocity pressure evaluated at height h

GC_p = product of external pressure coefficient and gust effect factor

GC_{pi} = product of internal pressure coefficient and gust effect factor

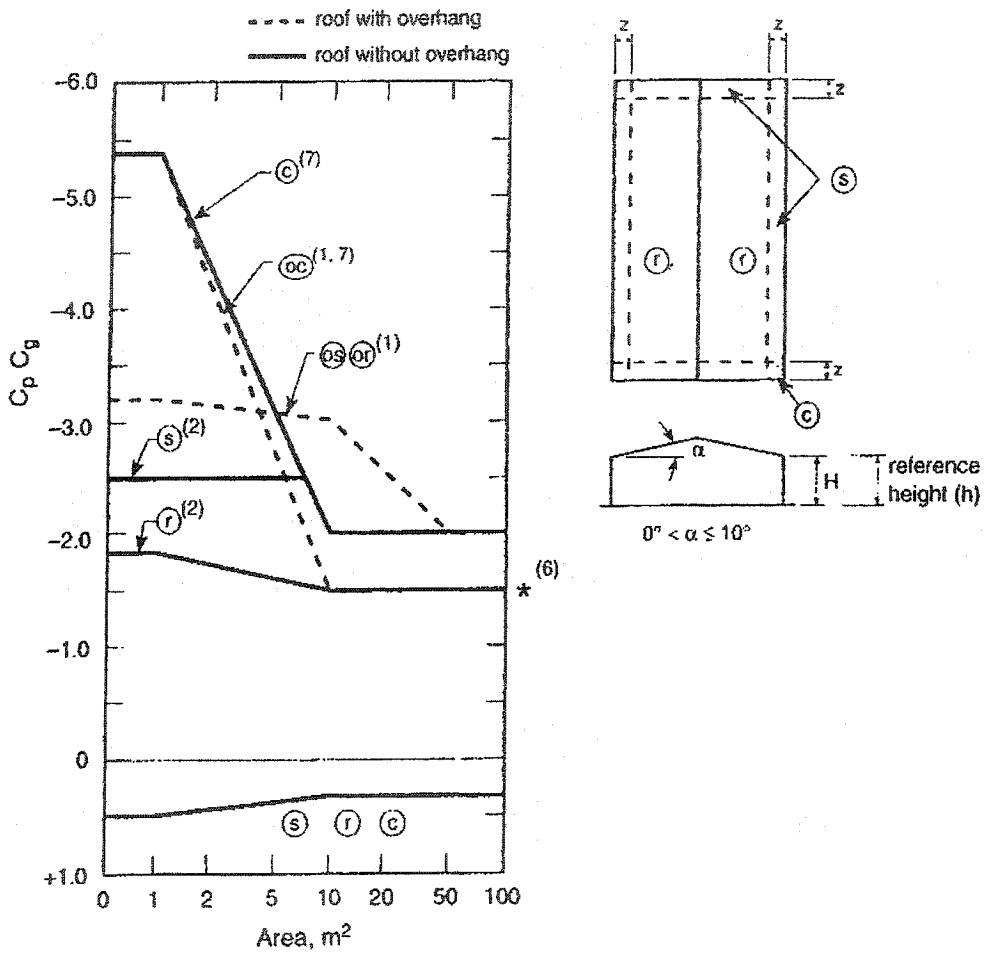

Figure 2.1 Existing design data based on building codes and practices (NBCC, 1995)

Figure 2.2 shows a typical design coefficient from ASCE 2002. The vertical axis shows {G. C_p} value instead of {C_p .C_g} the values used in the NBCC (Fig. 2.1). A design value of only 2.8 is recommended by the ASCE, for a similar configuration, namely, for a roof configuration with 10° slope and having a 1 m^2 corner roofing element.

2.2.3 Wind Tunnel Data

The {C_p .C_g} or {G. C_p} value for the North American codes are mainly determined from wind tunnel experiments. During wind tunnel experiments scaled models are tested under simulated wind conditions. Roof models are equipped with pressure taps to measure the induced pressure or suction. Figure 2.3 shows a photograph of a 3000 × 3000 mm PVC roof assembly in the wind tunnel. The test was carried out in the 9000 × 9000 mm wind tunnel at the National Research Council. For this test 81 pressure taps were fitted in the membrane to measure the wind induced pressure.

Measured pressures are analyzed statistically to provide mean, positive and negative maximum (peak) values corresponding to several locations on the roof. The negative or positive peaks represent suction or pressure. Such measured negative peaks are shown in Figure 2.4. Additional information on the wind tunnel investigation has been reported by Savage et al (1996). The data is for a square plan building exposed to oblique wind direction in open country exposure. It shows the spatial distribution of the peak pressure coefficients over the roof. For design purposes under similar conditions, these measured peak pressure coefficients can be used in Equation (2.1) in lieu of {C_p .C_g}.

As discussed, {C_p .C_g} can vary based on several factors. Building codes and standards recommend design values for most possible combinations. For example, NBCC provides roof design coefficients mainly for the following scenarios:

- Flat roofs – buildings greater in height than in width
- Stepped roofs
- Monoslope roofs – slope less than 30°
- Sawtooth roofs – slope less than 30°
- Gable and multi-gable roof – slope less than 45°.

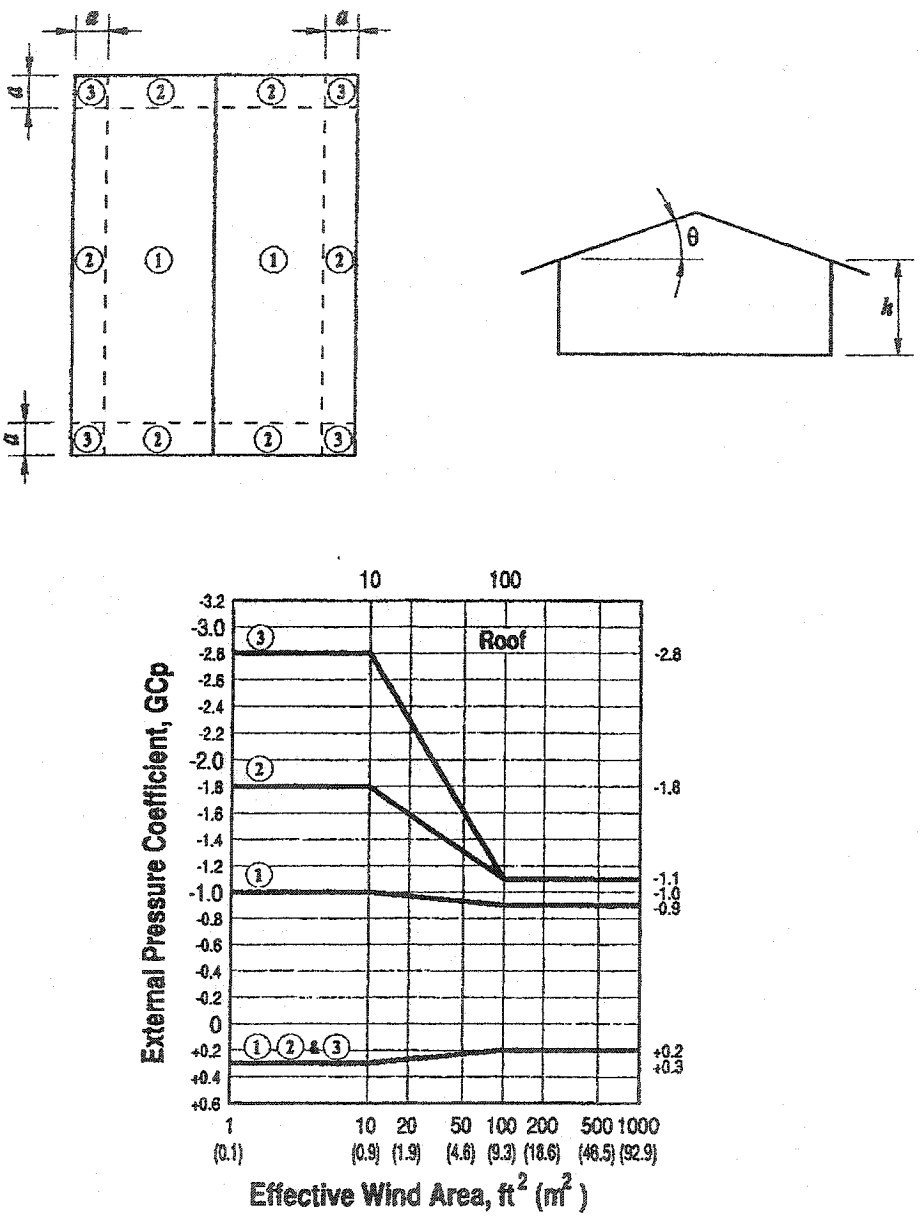

Figure 2.2 Existing design data based on building codes and practices (ASCE, 2002)

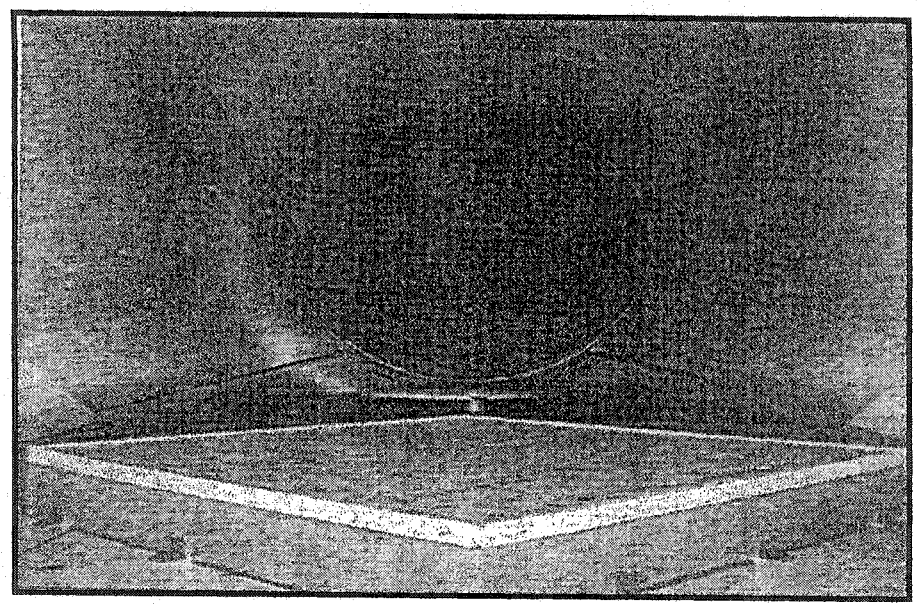

Figure 2.3 Photograph of a PVC roof assembly tested at NRC's wind tunnel

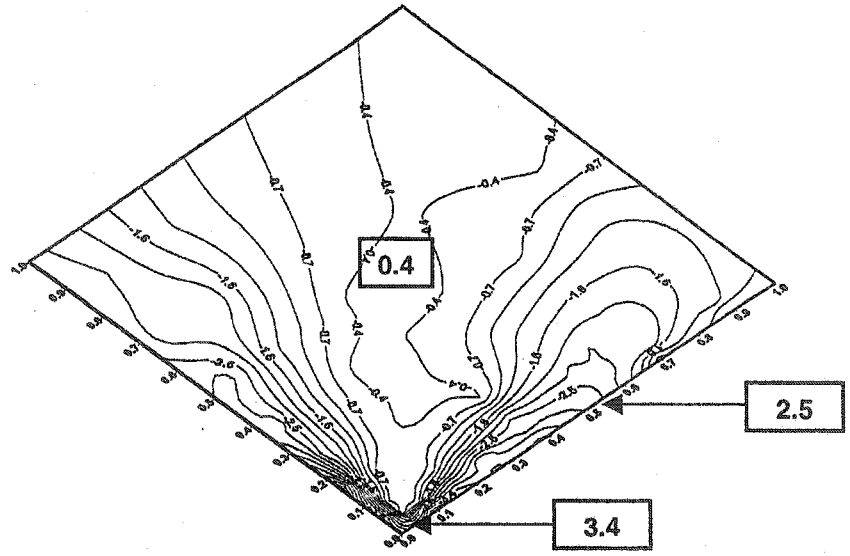

Figure 2.4 Typical roof wind pressure data from a wind tunnel study (Savage et al, 1996)

In practice, there are roofing configurations that fall outside those covered by the NBCC. The NBCC considers wind tunnel test results appropriate on buildings where the roof geometry deviates markedly from more common shapes for which information is already available. Moreover, the wind design roof data based on the code is mostly conservative. For example, NBCC defines one C_p .C_g constant value for a slope roof variation from 10 to 45. This value applies to the worst case in that range.

Alternatively, during the last four decades, several studies were carried out to quantify the C_p .C_g on roofs. Not all of this information is codified, therefore this knowledge is not accessible to designers. The data can be obtained by surveying researchers' works around the world.

2.3 Knowledge Extraction for Wind Load Estimation

Over the last forty years, there has been considerable research on wind-induced loads on roofs and chronicled in journal and conference papers quantifying the uplift pressure due to wind. The present study recently completed a survey documenting the state of the art for the roof design based on:

- Journals addressing wind effects on buildings and structures,
- Proceedings of the all ten International Conferences on Wind Engineering,
- Proceedings of all North American Conference on Wind Engineering (formerly known as U.S. National Conference on Wind Engineering).
-

A comprehensive review of the survey information has been made to extract useful design data. Emphasis was placed on papers that are dedicated to design data rather than papers addressing wind simulation techniques, comparison results and fundamentals of wind tunnel testing. More than 200 papers were found that provided roof wind uplift pressure distributions for different roof configurations. A further reduction was made to include only those articles for studies using boundary layer wind tunnels from 1970 and full measurement data. This resulted in 65 articles containing mean or peak pressure coefficients on various building roofs. From each article, information about the building geometry, building terrain, wind specification and distribution of pressure coefficient on roofs were scrutinized. Collected papers used by the present study are listed in Appendix A.

To enhance the collected data, all of them were converted to the common format. The common format provides consistency in unit and full-scale representation. For example, a number of

papers reported wind speed at levels other than eave height level. Present study converted all the reported wind speeds to eave height level. One can use either the log-law equation (2.4) or power-law equation (2.5). Engineers often prefer to use the power-law equation to convert the wind speed at different heights as it easier to evaluate and has enough accuracy. The present study also uses the equation 2.4 for the velocity conversion.

$$U = U_R \times Ln(H/H_0)/Ln(H_R/H_0) \qquad (2.4)$$

where U = wind speed at eave height

U_R = wind speed at reference height Z_R

H = building eave height

H_0 = roughness length

H_R = reference height

$$U = U_g(H/H_g)^{\alpha} \qquad (2.5)$$

where U = wind speed at eave height.

U_g = wind speed at gradient height.

H = building eave height.

H_g = gradient height.

α = power law index ranged from 0.1 to 0.4 based on the terrain type.

To make advantage of Computer Aided Design (CAD), full-scale representations were drawn by using the Corel Draw graphics program. All the graphic files have been saved in PDF format to make them more convenient for users to view using the Acrobat Reader program.

Figure 2.5, shows how typical source design data was converted to render the information useful for roof designer. The original data was from a full-scale study (Hoxey et al, 1983). This study reported results of different buildings instrumented to measure wind pressure on roofs in the open country condition. The reported pressure distribution on the windward and leeward roof is shown in Figure 2.5a for a building roof with 15-degree slope. These pressures were reported for a wind speed of 7 m/s at 10 meters height. The converted wind speed and pressure coefficient are

graphically shown in Figure 2.5b. By simplifying the two different graphs corresponding to the two roofs, the extracted design figure 2.5c shows variation of pressure coefficient graphically.

In all such figures, W, L, H and α parameters represent of width, length, eave height and roof slope respectively. In addition, V and θ wind speed and the angle of wind attack to the building represent wind specification. In some of the figures, the mean or peak pressure coefficients in corner, perimeter and field regions show the distribution of wind uplift pressure on roofs. Otherwise, mean or peak pressure coefficient show as arrows on top of the roofs. For the present study, more than 200 different design figures have been extracted from open literature. They cover building eave heights up to 200 meters. The collected data was organized based on building height, using advantage of computer technology. This will be described in the following section.

2.4 Database Development for Wind Load Estimation

By taking advantage of the growth of information technology, a user-friendly interface was created for searching the collected data more effectively. Microsoft Access 97 version 8, a 32-bit relational database management software to create a searchable database for wind load estimation. It has the capacity to integrate data from spreadsheets and other databases. Moreover, it has Internet related features for creating HTML documents for the World Wide Web. This would be helpful for future development of this ongoing project.

Overall functional structure of the database is shown in Figure 2.6. It has two query options:

- Search based on "Author".
- Search based on "Height".

These two modules have been connected to the wind pressure database, created as discussed in the previous section. By searching the database, the building geometry and pressure coefficient for any selected record will be displayed on the screen. Two other options Add/Edit and View data are also available for the users. These two modules and search modules constitute the framework of the database.

Each extracted wind pressure data is organized as a record for the pressure data table. In each record, there are seven fields: paper identification number (PIN), title, author, height, year, reference and design figures. Two other tables are also created, namely, height table and author table which related to the pressure data table.

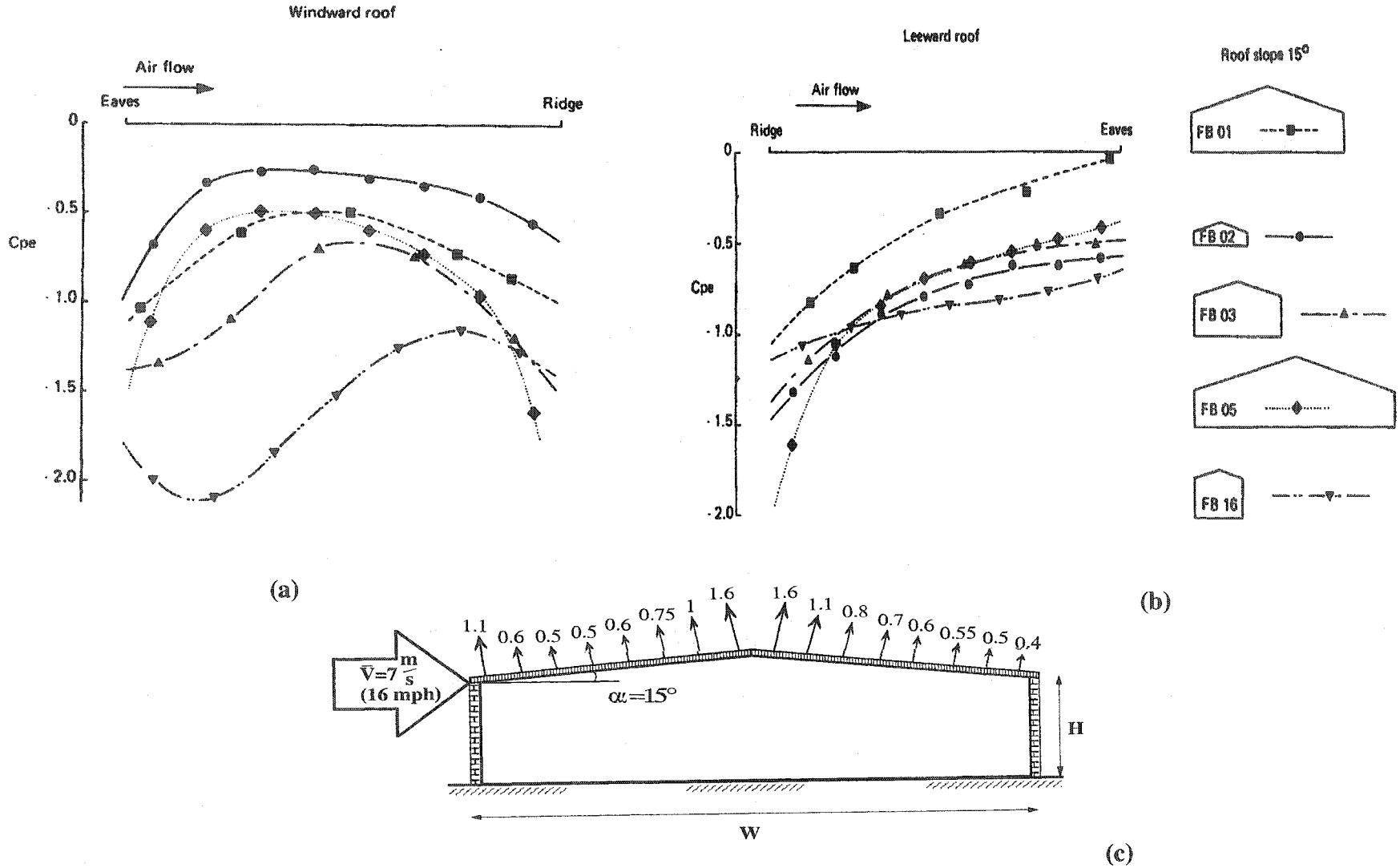

H=4.0m (13 ft) ; W=28m (92 ft) ; L=41m (135 ft)

Figure 2.5 Example of the extracted design knowledge from the source data

This is because some articles have design data for more than one height. Similarly, some articles have more than one author. The Author table contains name and PIN fields. The Height table includes height and PIN fields. The PIN field is used as a common field in all the tables. One can use the PIN field to develop relationships among the tables. This will enable a user to easily extract information. Thus, for a search based on an author, the design pressure related to various heights will be extracted. For a search based on height, all the work carried out by different authors will be generated.

As mentioned, the wind load database module is based on the existing data from the open literature. The accuracy of the published data is not the subject of the present study. Nevertheless, it was assumed that these published data from journals and conference papers have been scrutinized by the peer reviewer process. Also, the collected data does not depend on the specific region or any national building code therefore; it can complement to any national wind design tools. The database may provide options for the engineers to extract the pressure coefficients for building configurations that are not specified in the local code.

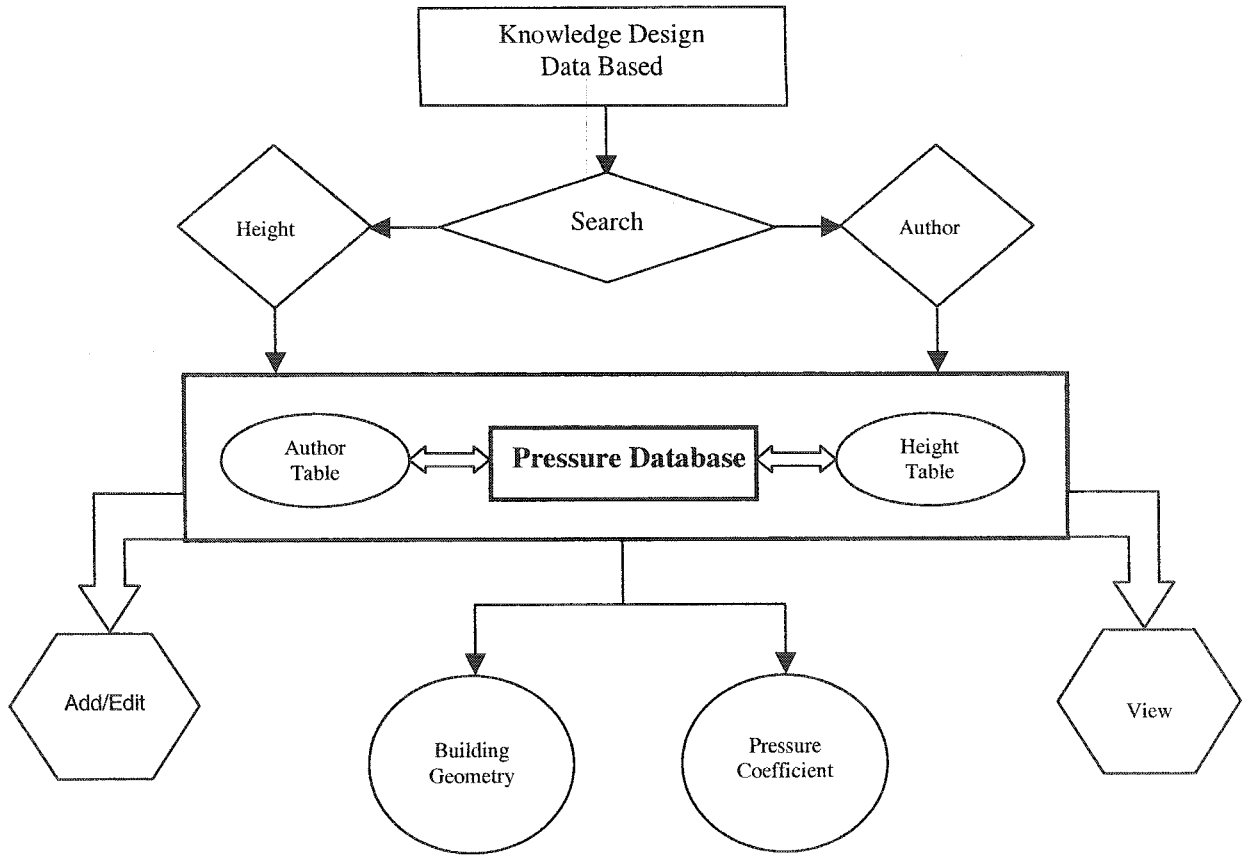

Figure 2.6 Framework of the developed data base

Figure 2.7 shows a typical view of the user interface. By selecting option 1 from the main menu, a new window will open. If the user selects Specified Author button, the program finds all papers corresponding to that author. Alternatively choosing the top button leads the user to enter the height range for the building using two different sub windows. For instance, Figure 2.7 shows selected height ranges of 4 to 5 meters. The program will search through the available database and find relevant records that meet the search criteria.

Figure 2.8 shows a typical output record for the input data in Figure 2.7 as explained below:

- The search identified 29 records that satisfy the search criteria; roof wind pressure records for building height ranging from 4 to 5 meters.
- Data is arranged in ascending order based on height; namely, record 1 out of 29 has the lowest building height whereas record 29 has the maximum building height of 5 meters.
- The output record shown in the figure corresponds to a building height of 4.9 and the corresponding fields such as paper title, author and source are also displayed.
-

By double clicking the design figure field (shown as a PDF in Fig. 2.8), the extracted design information complete with sketch is shown, using the Acrobat Reader program. The mean pressure coefficients, full scale building dimensions, wind direction, roof slope and the tested wind speed are also shown. To facilitate the design pressures, the information is presented in a format similar to building code representation. In other words, from the source article (Stathopoulos et al, 1991), the extracted data is displayed for the corner, edge and field region of the roof.

As mentioned, the wind load database module is based on the existing data from the open source. Although the accuracy of the design wind data is not the subject of this study, the data extracted from known published journals and conference papers, which are scrutinized by the peer review process. Also, the collected data does not depend on the specific region or any national building code therefore: it can be complemented to any national wind design tools. This will give a choice for the engineers to extract the pressure coefficients from the database rather that the local code.

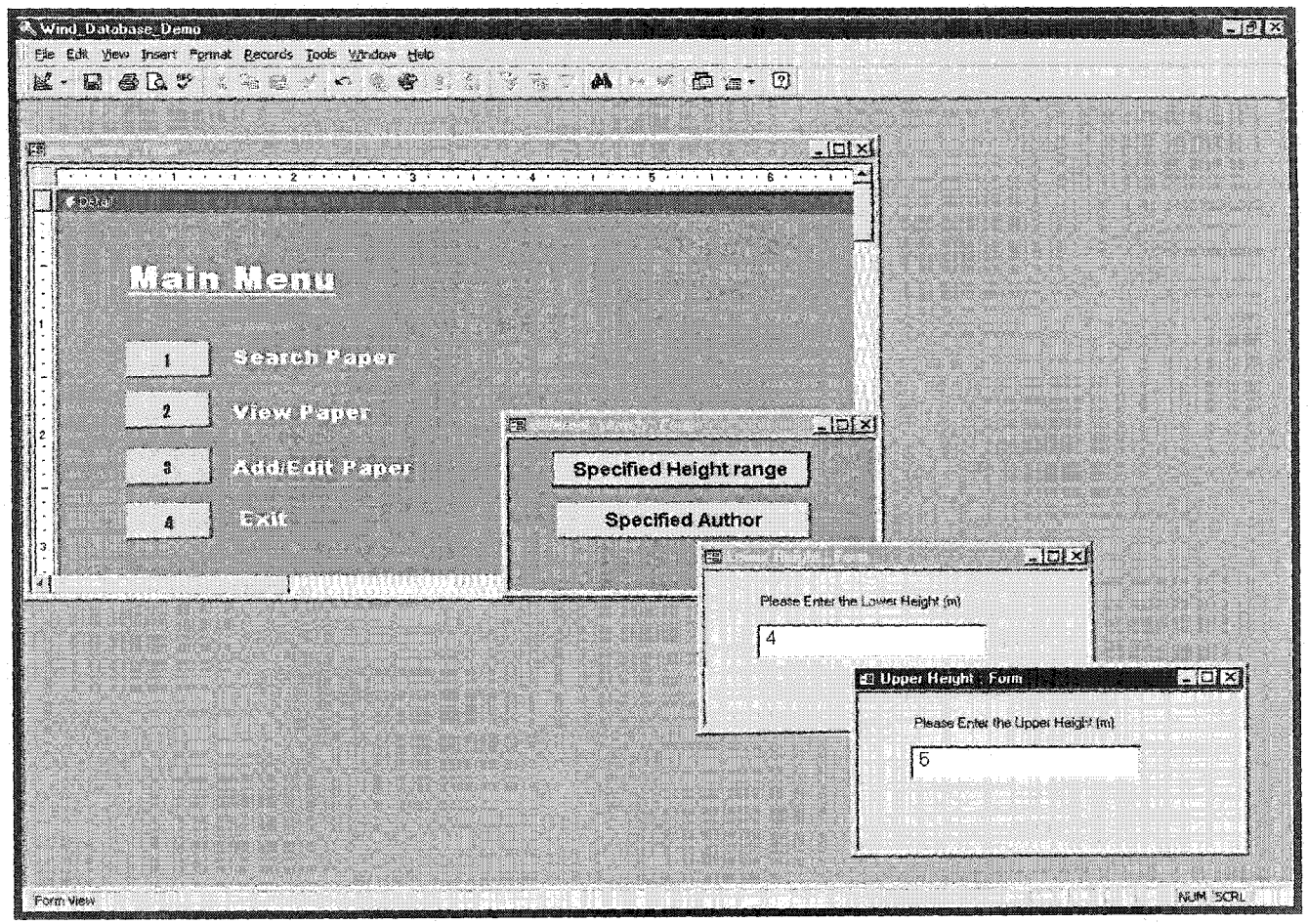

Figure 2.7 Typical inputs for searching

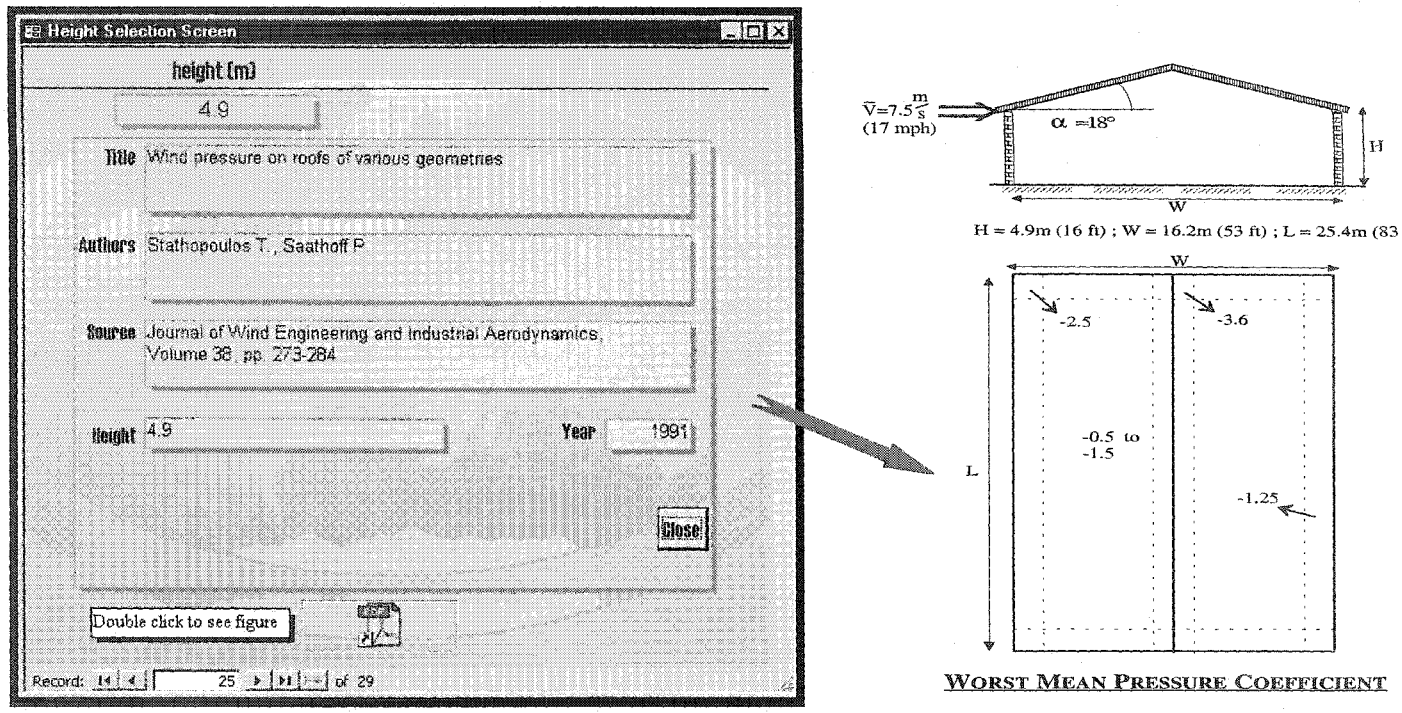

Figure 2.8 Typical output from the searching process based on building height

2.4 Database Limitation

Although the developed database can help the roof designer find the optimum wind load design easily, the following points are noted:

- The collected data is based on the available open literature. More data can be collected from other accredited sources.
- The database is developed based on existing data up to the year 1999. New data should be collected and integrated into the database so that it remains current.
- Although the developed application has a user-friendly interface, some computer knowledge is required by the users. A tutorial or a help document is provided to assist new users.
- Some collected data shows the mean pressure coefficients over the roof. The user has to find out the peak values prior to applying coefficient on wind load equation.
-

This chapter presented the fundamentals of wind load calculation and its distribution on the roof. It also introduced a wind load estimator that accesses a database to obtain design loads. This tool can facilitate roof designers to determine wind loads for a given roof for which the data is not available in the codes. In the next chapter, the roof system response to applied wind load pressure will be presented.

3 Wind Uplift Resistance of Roofing System

3.1 General

A roof can be classified as either a low-slope or a steep-slope roof system. A Low-slope roof is usually one that has a slope less than 14°. This type of roof is usually found on commercial and industrial buildings such as warehouses and factories. On the other hand, a steep-slope roofs with a slope more than 14°, is commonly used for residential houses. The latter one, usually made from asphalt shingle, fiber-cement, clay and concrete tiles.

In North America, two main types of low-slope roofs are in practice depending on the placement of the roofing membrane in the systems.

- *Inverted roofing system:* The membrane in the inverted roofing system (also called the upside-down roof) is placed below the insulation.
- *Conventional roofing system*: In the conventional roofing system the membrane is located at the insulation top. In this type, the membrane is directly exposed to environmental forces such as wind, snow, rain, UV and temperature fluctuation (Figure 3.1). The conventional roofs may be either the Single-ply roofing system (SPR) or a Built-Up roofing system (BUR).

3.1.1 Membranes Used in Single-Ply Roofing Systems

Conventionally, the BUR systems are introduced in low-slope roofs in Canada. The SPR was introduced in the early sixties as an alternative to BUR. In recent years, they have become a viable alternative because of the rising cost of labor as well petroleum-based bituminous materials. In addition, improvements in polymeric materials and the need for easily adaptable membranes for unusual roof configurations make SPR as an alternative option.

Figure 3.2 shows flexible roofing membranes that are in use for the single-ply roofing systems. Asphalt-based membranes are used mainly on Modified Bitumen roofing systems. The Modified Bitumen roofing membranes are composed of one or more pre-manufactured sheets consisting of asphalt, reinforcing layers and in some cases surfacing. During the manufacturer of Modified Bitumen roofing membranes, plastic or rubber is added to the bitumen while heating. It gives a higher softening point and greater elasticity (NRCA, 1999).

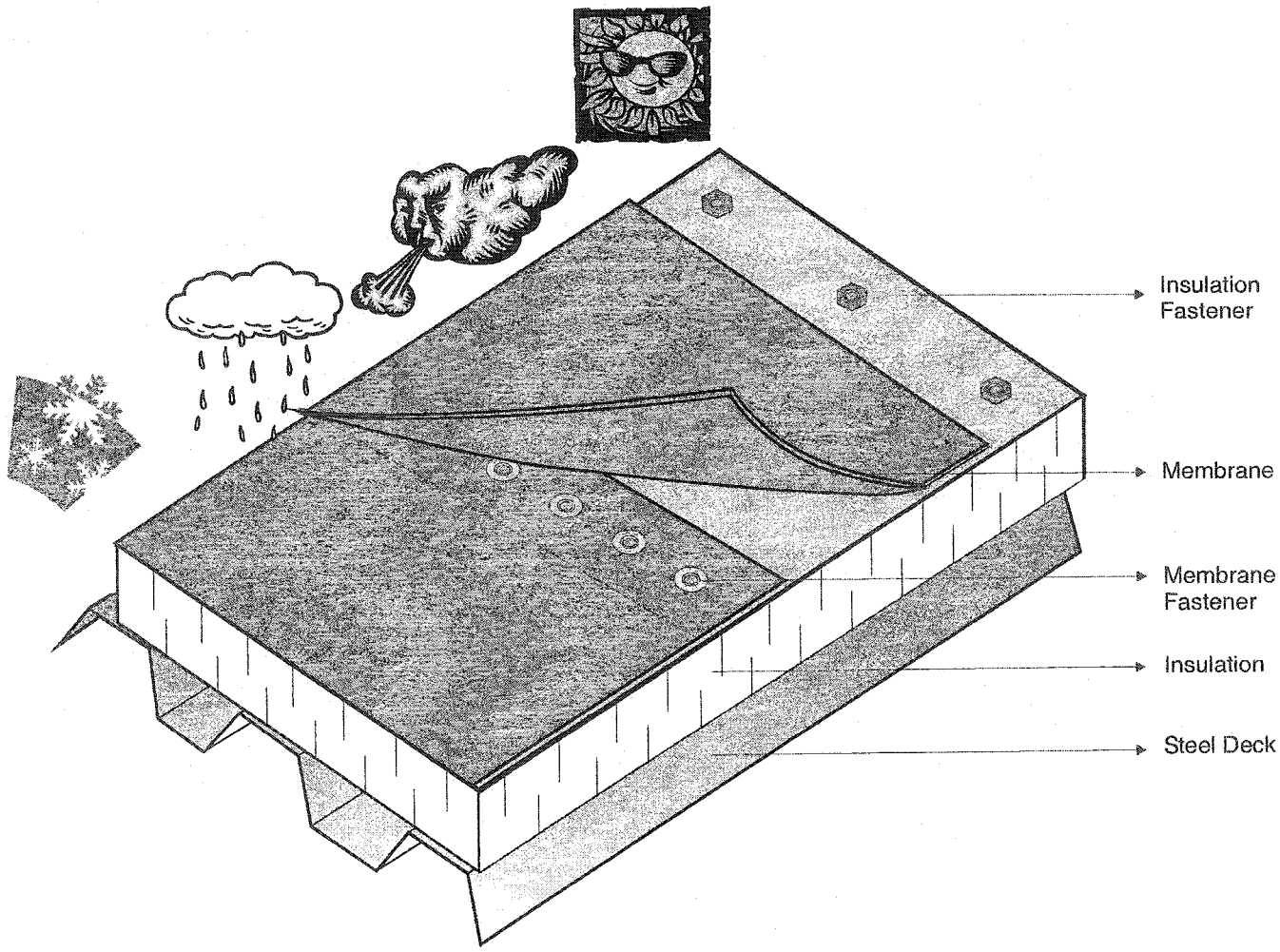

Figure 3.1 Typical conventional single-ply roofing system

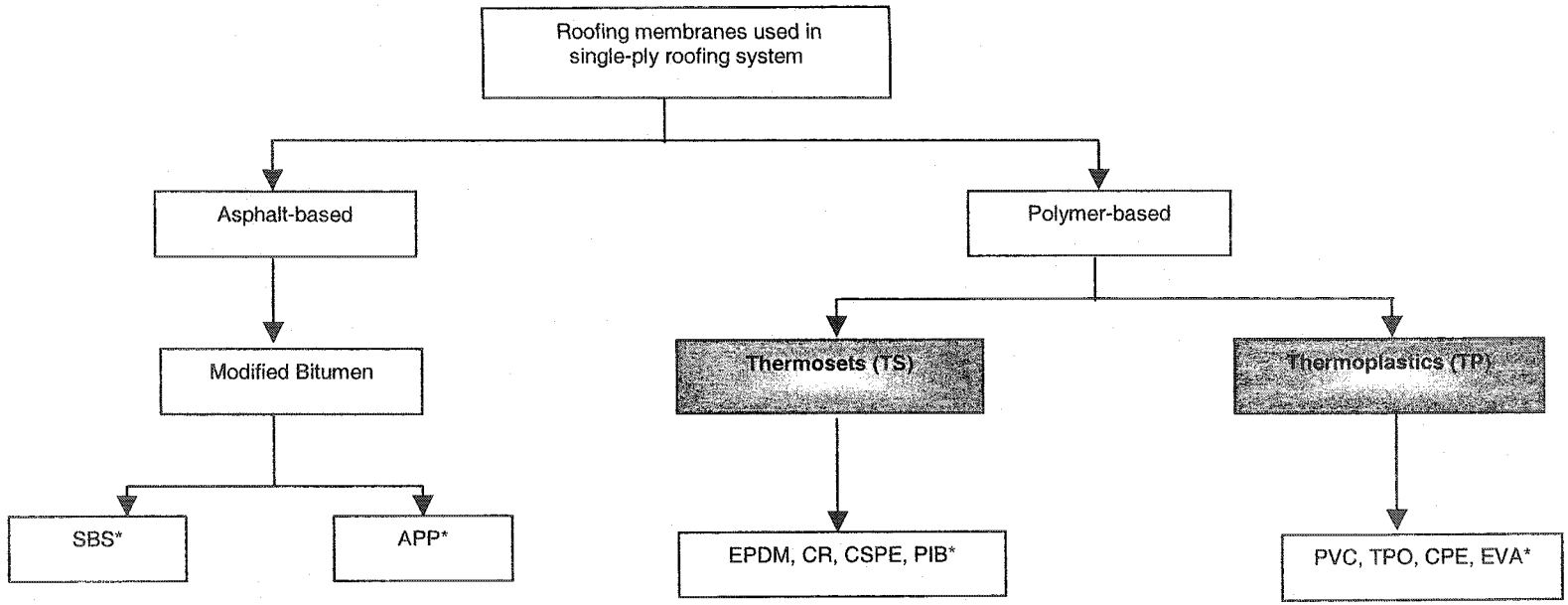

** Please refer abbreviation Section.*

Figure 3.2 Membranes used in single-ply roofing system

Thermoplastics (TP), referred to as plastics, are obtained from the polymerization of long chain molecules. This type of material softens when heated and can take new shapes by the application of heat and pressure, but does not cure or set. The changes seen in this type of membrane are purely physical and with the application of heat are wholly reversible. Therefore, a thermoplastic material can be reprocessed many times without undergoing any appreciable chemical change. This type of material is generally linear or slightly branched allowing it to flow under pressure when heated above the effective melting period. The thermoplastics can be subdivided in two groups: crystalline and non-crystalline polymers.

Thermoset (TS) materials, as the name indicates, is a material that cures or hardens into a given shape generally through the application of heat. Curing is an irreversible chemical reaction in which permanent connections (cross-links) are made between the molecular chains. These cross-links give the cured polymer a three-dimensional structure, as well as a higher degree of rigidity than it possessed prior to curing. A cured thermoset material will not flow or remelt or otherwise regain the processibility it had before curing. Thermosets can still be deformed after cross-linking but they regain their shape after removal of the stress. Thermoset polymers outperform other materials in a number of areas including mechanical properties, chemical resistance, thermal stability and overall durability.

Thermoplastic and thermoset materials are of great commercial importance in the building industry. However, they cannot always be used as engineering materials without improving properties such as strength. Polymer properties can be enhanced by adding reinforcing fillers. They are solid, chemically inert substances added to a resin to modify its properties and most of all, reduce cost. Most fillers are minerals and reduce cost, provide speed of cure, add strength, and provide special electrical, mechanical and chemical properties. The combination of the polymer (thermoplastic, thermoset, elastomer) and reinforcing-fiber materials such as glass or carbon results in a material known as a composite. A wide range of crystalline and amorphous materials can be used as the fiber. Carbon black and glass fiber are commonly used in the fabrication of construction materials e.g., roofing.

The present study focuses on the behavior of the two main kinds of single-ply roofing systems in which the membrane is polymer-based. Ethylene-Propylene-Diene-Monomer (EPDM) is a Thermoset (TS) elastometric compound synthesized from ethylene, propylene, and a small amount of diene monomer. Thermoplastic Olefin (TPO), a Thermoplastic (TP) type, is formulated from ethylene, alpha-olefin polymers and copolymers. Table 3.1 lists membrane mechanical and physical properties (ASTM 1996, 2003). Some of the advantages and

disadvantages of these two types of roof membranes (Baskaran et al 1997) are also highlighted in the Table 3.1.

3.1.2 Attachment Methods for Single-Ply Roofing Systems

There are generally three major types of attachments used to secure membranes in single-ply roofing systems. Mechanically-fastened SPR was shown in the Figure 3.1, whereas the other two types of attachments are shown in Figure 3.3. These figures depict the configurations along with the basic arrangement of roof components. The roof components include: membrane, insulation, deck, barriers and attachment systems.

- *Mechanically-fastened SPR*: The membrane is attached to the structural substrate either along strips or at numerous points using fasteners. The attachments consist of the mechanical fasteners and plates or metal or polymer batten.
- *Adhered SPR*: The membrane in adhered single-ply roofing system is fully bonded to the substrate by solvent or water-based adhesive or hot bitumen and the substrate is attached to the structural deck.
- *Loose Laid SPR (ballasted configuration)*: The completed membrane is loose laid and held down by the weight of gravels or concrete pavers. However, at the building perimeters, the membrane is attached with the roof/wall junctions.

Table 3.1 Typical TP and TS membrane material characteristics

Type	Properties	Typical	Pros	Cons
TP	Thickness mm (in)	10 (0.04)	• Highly elastic • Resistant to ozone • Resistant to Ultraviolet (UV) • Durable	• Requires careful seaming • Sensitive to oils, grease and solvent • Flammable • Shrinkage
	Elongation –Ultimate (%)	250		
	Breaking strength N (lbf)	400 (90)		
	Tear Strength N (lbf)	45 (10)		
TS	Thickness mm (in)	1.0 (0.04)	• Resistant to biological attack • Resistant to most acids and soils • Fire-resistant • Easy to apply • Good on-site seaming • Choice of colors	• Migration of plasticizers • Shrinkage and embrittlement • Heat-sensitive • UV-sensitive
	Elongation – Ultimate (%)	700		
	Breaking strength N (lbf)	976 (220)		
	Tear Strength N (lbf)	245 (55)		

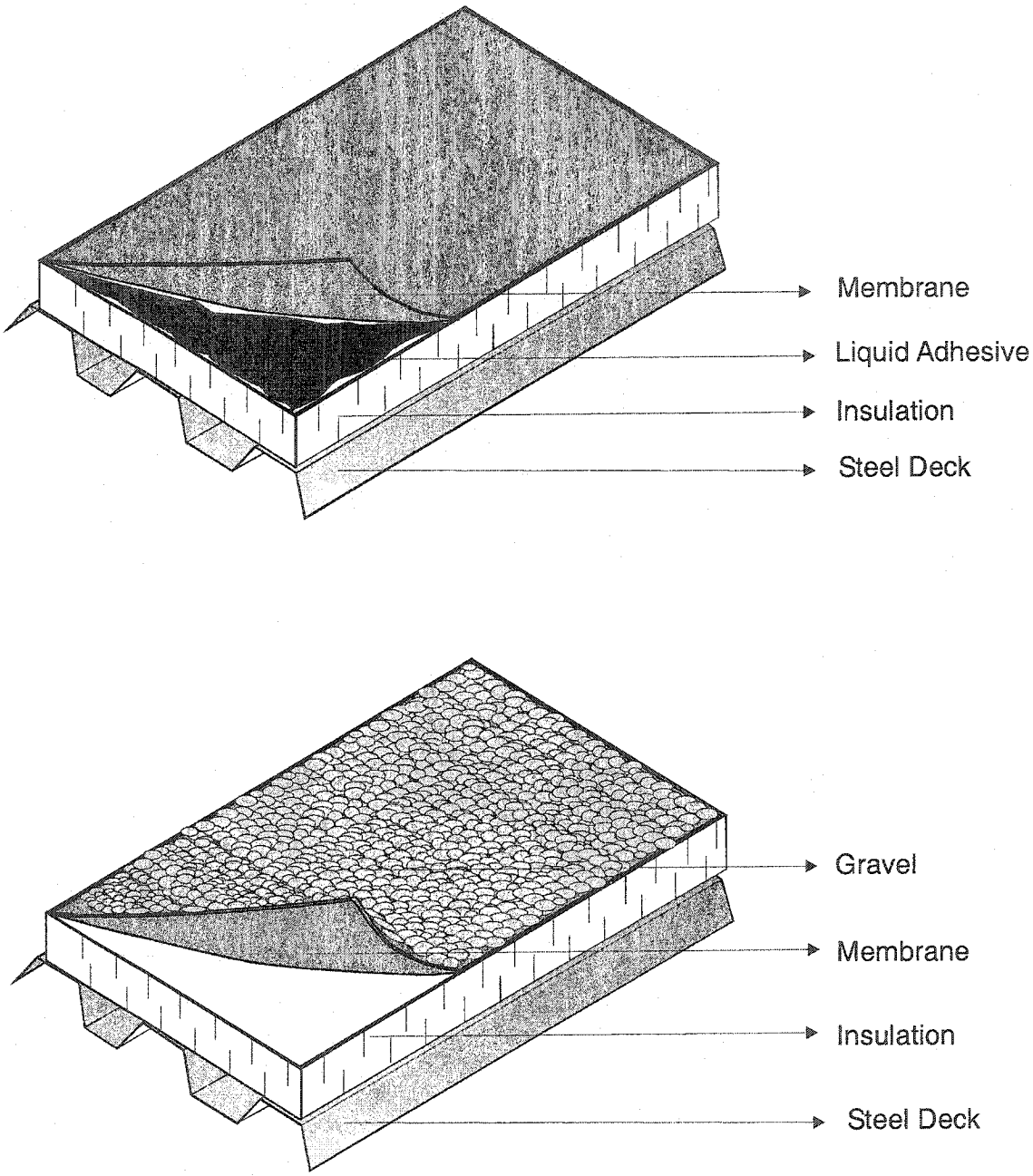

Figure 3.3 Attachment methods for single-ply roofing system

3.2 Evaluation Procedure

Wind performance investigation is critical in the evaluation of roofing systems. Wind-induced pressure on a roof varies with respect to time, as well as spatially over the roof. Wind loads are usually transferred to a roof assembly through pneumatic load path or a structural load path. If the external wind fluctuations are quicker than the membrane response, the load shared among the roof components by pressure difference across the components (Cook 1992). This is known as pneumatic load path. If, on the other hand, the fluctuation of the wind pressure is slower than the membrane response time the load is transmitted through membrane tension to the fasteners and there is a structural load path.

The design and evaluation of roofing systems are based on the standard test methods that involve placing the roof components in an apparatus and applying simulated wind loads to the roof system. Each component plays an integral role in the performance of a roofing system. Therefore, a roof designer should carefully pay attention to the selection of the compatible components. Although, a roofing manufacturer assembles the test specimens which are the same as the field, the simulation of wind load may not replicate the field environment properly. For instance, the Factory Mutual (FM) loading sequence overestimates the design parameters and yields different failure modes when compared with the developed dynamic load sequence. To elaborate more in this issue, a brief review of existing loading sequences for the evaluation of roofing systems summarized in the following section. More detail of the test procedures can be found in a review report by Baskaran and Dutt (1995).

3.3 Wind Uplift Simulation

3.3.1 Factory Mutual 4470 Standard

In the FM protocol (FM Research 1992), the pressure is supplied through the positive air pressure to the bottom of the apparatus using an air compressor. The initial test pressure of 1.44 kPa (30 psf) is applied and maintained for one minute. Then, the pressure is increased by 0.72 kPa (15 psf) in each successive minute until the failure of the test panel. The intention of this test procedure is the establishment of a windstorm classification for the roof assembly. The test assembly should withstand certain pressure levels for 1 minute to obtain approval for a Factory Mutual I roof cover. For example, to get an I-90 windstorm classification, the test assembly should sustain the 4.3 kPa (90 psf) pressure sequence for one minute. It should be noted FM is not a dynamic test

3.3.2 Underwriter Laboratories 580 Standard

The UL 580 (Haddock 1992) procedure applies loads on the chamber not only from the bottom as a steady positive pressure, but also from the top as steady and oscillating negative pressure. Table 3.2 shows the negative and positive pressures applied on different test phases at set times. The classification ratings for this protocol are: UL-15, UL-30, UL-60 and UL-90. For instance, to obtain approval for the UL-60 the following load sequences are applied to the roof assembly:

- In the first phase, a 1.55 kPa (32.3 psf) negative pressure is applied for 5 minutes.
- During the second phase, a 1.33 kPa (27.7 psf) positive pressure is added from the bottom of test assembly for an additional 5 minutes.
- Then, a negative oscillating pressure of 0.79 to 2.66 kPa (16.2 to 55.4 psf) is applied at a frequency of 10 second per cycles for 60 minutes.
- In the fourth phase, only a 1.94 kPa (40.4 psf) negative pressure is applied for 5 minutes.
- In the last phase, while the negative pressure is in effect, an additional 1.66 kPa (34.6 psf) positive pressure is applied for 5 minutes.

Similar procedures apply to other classifications considering that specimens must first pass the upper classes before starting the next class. The UL-90 classification takes around 5 hours to complete.

3.3.3 European Union of Agreement (UEAtc)

The following steps of the UEAtc standard wind load cycle were prepared according to a procedure developed by Gerhardt and Kramer (1986). Figure 3.4 shows the load cycle for a five-year return period

- Four cycles of 1415 gusts with a maximum load of 300 N per fastener are applied .
- If the back-out behavior of the fastener is unknown, then the roofing system must be subjected to 200,000 fluctuations with a loading of 100 N (22.5 lbf) per fastener and a frequency not exceeding 10 Hz. This is known as the conditioning cycle and it is applied between the third and fourth loading.
- 1415 gusts are applied on the condition the maximum load per fastener does not exceed 400 KN (90 lbf).
- The maximum load per fastener is increased in increments of 100 N (22.5 lbf) and applying 1415 gusts in each level until failure occurs.

Table 3.2 Underwriters Laboratories Standard Load Sequences

Rating	Test phase	Time duration minutes	Negative pressure kPa (psf)	Positive pressure kPa (psf)
UL 15	1	5	0.45 (9.4)	0.0 (0.0)
	2	5	0.45 (9.4)	0.25 (5.2)
	3	60	0.27-0.78 (5.7-16.2)	0.25 (5.2)
	4	5	0.7 (14.6)	0.0 (0.0)
	5	5	0.7 (14.6)	0.4 (8.3)
UL 30	1	5	0.79 (16.2)	0.0 (0.0)
	2	5	0.79 (16.2)	0.66 (13.8)
	3	60	0.39-1.33 (8.1-27.7)	0.66 (13.8)
	4	5	1.16 (24.2)	0.0 (0.0)
	5	5	1.16 (24.2)	1.00 (20.8)
UL 60	1	5	1.55 (32.3)	0.0 (0.0)
	2	5	1.55 (32.3)	1.33 (27.7)
	3	60	0.79-2.66 (16.2-55.4)	1.33 (27.7)
	4	5	1.94 (40.4)	0.0 (0.0)
	5	5	1.94 (40.4)	1.66 (34.6)
UL 90	1	5	2.33 (48.5)	0.0 (0.0)
	2	5	2.33 (48.5)	1.99 (41.5)
	3	60	1.16-2.33 (24.2-48.5)	1.99 (41.5)
	4	5	2.71 (56.5)	0.0 (0.0)
	5	5	2.71 (56.5)	2.33 (48.5)

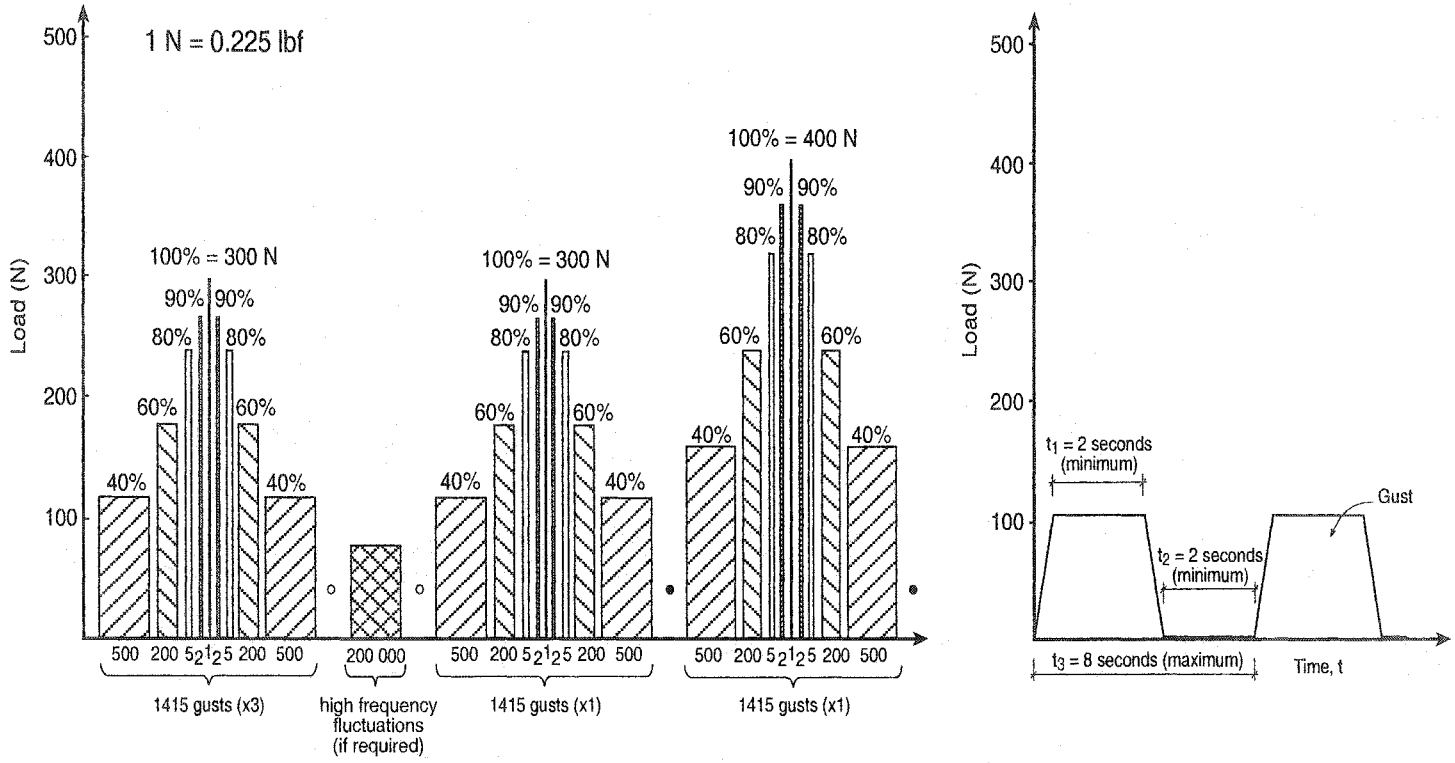

Figure 3.4 European Union of Agreement (UEAtc) load cycle

3.3.4 Norwegian Standard (NT BUILD)

NT BUILD 307 1986-11 (Paulsen 1989), "Roof coverings – Wind load resistance" is a standard method being used to test the strength of wind uplift on roof assemblies. This protocol is a standard method. In 1987, the Norwegian Building Research Institute (NBI), along with other participants from Scandinavian countries, initiated a study of dynamic load application on mechanically attached roof system. "NBI 162-90 Roof coverings – Dynamic wind load resistance" a modified version of the NT BUILD 307 static test procedure, developed from that study. In the test assembly, the specimen is situated between two lower and upper boxes. The lower box applies a static suction of 0.1 Pa (2.1 psf), while the upper box applies pulsating suction initiated at 0.2 kPa (4.2 psf). In each step the gust applies every 15 seconds for one hour. Figure 3.5 depicts the values and increments of gust intensities.

3.3.5 SIGDERS Dynamic Loading Cycle

The SIGDERS load cycle (Baskaran et al 1998) was developed based on the wind-tunnel studies of full-scale roof systems. Studies were made of 3048 × 3048 mm (120" × 120") roof systems using the National Research Council's (NRC's) 9000 × 9000 mm (360" × 360") wind tunnel. Two series of investigations were carried out using two distinct roofing membranes. The first series dealt with a reinforced Poly Vinyl Chloride (PVC) membrane and the other with a non-reinforced Ethylene Propylene Diene Monomore (EPDM) membrane. Different configurations were tested for variation in building heights, wind speed and wind direction. For PVC, there are 30 different test configurations, whereas in the case of EPDM, 48 configurations were tested.

The model roof systems instrumented with taps on different locations to record pressure time histories. For each configuration, 60 second pressure time histories were recorded, which represents 51 minutes duration in a full scale windstorm event. The obtained unsteady histories of wind pressures are used for the load cycle development. The details of the developed load cycle can be found in a report by Baskaran and Chen (1997).

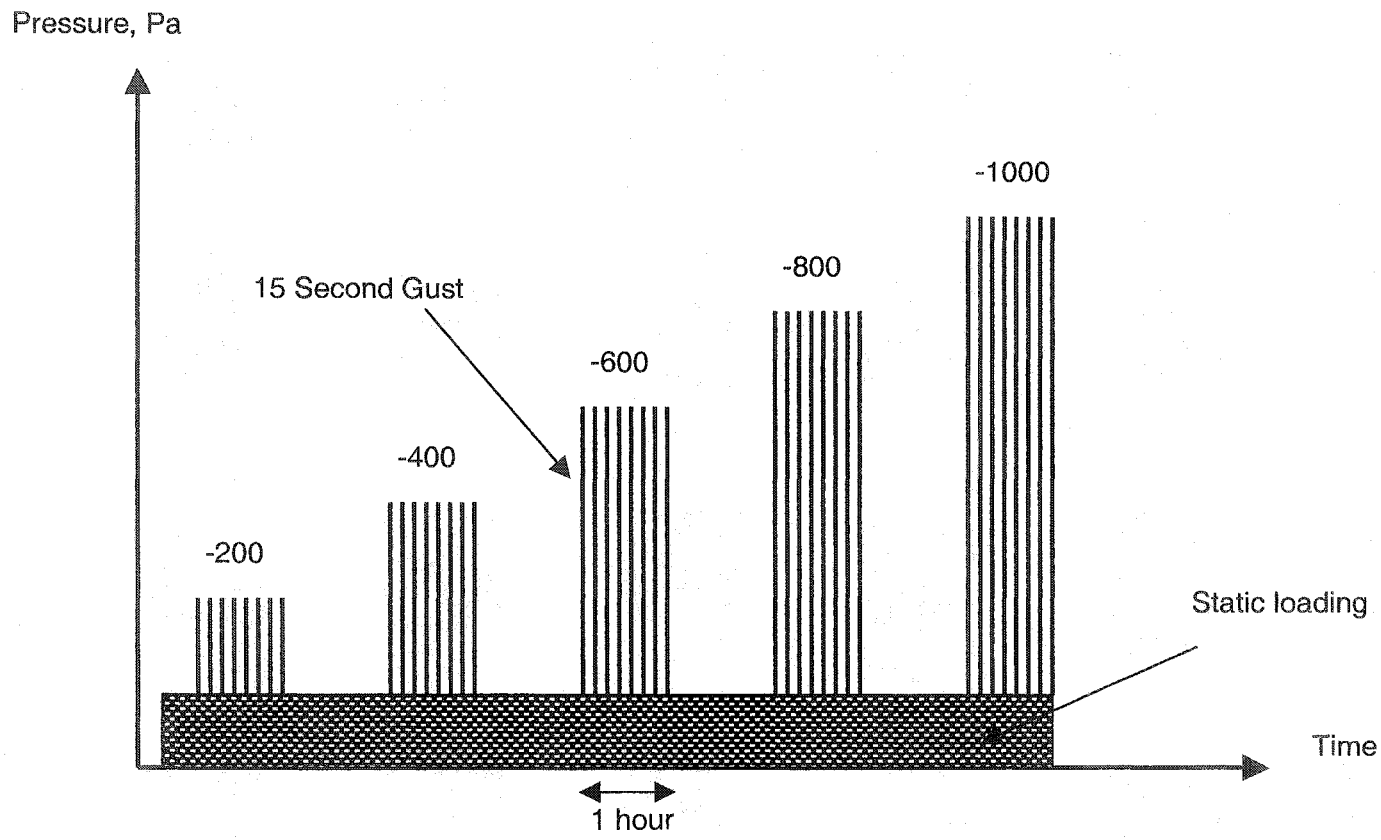

Figure 3.5 Norwegian load cycle

Figure 3.6 shows load cycle developed for the SIGDERS wind test procedure in five rating levels (A to E). The test pressure corresponds to the design pressure, in accordance with local building codes or wind standards. The pressures for each load sequence are calculated as percentages of the test pressure.

The load sequence is divided in two groups: Group 1 has a zero minimum value and for Group 2 the cycles are applied over a constant static component. Both groups are divided into four load sequences. The pressure level for Group 1, can be viewed as wind-induced suction over the roof assembly and applied as follows:

- 400 gust cycles are applied at 25% of the test pressure
- 700 gust cycles are applied at 50% of the test pressure
- 200 gust cycles are applied at 75% of the test pressure
- 50 gust cycles are applied at the test pressure

In Group 2, the simulation represents the effects of exterior wind fluctuations combined with a constant interior pressure. A constant suction of suction of 25% of the test pressure is applied. Then, four sequences of various gust pressures are applied as follows:

- 400 gust cycles are applied from 25% to 50% of the test pressure
- 400 gust cycles are applied from 25% to 50% of the test pressure
- 400 gust cycles are applied from 25% to 50% of the test pressure
- 400 gust cycles are applied from 25% to 50% of the test pressure

If the tested specimen passes all eight sequences of Group 1 and Group 2 at level "A", it can be tested with the design pressure increased incrementally by 0.25. Theses levels provide for the manufacturers systems with safety factors. Whereas the building codes or wind standards prescribe only minimum design value. Therefore, the load cycle can evaluate the design pressure or safety factor of two, where the specimen passed level "E".

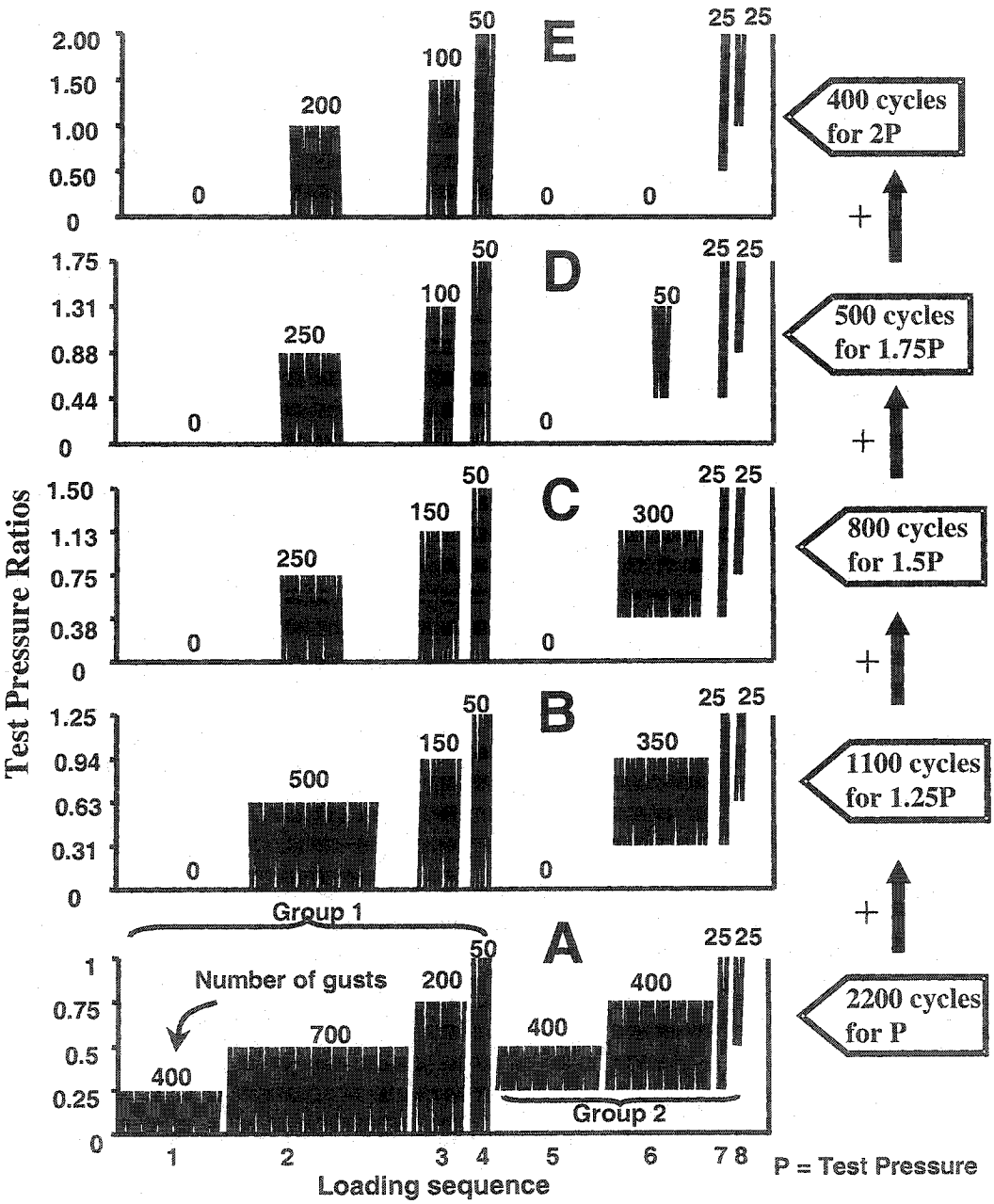

Figure 3.6 SIGDERS dynamic loading cycle

3.3.6 Other Test Procedures

Smith (1992) developed a procedure to test mechanically attached single-ply membranes for fatigue. The number of loading cycles was associated with wind speed increments by using the Weibull probability distribution. Letchford and Norville (1993) proposed a load sequence based on wind pressure records from the Texas Tech University's Wind Engineering Research Field Laboratory. They used level-crossing and mean-crossing and mean-range count analysis as the cycle-counting methods. This load sequence was also applied in the development of a test standard for determining impact resistance from windborne debris, SBCCI (1994). In Australia, Byrne (1976), Morgan and Beck (1977), Mahendran (1990, 1994) used an experimental setup to apply dynamic loading on sheet-metal roofing. Researchers' findings from this investigation were used to update the Australian Standard (TR – 1978). Clemson University in the United States acquired the Building Research Establishment Real-time Wind Uniform Load Follower (BRERWULF - 1988) facility for wind testing of building envelopes.

The above review of the existing test standards and procedures reveals the following:

- FM 4470 and UL 580 testing procedures do not account for the wind induced fatigue effects on the mechanically attached roofing system.
- Fatigue is an important factor in the two test procedures of UEAtc and NT BUILD 307. It illustrates that the European dynamic testing procedure is more advanced than in the North American' ones.
- The UEAtc procedure provides the fastener design load, whereas FM and UL certify a roof system for a design pressure.
- The UEAtc test is a time consuming procedure and may take more than 1 day for a typical test.

4 Evaluation of Wind Uplift Resistance

4.1 General

Numerical techniques can be useful for examining roof configurations that would be too expensive, or difficult to set up experimentally. In addition, the analytical models are generally faster than experimental approaches for solving problems where there is a need to investigate the impact of various influencing parameters. The effect of driving forces can also be easily modified more efficiently in the numerical models.

A limited number of numerical studies {Koike et al (1978), Lewis (1980), Rossiter and Batts (1985), Gerhardt and Gerbatsch (1989), Easter (1990), Zarghamee (1990), Gerhardt and Kramer (1992), Bienkiewic and Sun (1993), Brodland et al (1993)} attempted to evaluate the roofing system performance using numerical models. Baskaran and Kashef (1995) identified several research needs by systemically documenting the state-of-the-art in this area. A review of these studies shows numerical model or simplified methods have been used to:

- Determine induced stress in single-ply roofing membranes because of thermal gradients across the roof system.
- Investigate the mechanical failure behavior of fully adhered SPR under in-plane loading conditions.
- Investigate the static ballooning response of mechanically attached SPR membrane subjected to the wind uplift force.
- Predict the effect of wind pressure on the inflated SPR membranes and its attachment mechanism employing a quasi-static analysis.
- Investigate the fatigue failure of the fully bonded membranes caused by the fatigue rupture of substrates by solving the governing differential equations.
- Simulate wind loading distribution on SPR system with ballasted pavers by applying Darcy's law for flow movement and assuming linear pressure.

All the existing studies focused on the performance evaluation of a particular system rather than on the effect of various parameters on the system performance. The parameter variables such as fastener spacing, membrane size, roof component material and wind pressure load sequence can affect roof system responses. Also, there is no consensus on the test table size

to be used by testing protocols in spite of the concern that the test rig edge effect of the table may play a significant role in evaluating performance. The effect of table size on roofing system performance is an ideal opportunity to explore the modeling capabilities of numerical approaches. To address some of these issues, a numerical modeling approach has been selected by the present study. The steps for the numerical study are as follows:

- Select a suitable numerical model
- Simulate the wind uplift resistance of single-ply roofing system
- Benchmark the model using the experimental data

4.2 Selecting a Finite Element Based Numerical Model

Finite element based software programs for the design and analysis of structures have become more common in current Civil Engineering practice. A simple graphical user interface with extensive variety of structural modeling makes the simulation and analysis easy. A user can easily select a beam element to see the variation of shear stress or moment diagram for different loading options. The convenience comes from the numerical techniques used in the software. However, the numerical analysis has been rarely used by engineers to evaluate the behavior of SPR.

ABAQUS version 5.8 (1998), a commercially available Finite element program having potential to solve problems ranging from simple linear analysis to the more challenging nonlinear simulations, has been selected to carry out all the numerical analysis for the present study. ABAQUS contains a library of elements that can model various material geometries and simulate the behavior of an extensive list of materials including rubber, metal and polymers. It has the flexibility of defining complex system geometry and varying applied loads. For example, ABAQUS eliminates all unnecessary nodes before performing the analysis. This feature is useful since it allows points to be defined as nodes for node generation purpose only.

The present numerical model can predict the response of linear or nonlinear analysis systems. There are three sources of nonlinearity in the modeling of SPR: material, geometric and boundary. In a nonlinear analysis the solution cannot be calculated by solving a single system of linear equations, as would be done in a linear problem. Instead, the solution is found by specifying the loading as a function of time and incrementing time to obtain the nonlinear response. Using the Newton method, it often takes several iterations to determine an acceptable solution for each time increment.

4.3 Modeling of Single-Ply Roofing Systems

A numerical model was used to simulate the mechanically attached thermoplastic and thermoset systems. Since there are some similarities in the simulation model, first, the general input file format and analysis procedure for the numerical model of a generic single-ply roofing system is discussed. Then, in the next section, the detailed simulated model for each system is explained independently.

An input data file, which replicates the roofing system configuration, has been prepared. The file contains the model and history data. The model data defines the geometry system configuration such as nodes, elements and material properties while history data addresses the sequence of loading for which the model response is sought. The history data is also defined as a sequence of steps. Each step is a response period for a particular type of loading.

Finite element techniques were applied to analyze the input data file and the result of finite element analysis is created in the output text file. The output file format depends on which nodes and element are selected for analysis and it also could be shown in graphical format.

4.3.1 Model Data

Figure 4.1 shows a typical numerical model representation for the experimental single-ply roofing system. Only membrane properties were considered in the numerical modeling owing to the greater flexibility of membrane compared to other components in the roofing systems. In other words, the deflections of the steel deck and insulation were assumed to be negligible in comparison to the membrane deflection.

The model data defines the geometry layout and material characteristics of the roof components. As shown in Figure 4.1 a simulated layout model consisting of nodes and elements need to be defined. There are various approaches to identify the nodal points in the model. It is necessary for major node coordination to be defined in the x and y directions for both seam and membrane areas. The distances of the generated nodes are usually equal within the boundaries unless other options are applied. The option of BIAS that concentrates the nodes towards a boundary or reference point and in order to have accurate results in the stress concentrated seam areas, the BIAS parameter is used to concentrate towards fasteners compare to the mid span of the membranes.

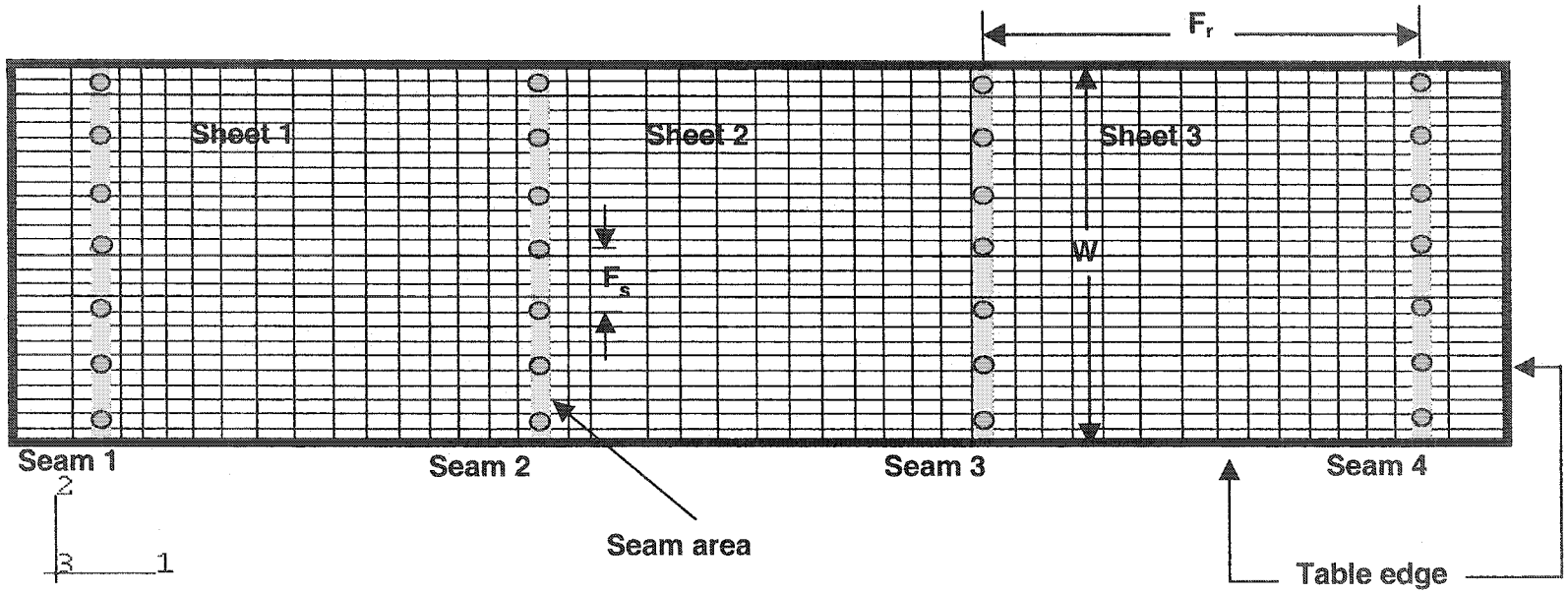

Figure 4.1 Typical roofing system layout for the numerical modeling

To simulate the membrane, a rectangular grid of 4-node and shell elements was used to discretize the elements. Element type S4 accounts for finite membrane strains and will allow for change in thickness. Therefore, it is suitable for large-strain analysis involving materials with a nonzero effective Poisson's ratio. This element fully integrates the finite-membrane-strain shell element. Membrane's response is treated with an assumed strain formulation that gives accurate solutions to in-plane bending problems and not sensitive to element distortion.

Figure 4.2 shows the simulated seam, plates and fastener of the roofing system. Seams details were modeled by doubling the thickness of shell element areas to simulate the overlap region of the membrane. The other material characteristics of the seams remain the same as membranes. SPRING elements were used to simulate fastener attachments with the steel deck. Fasteners were assumed as spring supports with axial stiffness (vertical degree of freedom). The fastener plates were simulated by changing the material properties on the corresponding shell elements.

4.3.2 History Data

The history data is added to input file for simulation of the applied forces on the model. A history data is defined by:

1. Dividing the problem history into steps;
2. Specifying an analysis procedure for each step; and
3. Prescribing loads, boundary conditions, and output requests for each step.

Dividing the problem history into steps: A basic concept in the present numerical approach is the division of the problem history into steps. In other words, a step is any convenient phase of the history or each step is a period of response of a particular type of loading. A general analysis step, whose response can be either linear or nonlinear, was chosen. The starting condition for each general step is the ending condition of the last general step, with the state of the model evolving throughout the history of general analysis steps as it responds to the loading history. The NLGEOM option was selected to include large-displacement effects. Nonlinearities can arise from large-displacement effects, material nonlinearity, and/or boundary nonlinearities such as contact and friction. When this option is chosen, most elements are formulated in the current configuration using current nodal position.

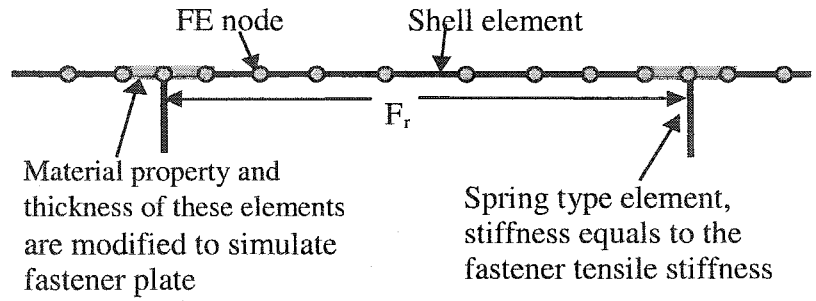

Figure 4.2 Typical seam, fastener and fastener plate details for numerical modeling

Therefore elements can distort from their original shapes as the deformation increases. In other words, the membrane which is flat at the beginning is allowed to balloon during the loading.

Specifying an analysis procedure for each step: The model has several types of analysis procedures to assign for each step. The static stress analysis was chosen for the numerical modeling since a) inertia effects can be neglected; b) the analysis can be liner or nonlinear and c) it ignores time-dependent material effects however it takes rate-dependent plasticity into account.

Prescribing loads, boundary conditions, and output requests for each step: During this step the initial time increment, the time period of the step, minimum and maximum time increment values are assigned. If the user does not provide a suggested initial increment size, the program will attempt to apply all of the loads defined in the step in a single increment. For highly nonlinear problems one can reduce the increment size repeatedly to obtain a solution, resulting in wasted CPU time. It is advantageous to provide a reasonable initial increment size because the loads in a step can be applied in a single increment only if the problem is quasi-nonlinear.

The boundary conditions are also defined in the history data. In the experimental layout, the membrane edges were held by clamps to restrict any movement. In the model, the perimeter edge nodes were simulated so as to have only rotational degree of freedom. The roofing system was subjected to a uniform static uplift pressure up to 4.31 kPa (90 psf). In the last step, the format of the output file was defined. This option allows the user to select the stresses and displacements for specific nodes and elements. The user can also request output results at the end of each step for multi-step analysis.

4.3.3 Analysis Procedure and Output

In the nonlinear analysis the solution cannot be calculated by solving a single system of linear equations, as would be done in a linear problem. Instead, the solution is found by specifying the loading as a function of time and incrementing time to obtain the nonlinear response. Therefore, the present study breaks the simulation into a number of time increments and finds the approximate equilibrium configuration at the end of each time increment. Then, the final solution from the previous load step is used as the initial solution for the next load step.

Newton's method has been used to solve the nonlinear equilibrium equations. Consider the system of n nonlinear equations of the form $f_i(x) = 0$, $(i = 1,\ldots, n)$, where x are the solution

variables. With an initial estimate of the solution $\{x_i\} = \{a_i\}$, the function can be expanded about a in n-space using Taylor's series:

$$f_i(a) + J(a)\,\delta = 0 \tag{4.1}$$

where J is the Jacobian of derivatives evaluated at a.

$$J(x) = \begin{bmatrix} \partial f1/\partial x1 & \partial f2/\partial x2 & \dots & \partial f1/\partial xn \\ \partial f2/\partial x1 & \partial f2/\partial x2 & \dots & \partial f2/\partial xn \\ \vdots & \vdots & \vdots & \vdots \\ \partial fn/\partial x1 & \partial fn/\partial x2 & \dots & \partial fn/\partial xn \end{bmatrix}$$

The solutions to the linear system are the set of deviations $\{\delta i\}$, which are used to calculate the new approximations to the solution variables of the nonlinear system from the initial solutions a_i, using Equation (4.2)

$$x_i = a_i + \delta_i \quad i = 1,\dots, n \tag{4.2}$$

In nonlinear problems the challenge is always to obtain a convergent solution in the least possible computational time. Convergence of the Newton's method is highly dependent on the nonlinearity of the functions and the choice of the initial solution. Thus for small loads, which produce small displacements, convergence is likely. For larger loads the convergence probability may be improved by splitting up the applied loads into incremental load steps, and applying them sequentially. Therefore, the solution usually obtained as a series of increments, with iterations to obtain equilibrium within each increment. Increments must sometimes be kept small (in the sense that rotation and strain increments must be small) to ensure correct modeling of history-dependent effects. Most commonly, the choice of increment size is a matter of computational efficiency: if the increments are too large, more iterations will be required. Furthermore, Newton's method has a finite radius of convergence; too large an increment can prevent any solution from being obtained because the initial state is too far away from the equilibrium state that is being sought—it is outside the radius of convergence. Thus, there is an algorithmic restriction on the increment size.

The selected model automatically adjusts the size of the time increments to solve nonlinear problems efficiently. The number of iterations needed to find a converged solution for a

time increment will vary depending on the degree of nonlinearity in the system. With the default incrementation control, the procedure works as follows. If the solution has not converged within 16 iterations or if the solution appears to diverge, the program abandons the increment and starts again with the increment size set to 25% of its previous value. It then attempts to find a converged solution with this smaller time increment. If the solution still fails to converge, the increment size is further reduced. This process is continued until a solution is found. If the time increment becomes smaller than the minimum defined by the user or more than five attempts are needed, the program stops the analysis.

The executable file for the analysis of the model could be run as a command followed by input filename and the desired options. It's possible to add the command lines on a batch file for more convenience. Various output files are created based on the options set in the input file and are distinguished by different file extensions. The major output file used for discussion has the extension of DAT.

4.4 Evaluation of Thermoplastic Systems

This section focuses on the evaluation of thermoplastic system in which a thermoplastic roofing membrane was used as the waterproof component has been subjected to wind uplift pressure. Both the experimental and numerical investigations are presented. However, the main focus of the present thesis is on the numerical model evaluation. Experimental data for this study was obtained from the Dynamic Roofing Facility (DRF) located at the National Research Council of Canada (IRC/NRC).

4.4.1 Experimental Investigation

4.4.1.1 Experimental Setup

As shown in Figure 4.3, the experimental apparatus consists of a bottom frame of adjustable height upon which the roof specimen and a removable top chamber are installed. The design allows for the installation and study of roof assemblies of different thicknesses up to 500 mm (18") as well as the evaluation of sloped roofs. The bottom frame and top chamber are 6100 mm (240") long and 2200 mm (86") wide and 800 mm (32") high. The top chamber is equipped with six windows for viewing, and with a gust simulator, which consists of a flap valve connected to a stepping motor through a timing belt arrangement. Pressure suction as high as 10 kPa (209 psf) over the roof assembly is produced by a 37 KW (50HP) fan with a flow rate of 2500 L/sec (5300 cfm).

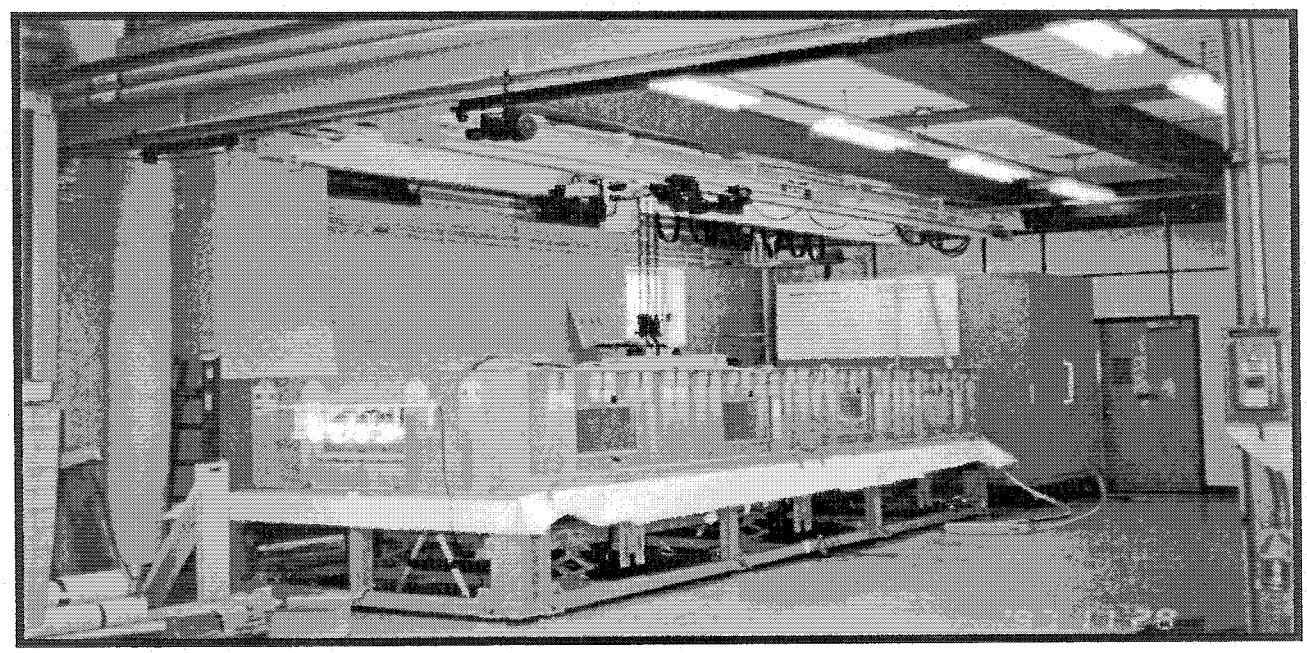

Figure 4.3 SIGDERS Dynamic Roofing Facility (DRF)

A computer, using feedback signals, controls the operation of the DRF. The computer regulates the fan speed in order to maintain the required pressure level in the chamber. Operation of the flap valve simulates the gusts in the form of uniform cyclic pressure loading over the surface of the roofing system. Closing the flap valve allows pressure to build in the chamber, while opening the valve bleeds the pressure. Also, the test facility has instrumentation for measuring the dynamic response for the specimen. More information of the DRF features is given in Baskaran and Lei (1997).

4.4.1.2 System Layout

Figure 4.4 shows a 67/12 mechanically attached thermoplastic system used in the experimental investigation. The first number in the pair represents the fastener row spacing and the second number accounts for the fastener spacing expressed in inches. For this configuration, three thermoplastic membrane sheets having width of 1830 mm (72") were installed on the experimental table and fastened to the structural deck along the four seams. Two different testing protocols, Factory Mutual (FM 4470) static test, and the SIGDERS dynamic load cycle, were used to compare static and dynamic evaluation of a roofing system. Instrumentation was used to monitor the system response (i.e., pressure, force, and deflection). Force balances and ultrasonic sensors were used to measure the tensile forces in the fasteners and uplift movements of the membrane. Applied suctions were also measured by means of a pressure transducer (P1). Signals from all of these instruments were monitored by a computer.

Figure 4.4 also shows the seam details consisting of the 22-Ga steel deck, 0.76 mm (0.03") thick, with a profile height of 38 mm (1.5") and a flute width of 150 mm (5.9") as structural support. Insulation boards as the thermal barrier with dimensions of 100 by 1500 by 3000 mm (4" by 48" by 96") were mechanically attached to the steel deck. Thermoplastic membrane sheets were attached by 127 mm (5") long fasteners with plastic plate 51 mm (2") in diameter to the deck along the seam. The seam had an overlap of 127 mm (5") with the fastener placed 38 mm (1.5") from the edge of the bottom sheets, and 89 mm (3.5") from the edge of the overlapping sheets. The portion of the seam beyond the fastener row was welded with hot air such that a waterproof top surface was obtained. The width of the welded portion varied between 38 and 45 mm (1.5" and 1.75").

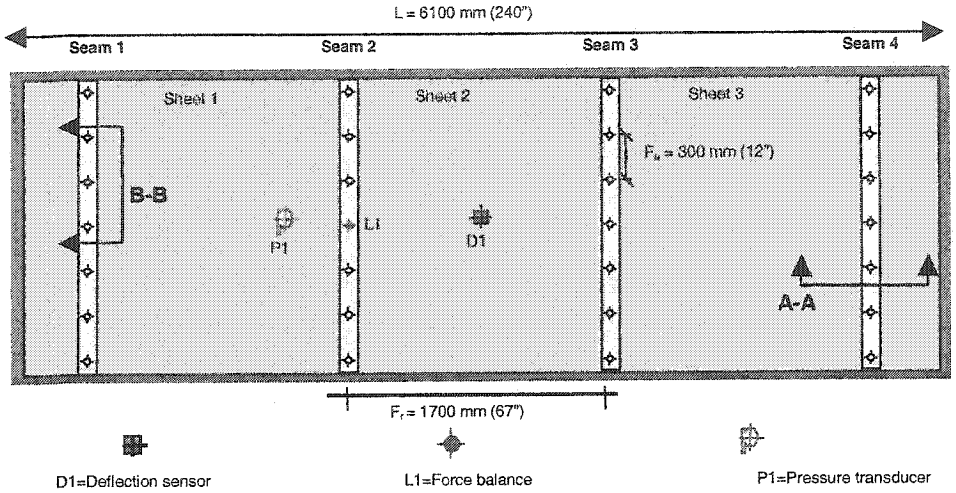

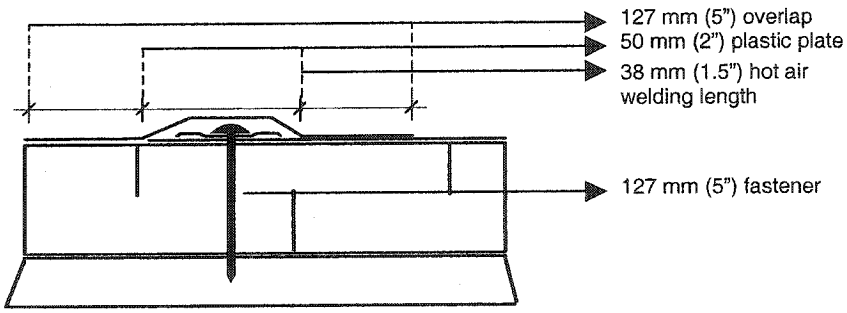

Section A-A

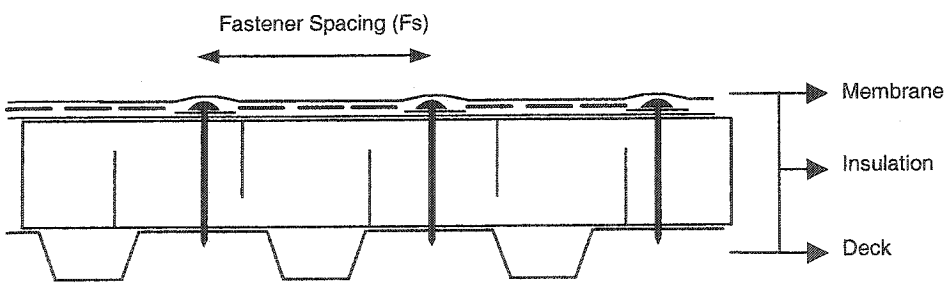

Section B-B

Figure 4.4 67/12 thermoplastic system configuration and seam details

4.4.1.3 System Response

Figure 4.5 shows the time histories for the measured pressure, fastener forces and membrane deflections. The test conforms to the FM-4470 standard requirements for load sequences. At first, a pressure level of 1.44 kPa (30 psf) was applied and maintained for 60 seconds prior to increasing to the next pressure of 2.15 kPa (45 psf). The pressure increased in each level until failure occurred. The specimen sustained the applied pressure level of 3.59 kPa (75 psf) and failed at the pressure close to 4.31 kPa (90 psf). The measured fastener force and membrane deflection at 3.59 kPa (75 psf) were 1187 N (267 lbf) and 217 mm (8.5") respectively.

A similar system configuration was also investigated by subjecting it to the SIGDERS dynamic load sequence. The dynamic pressure level starts at 0.86 kPa (18 psf) for 400 gust cycle and takes 45 minutes prior to reaching to next level. The system sustained a maximum pressure of 3.4 kPa (70) psf and passed all eight steps of the SIGDERS test (ref. to Figure 3.6). The time histories for the measured pressure, fastener forces and membrane deflections are shown in Figure 4.6. The specimen sustained the applied pressure level of 3.40 kPa (71 psf). The measured fastener force and membrane deflection were 1133 N (255 lbf) and 211 mm (8.3") respectively.

For benchmarking the numerical model two additional thermoplastic system configurations (48/18 and 72/18) were selected. The roof system configurations were evaluated using both the FM and SIGDERS dynamic load sequences to measure the maximum fastener force and membrane deflection. The data derived from the time histories response measurements are tabulated in Table 4.1.

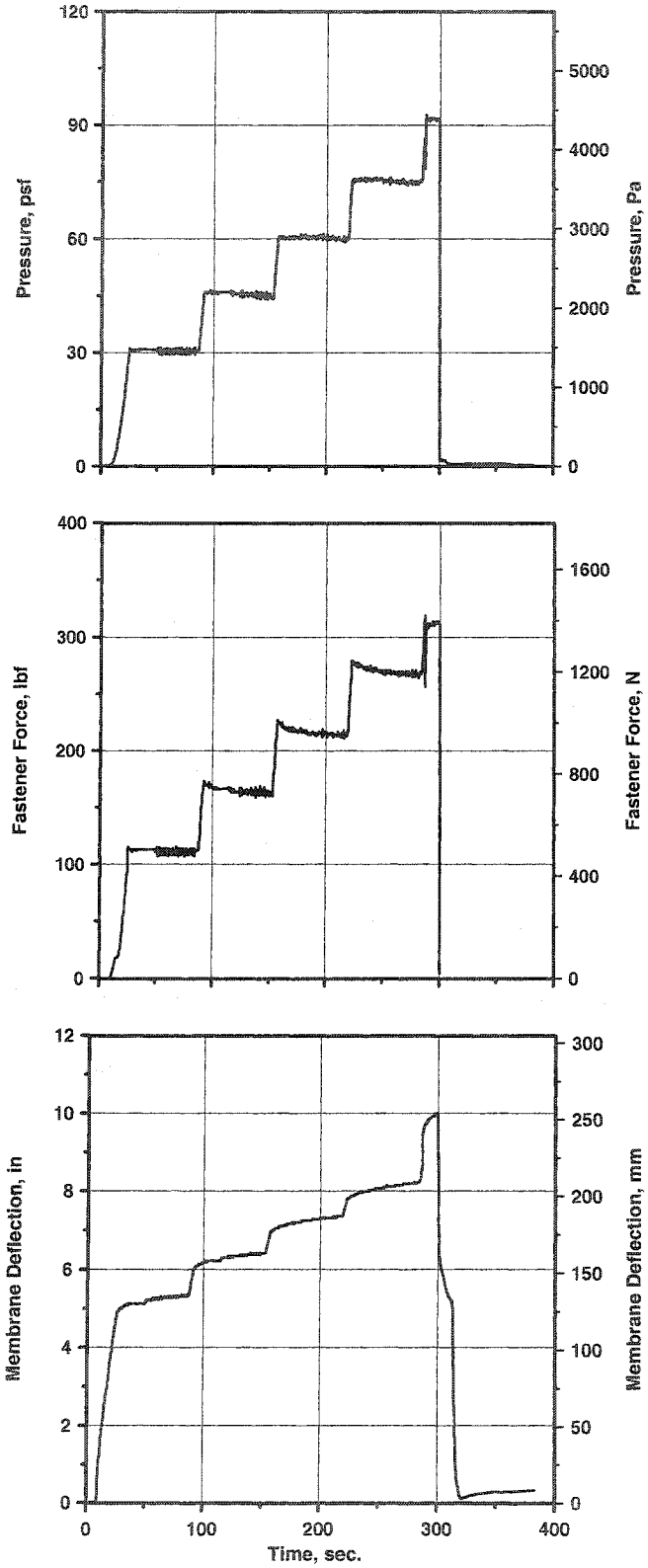

Figure 4.5 Response of the 67/12 thermoplastic system configuration during FM test

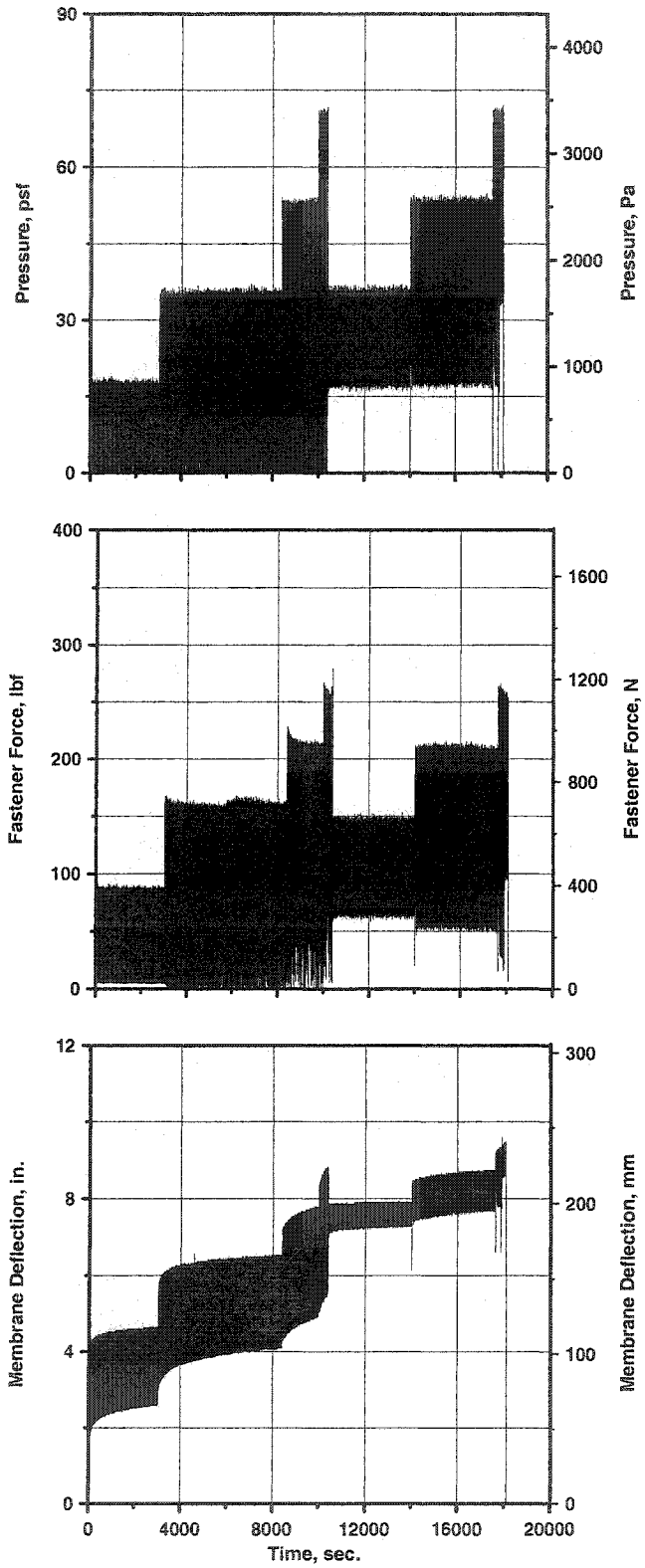

Figure 4.6 Response of the 67/12 thermoplastic system configuration during SIGDERS test

Table 4.1 Experimentally measured pressure, fastener load, and membrane deflection for thermoplastic systems

Configuration type	Wind Load cycle	Pressure kPa (psf)	Fastener force N (lbf)	Membrane Deflection mm (in)
48/18	FM	1.44 (30)	769 (173)	110 (4.3)
		2.15 (45)	1071 (241)	135 (5.3)
		2.87 (60)	1382 (311)	155 (6.1)
		3.59 (75)	1667 (375)	200 (7.9)
	SIGDERS	0.91 (19)	444 (100)	95 (3.7)
		1.82 (38)	844 (190)	125 (4.9)
		2.73 (57)	1133 (255)	155 (6.1)
67/12	FM	1.44 (30)	516 (116)	136 (5.4)
		2.15 (45)	764 (172)	170 (6.7)
		2.87 (60)	1004 (226)	198 (7.8)
		3.59 (75)	1187 (267)	217 (8.5)
		4.31 (90)	1347 (303)	228 (9.0)
	SIGDERS	0.86 (18)	369 (83)	120 (4.7)
		1.72 (36)	707 (159)	160 (6.3)
		2.59 (54)	951 (214)	190 (7.5)
		3.40 (71)	1133 (255)	211 (8.3)
72/18	FM	1.44 (30)	591 (133)	140 (5.5)
		2.15 (45)	867 (195)	170 (6.7)
		2.87 (60)	1178 (265)	195 (7.7)
		3.59 (75)	1378 (310)	233 (9.2)
	SIGDERS	0.72 (15)	333 (75)	55 (2.2)
		1.44 (30)	644 (145)	130 (5.1)
		2.15 (45)	844 (190)	155 (6.1)
		2.87 (60)	1000 (225)	175 (6.9)

4.4.2 Numerical Investigation

4.4.2.1 Development of Input File

As explained in the Section 4.3, the input file consists of model and history data which represent the simulated configuration. Three different input files are created for the simulation of 48/18, 67/12 and 72/18 configurations. Nodes coordinate and element sizes are generated accurately to simulate, the testing table, membrane size, seam area and fastener locations. Then, the material characteristics are defined in the input file. Table 4.2 shows the thermoplastic system components characteristics used for the numerical models. The membrane and seam dimension varies since the generated element meshes are not the same size in the models. The smaller element sizes are considered in the stress concentrated seam areas. Fixed bar type elements are used to simulate fastener attachments with the steel deck. Fasteners are assumed as spring supports with axial stiffness of 20 N/mm (114 kip/in). The stiffness rate is the result of dividing the fastener force value by the fastener displacement value.

Table 4.2 Material characteristics used for the modeling of thermoplastic system

	Thickness mm	**Modulus of Elasticity Mpa**	**Poisson ratio**
Thermoplastic membrane	1.04	300	0.4
Seams	2.08	300	0.4
Plate	3 - Diameter (50)	500	0.4

The input files include the history data applied to the simulated models. The models have a uniform static uplift pressure up to 4.31 kPa (90 psf) on the membrane. The load is defined as a function of time in order to obtain nonlinear system response. The initial pressure starts at 0.00001 of maximum one and the model automatically adjust the size of time increment when the load increases from one step to other. At the end of the input file preparation, the output file format is defined. This option allows the user to obtain the stress and displacement for specific nodes and elements. The user can also obtain the output results by the end of each step if the analysis takes more than one step. A typical input file used for 67/12 thermoplastic system configuration is included in Appendix B.

4.4.2.2 Predicted System Response

A typical computer generated depiction of a deflected membrane is shown in Figure 4.7. It shows the membrane ballooning occurring between fastener rows and table edges. A full model of the configuration is also shown to reveal the existence of symmetry. This modelled 67/12 configuration has a maximum deflection of 117 mm (4.6") at the middle of the membrane for the wind uplift pressure of 1.44 kPa (30 psf).

Figure 4.8 shows the computed fastener forces for the 67/12 configuration. The results show that the fastener forces increase along the seams (for the location of the seams refer to Figure 4.4) when the fasteners are away from the edges. For the 1.44 kPa (30 psf) pressure the seam two, has the maximum fastener force of 533 N (120 lbf), while the minimum fastener force for the same seam is 80 N (18 lbf). Also, the fastener forces in the seam two are higher compare to the seam one. These changes reveal the edge effect on the fastener force. This will be further discussed in Chapter 5.

4.5 Evaluation of Thermoset Systems

4.5.1 Experimental Investigation

4.5.1.1 System Layout

Figure 4.9 shows a 78/12 mechanically attached thermoset system used in the experimental investigation. The first number in the pair represents the fastener row spacing and the second number accounts for the fastener spacing expressed in inches. For this configuration, three thermoset membrane sheets having width of 2130 mm (84") were installed on the experimental table and fastened to the structural deck along the three seams. Two different testing protocols, Factory Mutual (FM 4470) static test, and the SIGDERS dynamic load cycle, were used to compare static and dynamic evaluation of a roofing system. Instrumentation was used to monitor the system response (i.e., pressure, force, and deflection). Force balances and ultrasonic sensors were used to measure the tensile forces in the fasteners and uplift movements of the membrane. Applied suctions were also measured by means of a pressure transducer (P1). Signals from all of these instruments were monitored by a computer.

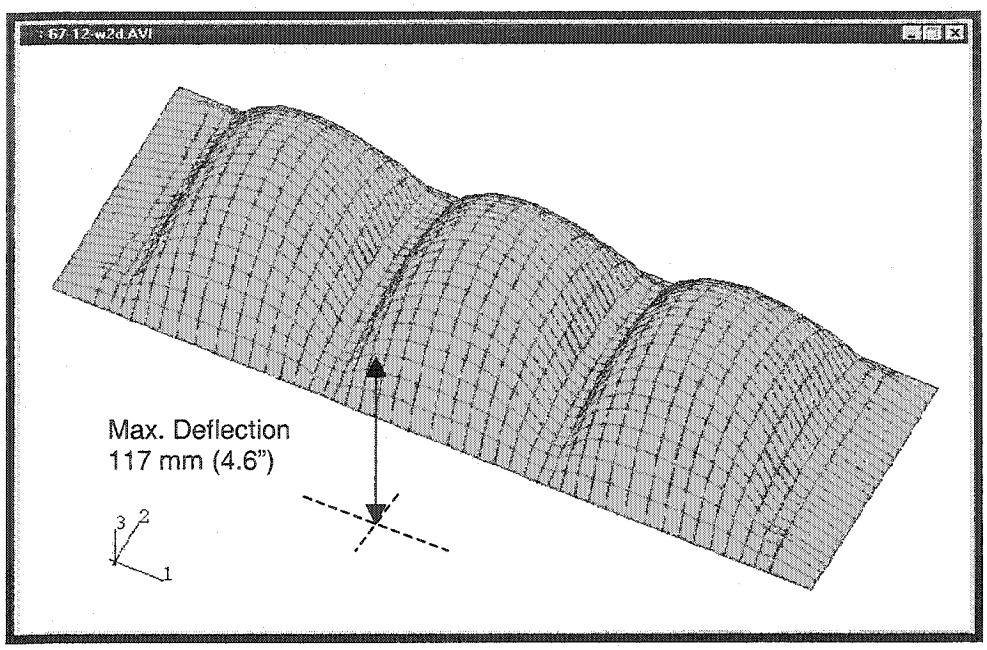

Figure 4.7 Computed membrane deflected shape for the 67/12 configuration

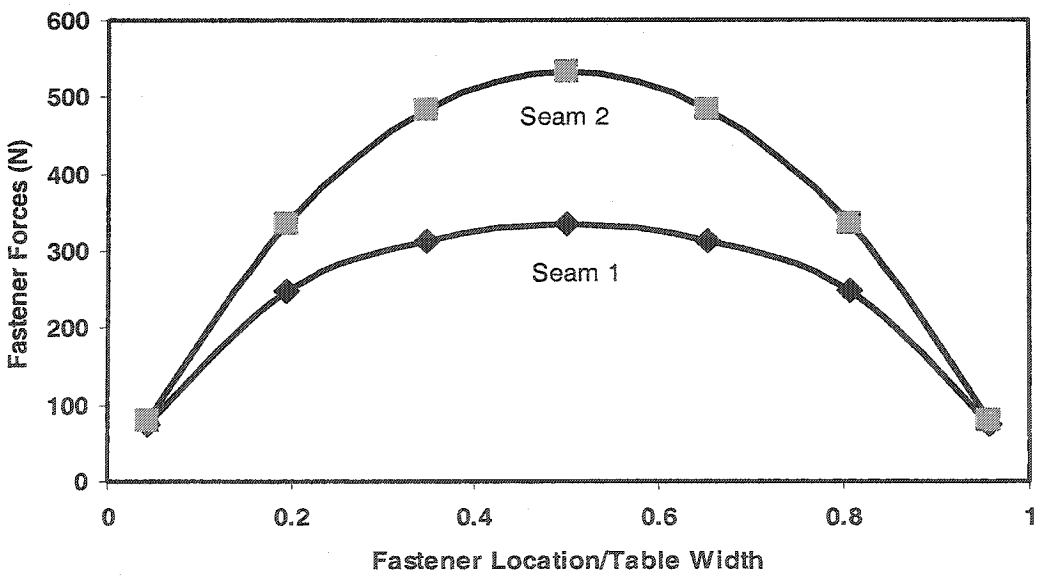

Figure 4.8 Variation of computed fastener forces for 67/12 configuration

Figure 4.9 shows the seam details consisting of the 22-Ga steel deck, 0.76 mm (0.03") thick, with a profile height of 38 mm (1.5") and a flute width of 150 mm (5.9") as structural support. Insulation boards as the thermal barrier with dimensions of 100 by 1500 by 3000 mm (4" by 48" by 96") were mechanically attached to the steel deck. Thermoset membrane sheets were attached by 127 mm (5") long fasteners with metal plate 51 mm (2") in diameter to the deck along the seam. The seam had an overlap of 152 mm (6") with the fastener placed at the centre of the seam area leaving 51 mm (2") on both sides. The top and bottom membranes are fully bonded together in seam area by liquid adhesive.

4.5.1.2 System Response

Table 4.3 shows the data derived from the time histories response for the measured pressure, fastener forces and membrane deflections. The test conforms to the FM-4470 standard requirements for load sequences. At first, a pressure level of 1.44 kPa (30 psf) was applied and maintained for 60 seconds prior to increasing to the next pressure of 2.15 kPa (45 psf). The pressure increased in each level until failure occurred. The specimen sustained the applied pressure level of 3.59 kPa (75 psf) and failed at the pressure close to 4.31 kPa (90 psf). The measured fastener force and membrane deflection at 3.59 kPa (75 psf) were 1624 N (365 lbf) and 234 mm (9.2") respectively.

A similar system configuration was also investigated by subjecting it to the SIGDERS dynamic load sequence. The dynamic pressure level starts at 0.91 kPa (19 psf) for 400 gust cycle and takes 45 minutes prior to reaches to next level. The system sustained a maximum pressure of 1.77 kPa (37) psf and failed at the pressure close to 2.59 kPa (54 psf). The measured fastener force and membrane deflection at 1.77 kPa (37) psf were 1133 N (255 lbf) and 211 mm (8.3") respectively.

For benchmarking the numerical model one additional thermoset system configuration 78/6 was selected. The roof system configuration was evaluated using the FM load sequences to measure the maximum fastener force and membrane deflection. The data derived from the time histories response measurements are tabulated in Table 4.3.

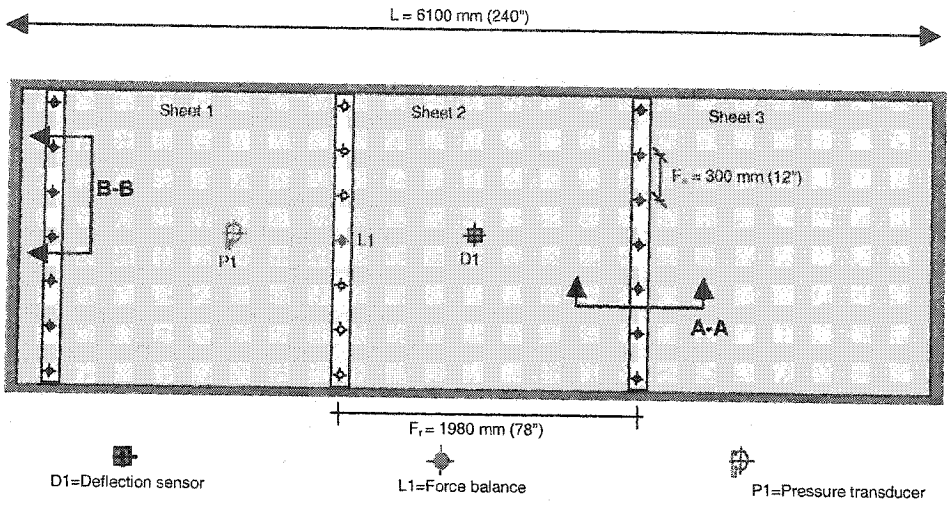

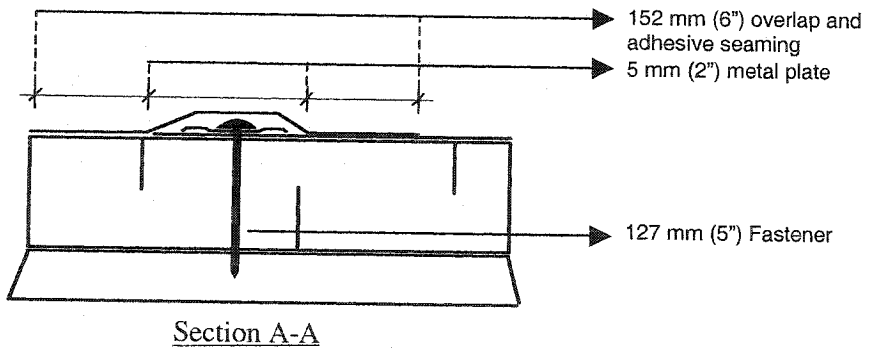

Section A-A

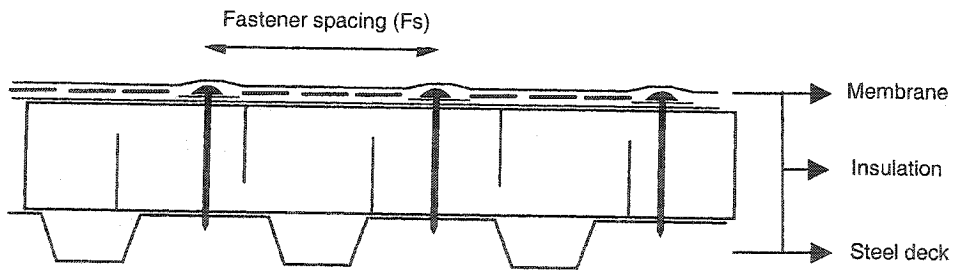

Section B-B

Figure 4.9 78/12 thermoset system configuration and seam details

Table 4.3 Experimentally measured pressure, fastener load, and membrane deflection for thermoset systems

System Configuration	Wind Load Cycle	Pressure kPa (psf)	Fastener Force N (lbf)	Membrane Deflection mm (in)
78/6	FM	1.44 (30)	423 (95)	140 (5.5)
		2.15 (45)	667 (150)	165 (6.5)
		2.87 (60)	823 (185)	191 (7.5)
		4.31 (90)	1001 (225)	244 (9.6)
		5.03 (105)	1246 (280)	267 (10.5)
78/12	FM	1.44 (30)	845 (190)	152 (6)
		2.15 (45)	979 (220)	180 (7.1)
		2.87 (60)	1268 (285)	206 (8.1)
		3.59 (75)	1624 (365)	234 (9.2)
		4.31 (90)	1890 (425)	259 (10.2)
	SIGDERS	0.91 (19)	480 (108)	127 (5)
		1.77 (37)	907 (204)	160 (6.3)
		2.59 (54)	1085 (244)	188 (7.4)
78/12*	FM	1.44(30)	885 (199)	178 (7)
		2.15 (45)	1112 (250)	211 (8.3)
		2.87 (60)	1467 (330)	236 (9.3)
		3.59 (75)	1757 (395)	264 (10.4)

* *Repeated test*

4.5.2 Numerical Investigation

As discussed in the Chapter three, thermoset membranes are widely used in single-ply roofing systems. Thermoset membrane tensile properties are significantly different from thermoplastic membranes which warrant modification in the developed model. Figure 4.10 shows the stress-strain relation for thermoplastic and thermoset membranes based on a tensile testing of the membranes in accordance to the ASTM D 751-98. A minimum of five tensile tests is needed for each membrane type. The specimens were cut using a die with a width of 25.4 mm (1") and length of 152.4 mm (6") and tested using an Instron 4502 Automated Materials Testing System, with a pneumatic grip. A 1000 N (225 lbf) load cell was used for the testing in the machine direction. The specimens were pulled at a cross-head speed of 300 mm/min (11.8 in./min), a sampling rate of 10 pt./sec, and a gauge length of 101.6 mm (4"). The results of testing are converted to the stresses and strains shown in Figure 4.5.

4.5.2.1 Development of Input File

Two input files were created to simulate the configurations of 78/6 and 78/12. The data represents the experimental table layouts, the system characteristics and the applied load. The nodes and elements are defined to model the table, membrane, fasteners, seams and plates locations. The shell element for the thermoset membrane have a thickness of 1.1 mm (0.04"), an equivalent modulus of 150 MPa (21.8 ksi) and a Poisson Ratio of 0.22.

The seam areas are modeled by doubling the thickness of the shell elements. Therefore, the seam area properties remain the same as those of the shell element except for the thickness change to 2.2 mm (0.09"). Fasteners are modeled as spring supports with an axial stiffness of 60 N/mm (342 kip/in). The fastener plates are simulated by changing the material properties on the corresponding shell elements. The fastener plate diameter was 50 mm (2") in and 2 mm (0.08") thick with the equivalent modulus of elasticity and Poisson ratio were 200,000 MPa (29,008 ksi) and 0.2 respectively. A typical input file for a 78/6 thermoset system is presented in Appendix C.

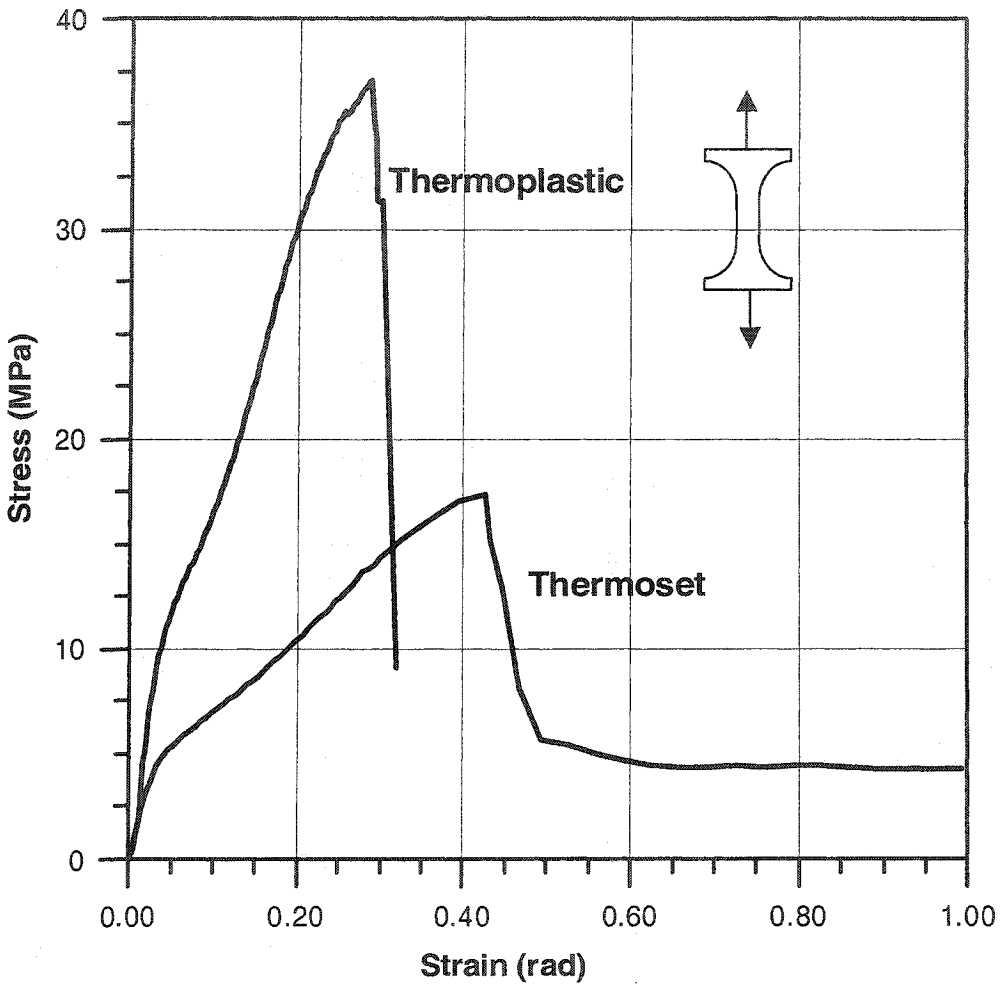

Figure 4.10 Comparison of the tensile strength for thermoplastic and thermoset membranes

4.5.2.2 Predicted System Response

Figure 4.11 shows the typical membrane deflection for the 78/12 configuration in which the membrane ballooning occurs between fastener rows and table edges. The maximum membrane displacement happens in the mid span of the layout. For the sustained uplift pressure of 4.31 kPa (90 psf) the deflection was 242 mm (9.5"). Computed fastener forces and deflections are presented in the next section.

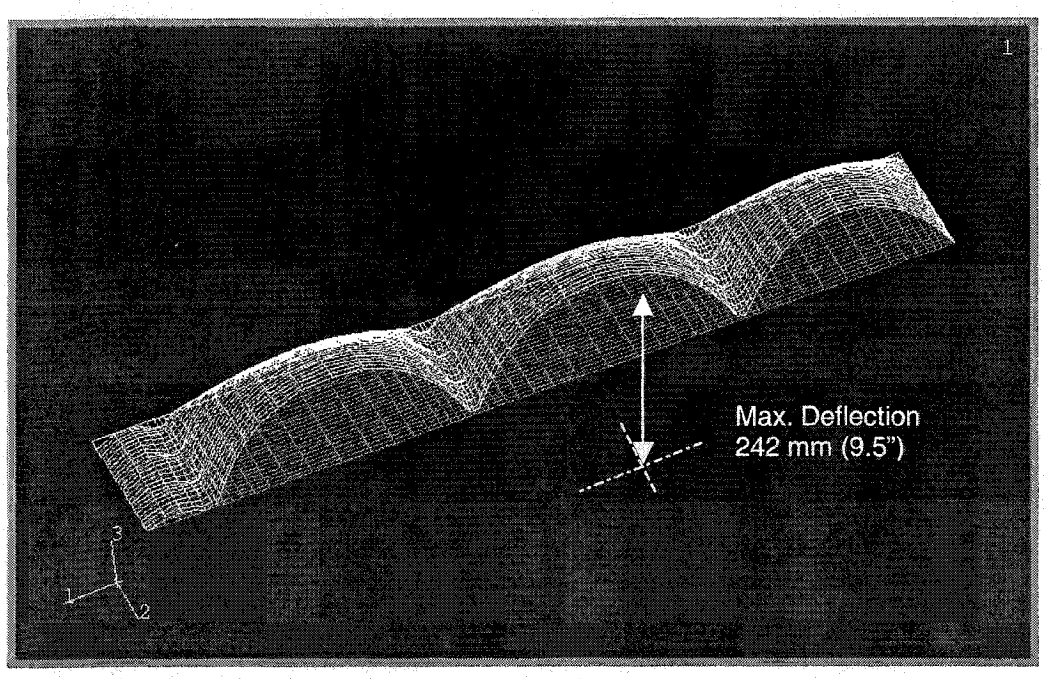

Figure 4.11 Computed membrane deflected shape for the 78/12 configuration

4.6 Validation of the Developed Model

Experimental data (refer Table 4.1 and 4.3) obtained from the Dynamic Roof Facility (DRF) were used to benchmark the developed model for the thermoplastic and thermoset systems. It is worth to note that the numerical model has been developed to predict the performance rather to simulate the failure mode or ultimate strength of the experimental roofing systems.

The average values of two characteristic parameters - fastener loads and membrane deflections measured from the DRF experiments - were compared with the output of the numerical model. The fastener force measured at the centre location L1 on the seam and deflection at the mid-span location D1 of the membrane, as indicated in experimental layout (refer to Figure 4.4 and 4.9), are selected. Although both membrane deflections and fastener forces are used to validate the numerical model, only fastener forces are used for the design purpose of roofing system and it will be further discussed in the next chapter.

4.6.1 Validation for Thermoplastic Systems

Comparisons of fastener forces between the experimental and numerical modeling for thermoplastic systems are shown in Figure 4.12. The horizontal axis represents the applied suctions on the roof assembly and the vertical axis represents the fastener forces of the roofing systems response for the applied pressure. In the experiments, depending on the test protocols (Factory Mutual or SIGDERS) the required pressures are applied and maintained for a specific duration. The following expression was used to establish deviations between the two data sets (Experiments versus Numerical Model):

$$\Delta F = \sum_{i=1}^{N} \left(\frac{F_{NM} - F_{EXP}}{F_{EXP}} \right) \times 100 \qquad (4.3)$$

where: F_{NM} is the fastener force obtained from the numerical model,

F_{EXP} is the fastener force measured from the experimental evaluation,

N is the number of cases (pressure levels) considered for each configuration, and

ΔF is the fastener force deviation between F_{NM}, and F_{EXP}. ΔF with a negative sign (-) means that the model underestimates the roofing system response compared to the experimental approach and vice versa.

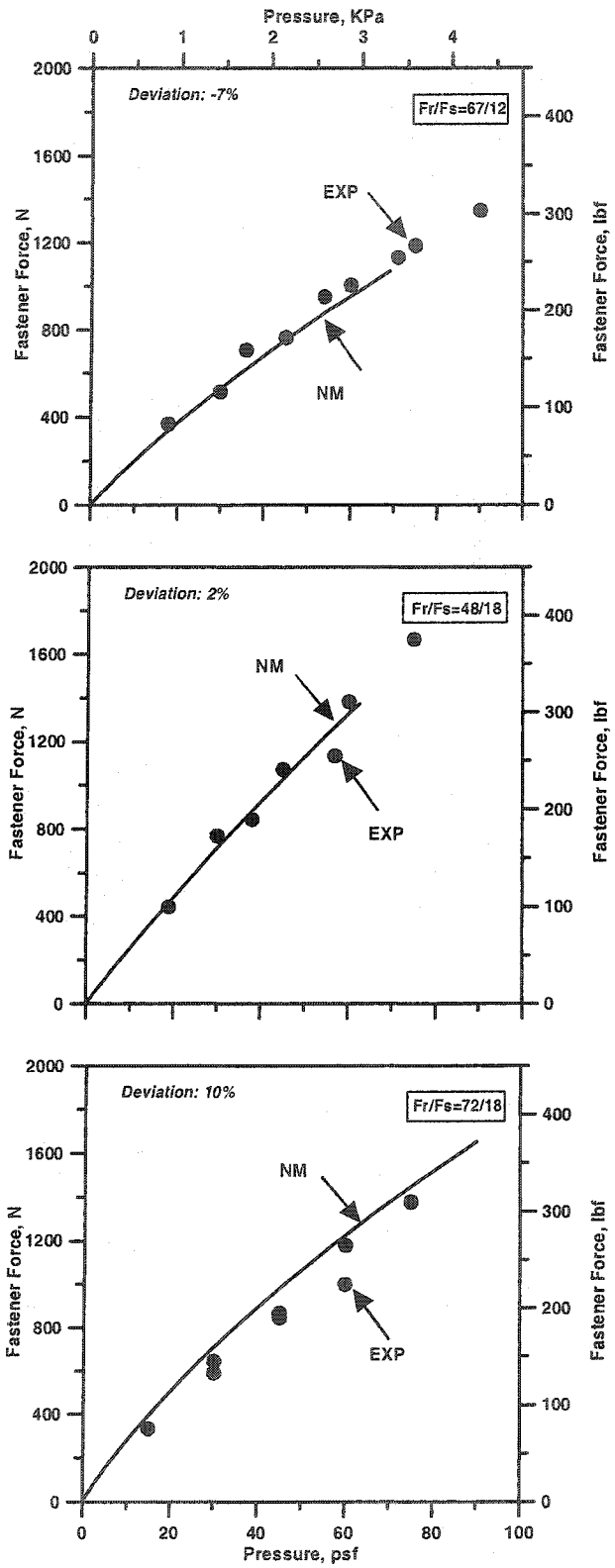

Figure 4.12 Model validation for thermoplastic system - fastener force

Using Equation (4.3), for the case of F_r/F_s = 67/12, an under-estimation of 7% by the numerical model was found. Similar comparisons for the 48/18 and 72/18 configurations respectively revealed 2% and 10% deviations (over-estimations) of the numerical model from the measured fastener loads. These comparisons demonstrated that the numerical model is a viable tool that can be used to predict the fastener forces of test specimens at any uniform static pressure level.

Figure 4.13 presents the model validation for the prediction of the membrane deflection. Using deflection instead of forces in the equation (4.3), deviations for the 67/12, 48/18 and 72/18 configurations are 18%, 19% and 7% respectively. Irrespective of the roofing system configurations, the membrane deflections are always underestimated by the numerical model. One of the reasons for the difference between these results is owing to difference in the edge conditions of the model. In the numerical model, all four edges are restrained from any movements, whereas membrane slippage from the edges of the test frame may happen during the lab experiments. Therefore, the measured deflection in the lab is the summation of the true membrane uplift and membrane slippage whereas the model computes only membrane uplift.

Table 4.4 shows the average deviations for the fastener force and membrane deflection. The average results reveal the finite element model is a viable tool that can be used to predict the fastener forces and membrane deflections of thermoplastic test specimens at any pressure level.

Table 4.4 Model validation for thermoplastic systems

	67/12	**48/18**	**72/18**	**Average**
Force Deviation	-7%	2%	10%	1.7%
Deflection Deviation	-18%	-19%	-7%	-14.7

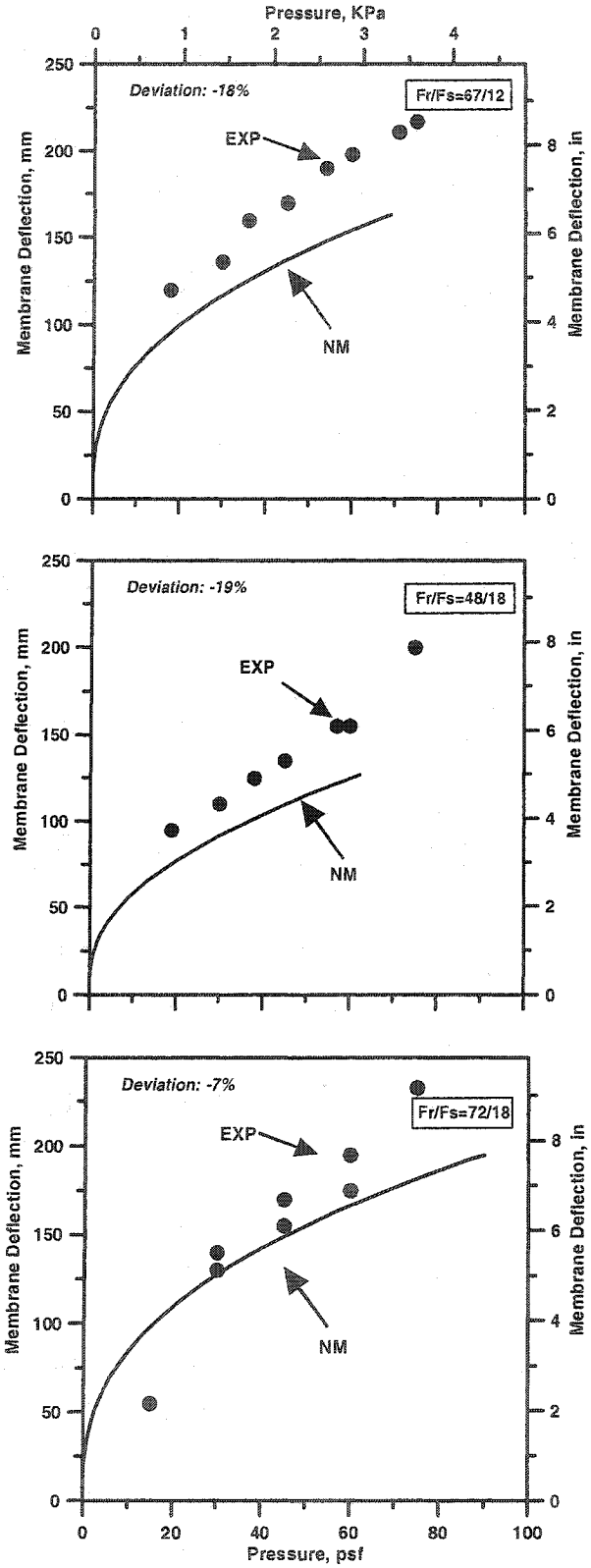

Figure 4.13 Model validation for thermoplastic system - membrane deflection

4.6.2 Validation for Thermoset Systems

Comparisons of fastener forces between the experimental and numerical modeling for thermoset systems are shown in Figure 4.14. The horizontal axis represents the applied suctions on the roof assembly and the vertical axis represents the fastener forces of the roofing systems response for the applied pressure. In the experiments, depending on the test protocols (Factory Mutual or SIGDERS) the required pressures are applied and maintained for a specific duration.

Using Equation (4.3), for the case of F_f/F_s = 78/12, an under-estimation of 3.5% by the numerical model was found. Similar comparisons for the 78/12 configuration revealed 5% deviations (under-estimations) of the numerical model from the measured fastener loads. These comparisons demonstrated that the numerical model is a viable tool that can be used to predict the fastener forces of test specimens at any uniform static pressure level.

Figure 4.15 presents the model validation for the prediction of the membrane deflection. Using deflection instead of forces in the equation (4.3), deviations for the 78/6 and 78/12 configurations are 2.5% and -4.5% respectively.

Table 4.4 shows the average deviations for the fastener force and membrane deflection. The average results reveals the finite element model is a viable tool that can be used to predict the fastener forces and membrane deflections of thermoset test specimens at any pressure level.

Table 4.5 Model validation for Thermoset systems

	78/6	**78/12**	**Average**
Force Deviation	-5%	-3.5%	-4.3%
Deflection Deviation	2.5%	-4.5%	-1.0%

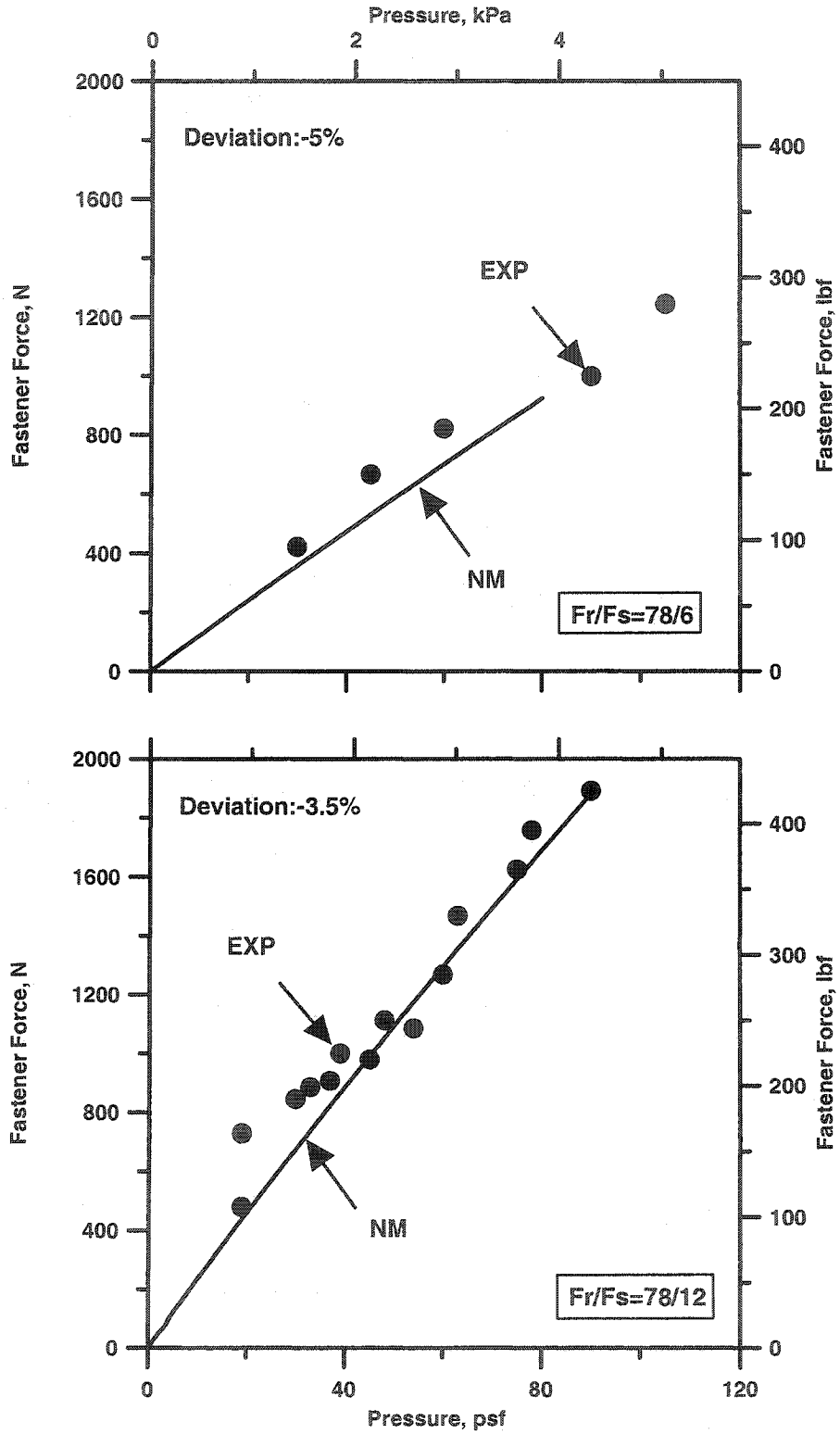

Figure 4.14 Model validation for thermoset system - fastener force

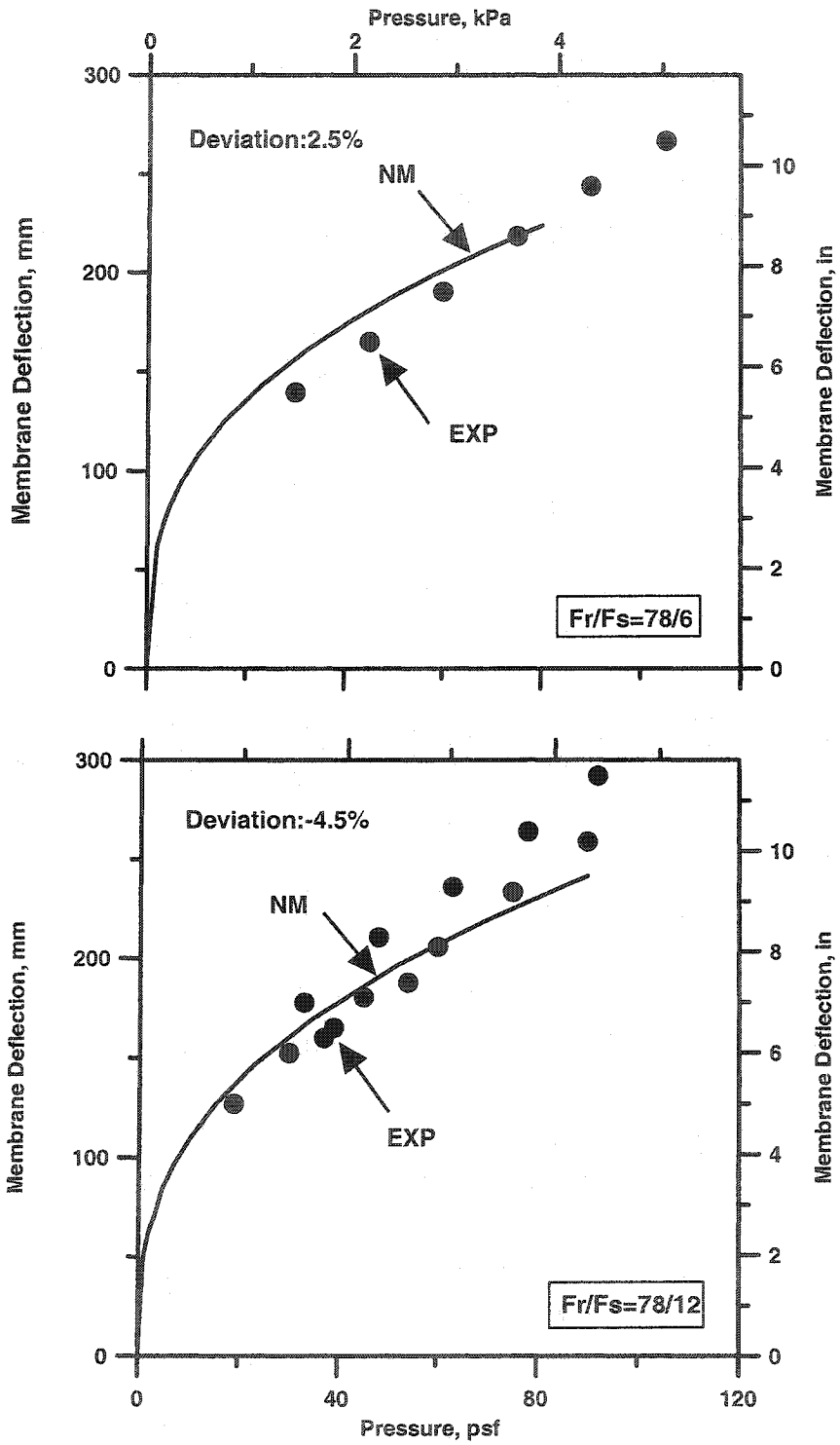

Figure 4.15 Model validation for thermoset system - membrane deflection

5 Application of the Developed Numerical Model

5.1 General

Currently, the membranes available in the market have the widths of up to 3660 mm (144"). The wider membranes provide savings installation cost by reducing the number of overlaps to be seamed in the field. Wider membranes also reduce fasteners and plates for attachment, fewer rolls for the roofing applicator to handle on the roof, and less membrane being utilized in the seam overlaps.

Field performance of systems with wider membrane remains questionable, as they have yet to be experience an extreme wind event such as hurricane. With wider membranes wind uplift resistance design of roofs is more challenging. Compare to the past wider membrane or longer fastener row spacing increase the influence area over the fasteners and induces higher loads. Care should be taken for the deck attachment so that it can accommodate the increased wind uplift within the existing span. Therefore, the current test apparatus may not mimic field behavior while the table sizes are not wide enough for the wind uplift performance evaluation. One approach is to apply appropriate correction factor on the roofing system response that are tested on a narrow table.This chapter presents the development of correction factors using the validated numerical model. The steps for the study are as follows:

- Review the sizes of the existing tables
- Investigate the effect of table size on the roofing system response
- Develop correction factors for both thermoplastic and thermoset systems
- Develop generalized correction factor

5.1.1 Review of the Existing Testing Table Size

The research shows that testing table size can significantly influence the wind uplift resistance used for the certification process. It is important to select an appropriate test table size. For example, the use of narrow tables would increase the edge effects on the system response particularly for roofing systems having wider membranes. In other words, boundary effects can reduce the fasteners load transferred from membrane during a test. On the other hand, use of wide tables may not be economical for routine testing procedures. If the testing table sizes are sufficient, then the roofing system response remains constant or minimum changes may occur.

Table 5.1 Table sizes used for the certification of roofing systems

No.	Test Protocol	Table Size, mm (in)	Country	Reference
1	FM 4470 Standard	2700×1500 (108"×60")	U.S.A.	FM research 1986
2	Revised FM 4470	7300×3800 (288"×144")	U.S.A.	FM Research 1992
3	UL 580 Standard	3000×3000 (120"×120")	U.S.A.	UL Inc. 1991
4	UEAtc Standard	6100×1500 (240"×60")	Europe	Gerhardt and Karmer 1986
5	BRERWULF	5000×5000 (196"×196")	UK	Cook et al 1988
6	NT Build 307 Standard	2400×2400 (96"×96")	Norway	Paulsen 1989
7	SIGDERS	6100×2200 (240"×86")	North America	Baskaran and Lei 1997

As shown in Table 5.1, existing test methods use different table sizes for the certification of roofing systems. For instance, the Factory Mutual (1986) test uses a table size of 1500 by 2700 mm (60" by 108"') or 3700 by 7300 mm (144" by 288") depending on the roofing system. A chamber size of 3000 by 3000 mm (120" by 120") is used by the Underwriters Laboratories (1991) standard and SIGDERS (1997) uses a table size of 2200 by 6100 mm (86" by 240"). None of these test procedures uses correction factors.

UEAtc (1986) is the only test protocol that specified a correction factor for evaluation of roofing systems under wind pressure. Since the table width is rather narrow, the calculated failure load is not necessarily equal to the actual fastener load. In this protocol, the fastener load is determined by multiplication of the area of influence by the applied pressure load. The area of influence, which is called the tributary area, is determined by multiplication of fastener spacing and fastener row spacing.

To obtain the corrected load (W_{corr}), the calculated fastener load is reduced by two factors C_a and C_d using the equation:

$$W_{corr} = W_{test} \times C_d \times Ca \tag{5.1}$$

where W_{test} = calculated fastener load

C_d = statistical factor considers the probability of one fastener failure, when the number of fasteners decreases

C_a = geometric factor which depends on the variation of the fastener row spacing, "a", the fastener spacing, "b", and the table width, "m" as shown in Figure 5.2.

The proposed geometric factor is only applicable to the UEAtc test protocol and should be verified for other table tests that make use of it. In addition, the effect of membrane type is not accounted in the calculation of the correction factor.

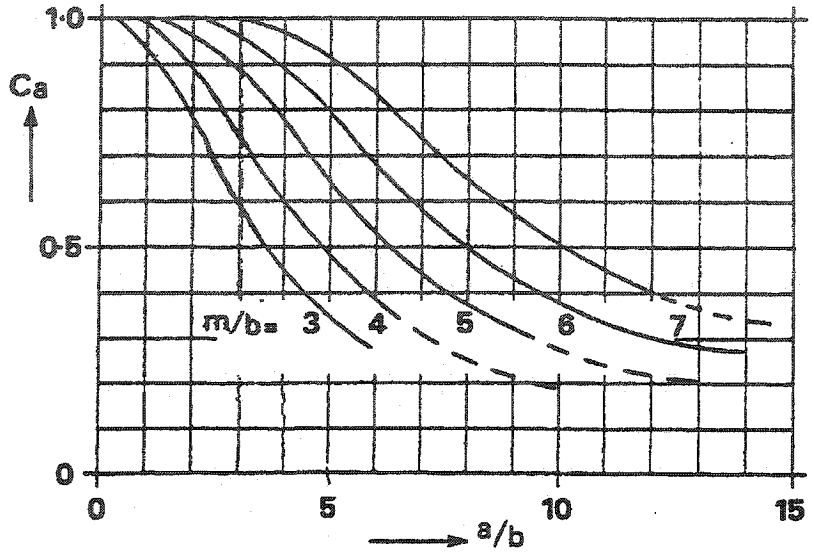

Figure 5.1 Geometric factor from the UEAtc test procedure (Gerhardt et al 1986)

Smith (1989) compared the failure pressures obtained from FM (2700 × 1500 mm) with data obtained from the FM table size of 7300 × 3800 mm. The results showed that the failure pressure with the 7300 × 3800 mm was consistently 2.16 kPa (45 psf) lower than that with the 2700 × 1500 mm table.

David et al (1998) measured the failure pressure and failure fastener force for six different table sizes to determine whether a minimum table size could be identified. The study focused on thermoset systems and reveals the following recommendations:

- A 2.4 × 2.4 m (96" × 96") table appears to be sufficient for providing reasonable accurate results to allow the calculated fastener load based on the assumed tributary area times the system failure pressure
- The minimum table width should be at least 1.5 times the fastener row spacing (aspect ratio greater than 1.5)
- If a table has an aspect ratio less than 1.5, a correction factor needs to be developed to convert the calculated fastener load to actual fastener load.

5.2 Investigating Table Size Effect

5.2.1 Ideal Table Size

An ideal table size is one that provides accurate results and is modestly sized such that test preparation can be easier. All three dimensions (length, width and depth) define the table size. However, all the components used in the lab experiments are similar to those used in the field. In other words, there is no variation in the thickness of components such as the insulation and membrane. For this reason, the depth does not affect the system response as table length or width does.

The table length effect was investigated using validated finite element numerical models. A SIGDERS roofing table with the configuration of 48/12 and static pressure of 1.44 kPa (30 psf) was selected. Then the table length was increased by increments of 300 mm (12") while all other parameters were kept constant. The maximum table length for this exercise was 7300 mm (288"), which is the maximum available table length used by the Factory Mutual testing. The results of the three fastener forces on the middle seams are shown in Figure 5.2. As shown, the difference of fastener forces in each configuration is less than 1.0%. This confirms that table length does not significantly influence the system response. This is mainly because during the system installation, membrane width forms parallel to the table width. This means the effect of the table length is negligible as long as the table length remains at least three times the table width.

To investigate the table width effect, two existing tables (SIGDERS and UEAtc) were selected from Table 5.1. Both tables had the same length of 6100 mm (240") and had difference in widths, 2200 mm (86") for the SIGDERS versus 1500 mm (60") for the UEAtc. A static pressure of 1.44 kPa (30 psf) was applied to a roof system with a 48/6 configuration. The resulting fastener force variations along a seam are presented in Figure 5.3 with respect to the normalised table width. The numerical model computed maximum fastener force at the middle of the seam and minimum at the end of the seam. This reveals the edge influence on the fastener forces as the slope of the curve shows a diminishing edge effect on the fastener forces from the edge to the middle. An ideal condition is one where edge effects are minimal and most of the fasteners have equal forces since they are subjected to the same magnitude of wind uplift pressure. However, during the laboratory experiments, the edge will always offer some resistance. In the case of the SIGDERS' table which is 2200 mm (86") wide, three fasteners at the centre (mid-width) will have equal or similar forces to confirm they are not influenced by the edges. Results showed a variation of about two percent between the centre fastener and the adjacent ones. This confirms that the edge influence is negligible. Moreover, decreasing the table width to 1500 mm (60") decreases the overall magnitude of the fastener force.

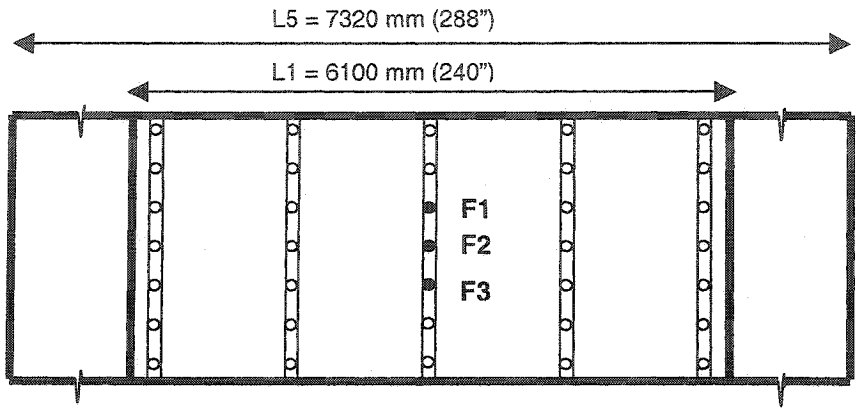

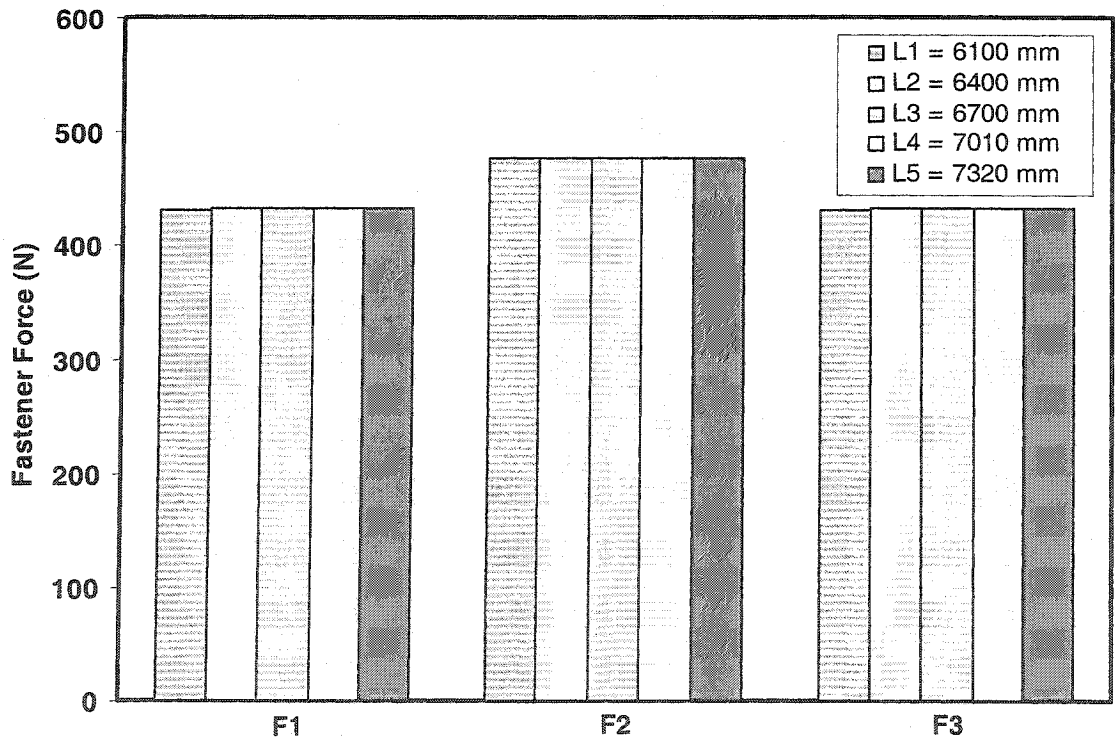

Figure 5.2 Effect of table length on the fastener force

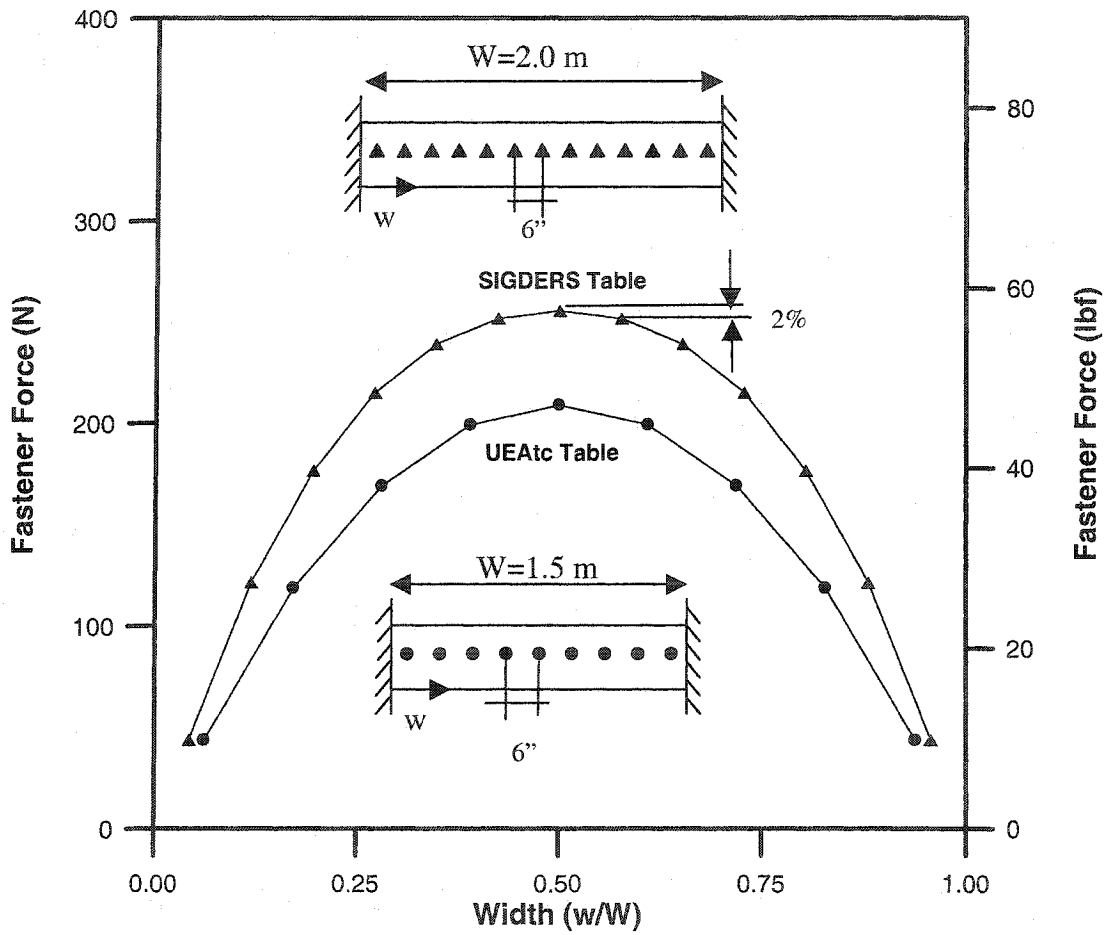

Figure 5.3 Computed fastener force variation along the seam for SIGDERS and UEAtc tables

5.2.2 Required Table Width

The present investigation focuses to isolate the effect of table width effect on the system response using the validated FE model. With all other parameters maintained constant, the Required Table Width (RTW) is one that will provide roofing system response in the lab similar to that of the field. Moreover, the development of RTW requires several levels of generalization of the true wind-induced effect over a roof assembly. Often, these generalizations warrant compromise from the technically sound approach to the practically acceptable procedure. This research work had the luxury of receiving input from all parties concerned with roofing, including researchers, manufacturers, roofing associations representing the contractors, and building owners. (Refer to the acknowledgment section for the SIGDERS consortium participants.) Based on the numerical investigation and the practical inputs the following criteria were established to identify the RTW:

"The table with RTW should provide no change in the maximum fastener forces or change in the maximum fastener force should be within 5% compared to those obtained while decreasing the table width by 305 mm (12")".

To identify the RTW for the roofing systems, simulations were performed for various table widths. The modelled table width ranged from 781 to 5048 mm (31" to 199"). This range covered the different tables that are used for the current roofing system evaluation (Table 5.1). For illustrating the above criteria and involved calculations, a typical example is shown in Table 5.2. It shows the computed maximum fastener forces for the themoplastic system with a 1220 mm (48") fastener row spacing (F_r) and a 305 mm (12") fastener spacing (F_s). A suction pressure of 1436 Pa (30 psf), was applied on this system. A computed fastener force of 800 N (180 lbf) was calculated for a table width of 5048 mm (199"). No change on the fastener force resulted from decreasing the width to 4134 mm (163"). Further reductions of the width reduced the fastener force. For a table width of 2000 mm (79"), the computed fastener force was only 650 N (146 lbf). This reduction from 800 N to 650 N (180 lbf to 146 lbf) is owing to the edge effect. By applying the established criteria, a table width of 2610 mm (103") can be selected as the RTW for this configuration where the variation of fastener force is less than 5%.

Table 5.2 Example to illustrate the RTW criteria

Simulation No.	Table Width mm (in)	Configuration 48/18	
		Fastener Force N (lbf)	Change (%)
1	5048 (199)	800 (180)	0
2	4743 (187)	800 (180)	0
3	4438 (175)	800 (180)	0
4	4134 (163)	800 (180)	0
5	3829 (151)	799 (180)	0.1
6	3524 (139)	796 (179)	0.5
7	3219 (127)	789 (177)	0.9
8	2914 (115)	774 (174)	1.9
9	**2610 (103)**	**751 (169)**	**3.0**
10	2305 (91)	713 (160)	5.1
11	2000 (79)	650 (146)	8.8
12	1695 (67)	569 (128)	12.5
13	1390 (55)	466 (105)	18.1
14	1086 (43)	343 (77)	26.4
15	781 (31)	207 (47)	39.7

5.2.3 Parameters Influencing the RTW

A number of factors can influence the RTW. Three critical parameters, namely, variations in the membrane properties, fastener spacing (F_s) and fastener row spacing (F_r) are investigated and discussed below.

Variation in the thermoplastic membrane: There are two main types of thermoplastic membranes used for industrial roofing, namely, TPO and PVC. A roofing system, with PVC membrane instead of TPO, was modelled to investigate the effect on the RTW for membrane variations in the thermoplastic group. The same finite element model was used with the exception of different input parameters. A typical 67/12 configuration has been selected with appropriate modulus of elasticity and details are documented in Zahrai and Baskaran (1999). Computed fastener forces for different table width ranging from 781 to 5048 mm (31" to 199") are shown in Figure 5.4. A comparison shows minimum variations in fastener forces between the PVC and TPO roof systems. Therefore, it was decided to use one set of RTW for the evaluation of roofs with thermoplastic membrane.

Fastener row spacing (F_r): To quantify the impact of F_r on the RTW, two thermoplastic configurations were selected. The layouts were 48/18 and 114/18 and all other parameters such as fastener spacing and applied pressure were maintained constant. The selected fastener row spacing of 1220 and 2900 mm (48" and 114") can cover systems with minimum and maximum fastener row spacing available in the roofing industry. Computed fastener loads for both configurations and for different table widths are presented in Figure 5.5. Fastener forces were calculated for a 1436 Pa (30 psf) uplift pressure. For the system with a 2900 mm (114") fastener row spacing, the RTW is 4130 mm (163"), whereas for a system with an F_r of 1220 mm (48") the RTW is 2610 mm (103"). This reveals that the F_r has a direct influence on the RTW and that its dependency is not linear.

Fastener spacing (F_s): In order to investigate the influence of fastener spacing on the RTW, computed fastener forces for 48/6 layout are added in to the Figure 5.5. It is evident that decreasing fastener space from 460 to 152 mm (18" to 6") caused a decrease in the computed fastener force. This has been the case for all simulated table widths. For the system with 152 mm (6") fastener spacing the RTW is 2000 mm (79"). Comparison of RTW between 460 and 152 mm (18" and 6") fastener spacing, ranged from 2610 to 2000 mm (103" to 79"), indicate a small influence. Overall, the Figure 5.5 data confirms that one should consider the effect of fastener row spacing (F_r) and fastener spacing (F_s) in determining the RTW. One can assign higher importance factor for F_r than F_s when generalising the RTW. This will be further explained in the following section in which RTW is used to develop correction factors.

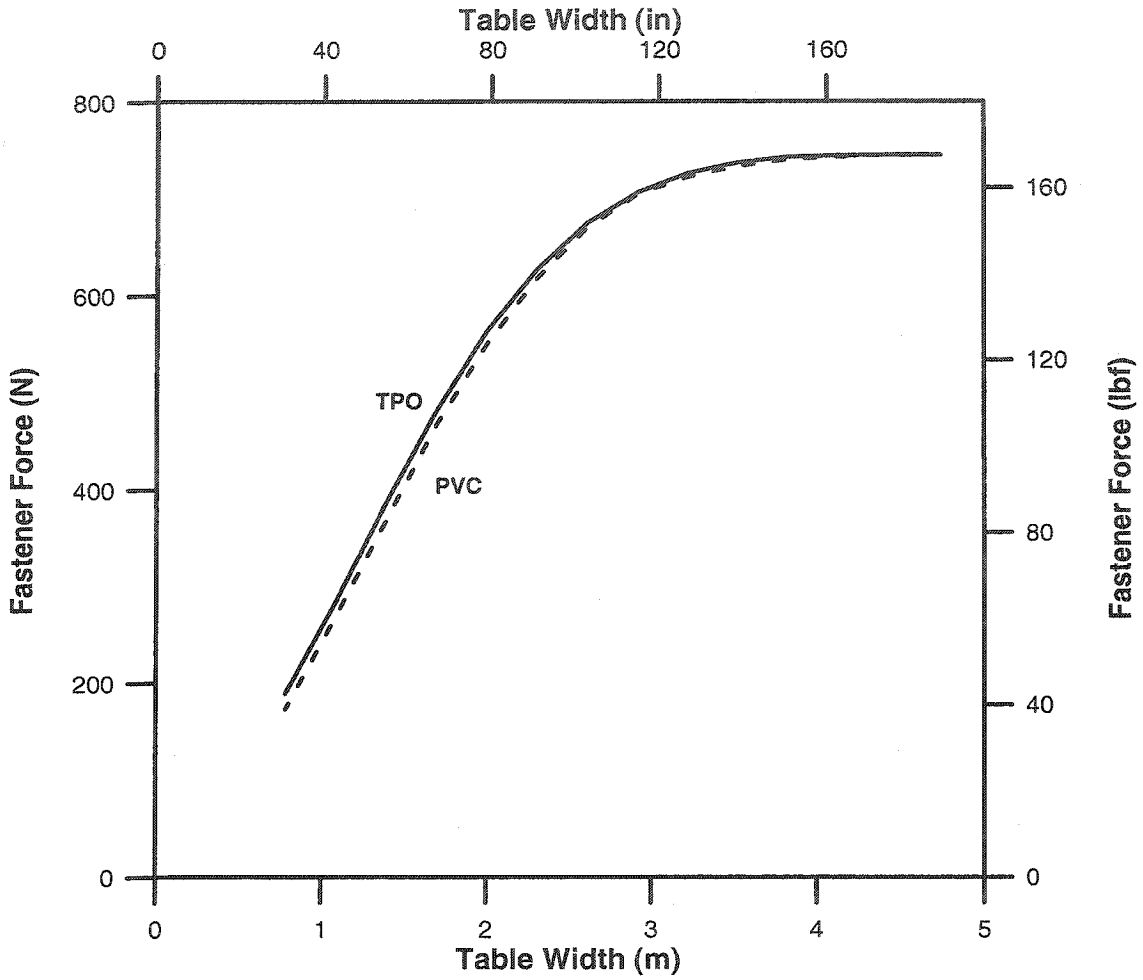

Figure 5.4 Effect of membrane on the computed fastener force

5.3 Development of Correction Factor

One objective of the present study was to develop correction factors (C_f) for the tables having width smaller than the established RTW. This section explains the development of C_f for various configurations of thermoplastic systems.

The correction factors can be calculated by dividing the fastener force obtained from the RTW table with that of the narrow ones. Tables having larger widths than RTW have correction factors equal to one. For instance, in Table 5.2, the width of 2610 mm (103") was identified as the RTW with 751 N (169 lbf) as fastener force. Using a 2000 mm (79") table would reduce the fastener force to 650 N (146 lbf). To correct this situation, the fastener force obtained from the table that has a width of 2000 mm (79") needs to be multiplied by the correction factor of 1.15 (751/650).

Table 5.3 shows the correction factor for the configurations of F_r equal to 1220 mm (48") while F_s changes from 152, 305, 460, 610 mm (6", 12", 18" to 24"). Using a 48/24 roofing system configuration on a table width of 2000 mm (79") required the application of a correction factor of 1.35 to rectify the measured fastener force. The same table width does not need any correction factor on measured fastener force when the 48/6 configuration is evaluated. The RTW for each configuration can also be identified from this table. As discussed, increasing the table width decreases the edge effect. Therefore the correction factor reduces until the factor becomes 1.0. Therefore, Required Table Width is one when the correction factor equals one (shown bold in the table). For instance, the configuration of 48/6 has the RTW of 2000 mm (79") whereas the configuration of 48/24 has the RTW of 2914 mm (115").

More than 200 simulations were performed for the variations of the two influencing factors discussed in the previous section, namely, fastener row spacing (F_r) and fastener spacing (F_s) for the thermoplastic systems. The results of the study are tabulated in Appendix D. Four F_r configurations 2900, 1830, 1700 and 1220 mm (114", 72", 67" and 48") with four F_s configurations 152, 305, 460 and 610 mm (24", 18", 12" and 6") were considered. These (F_r/F_s) combinations represent most of the thermoplastic systems currently available in the roofing industry. For each configuration, correction factors were developed and the curves of correction factors for different fastener row spacing and fastener spacing are presented in Figure 5.6 and 5.7. The intent was to achieve characteristic curves such that generalised guidelines can be developed for the C_f. The comparison of these curves revealed the following based on which generalised correction factors can be developed in section 5.4.

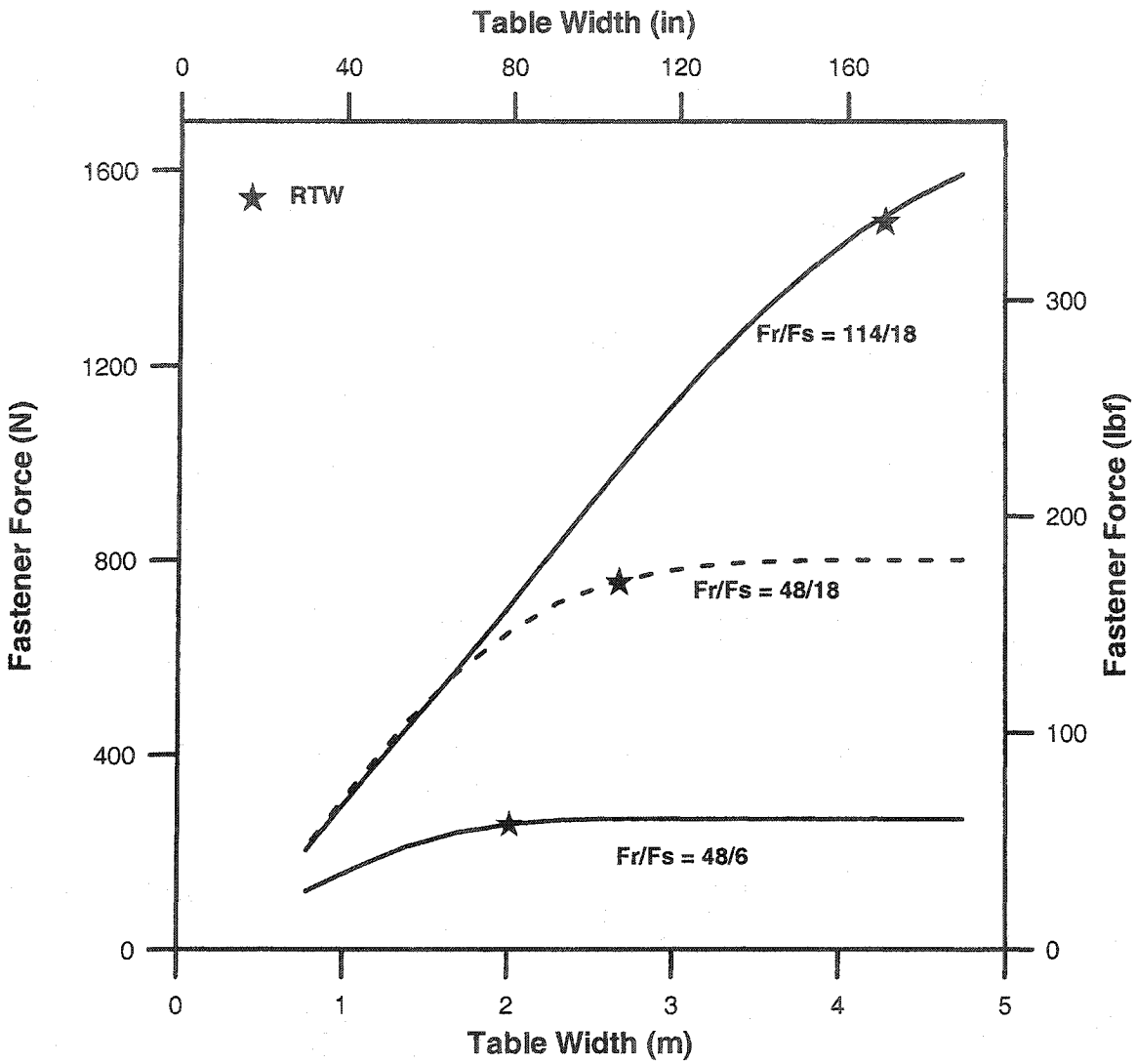

Figure 5.5 Impact of roofing system configuration on the computed fastener force

- The RTW for different roofing layouts ranged from 2000 to 4000 mm (79" to 157"). For instance, using a table width of 3000 mm (118"), one can evaluate all layouts for F_r equal to 1220 mm (48"). On the other hand, a minimum table width of 4000 mm (157") is necessary if one wants to evaluate all F_r/F_s combinations without applying any correction factor.
- Increasing F_s from 460 mm (18") to 610 mm (24") increased C_f more than any other changes in the F_s. This is valid irrespective of the F_r.
- In experimental set up, at least three fasteners along each seam are required to provide sufficient roofing system response. To investigate a system with an F_s of 610 mm (24"), the table width should be greater than 1400 mm (55"). Then, in general, application of C_f for tables less than 1400 mm (55") wide is not appropriate. Therefore, only table widths more than 1400 mm (55") can be used with correction factors. The required correction factors for all F_r/F_s combinations can be obtained from Figure 5.6.

Table 5.3 Developed correction factor for various table with F_r = 1219 mm (48")

Simulation No.	Table Width mm (in)	48/6	48/12	48/18	48/24
1	5048 (199)	1	1	1	1
2	4743 (187)	1	1	1	1
3	4438 (175)	1	1	1	1
4	4134 (163)	1	1	1	1
5	3829 (151)	1	1	1	1
6	3524 (139)	1	1	1	1
7	3219 (127)	1	1	1	1
8	**2914 (115)**	1	1	1	1
9	**2610 (103)**	1	1	1	1.061
10	**2305 (91)**	1	1	1.053	1.166
11	**2000 (79)**	1	1.065	1.1554	1.353
12	1695 (67)	1.071	1.179	1.320	1.706
13	1390 (55)	1.220	1.404	1.612	2.405
14	1086 (43)	1.527	1.811	2.190	4.025
15	781 (31)	2.161	2.697	3.628	10.457

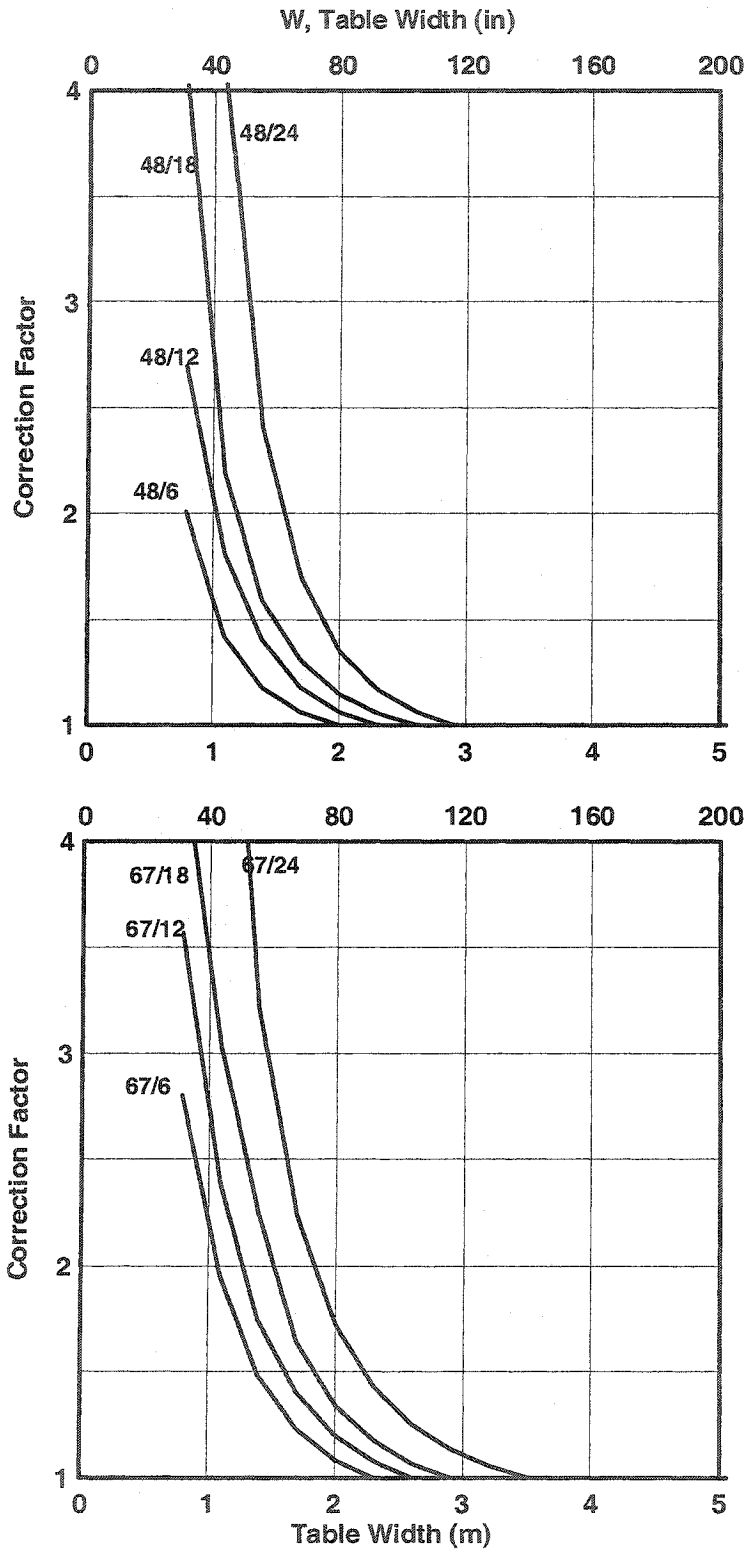

Figure 5.6 Developed correction factors for Fr = 48 and 67 – Thermoplastic system

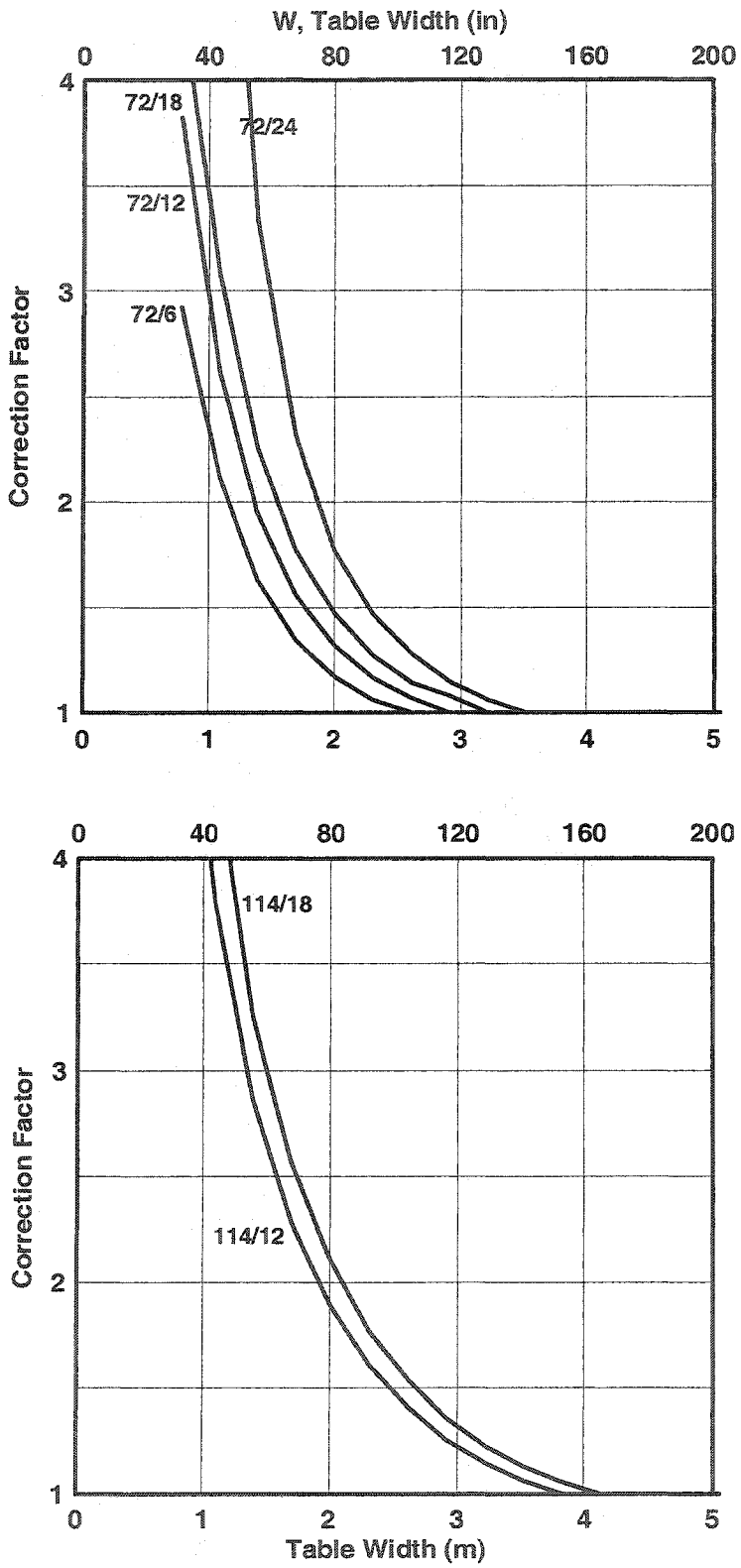

Figure 5.7 Developed correction factors for Fr = 72 and 114 – Thermoplastic system

5.4 Generalization of Correction Factor

5.4.1 Thermoplastic System

To generalize the developed correction factor, in this section attempts have been made to identify the relationship between the correction factor and influenced parameters (F_r, F_s and W). A database table was created by grouping all the simulated configuration data from the Appendix D and a segment is shown in Table 5.5. Three more parameters (ratios) were calculated from the grouped data. Those values consist ratio of:

- Fastener row spacing to fastener spacing (F_r/F_s)
- Table width to fastener spacing (W/F_s)
- Table width to fastener row spacing (W/F_r)

First, the trend of systematically decreasing the correction factor becomes clear for each set of (F_r/F_s). Then, the table was grouped based on F_r/F_s ratio. In doing so, the 14 different layout configurations shown in the Figure 5.6 reduces to 13. It was owing to configurations 72/18 and 48/12 having the same F_r/F_s ratio of four. Then, the data in each category was sorted in descending order according to correction factor values. It was noticed that the W/F_s and W/F_r ratios increases for each set of Fr/Fs as the correction factor decreases. In the Table 5.5 this trend of the F_r/F_s is shown when F_r/F_s ratio of 2, 5.6 and 12. Note that the maximum and minimum ratios of F_r/F_s by the present study were 2 and 12 respectively. The Appendix D provides similar data for other Fr/Fs configurations.

In order to investigate the result of this study in more detail, the computed values are shown in graphic format in Figure 5.8 by introducing a constant value of m, which is the ratio of F_r/F_s. The X-axis shows the relation between the width (W) over fastener spacing (F_s) and correction factor were presented in the Y-axis. As shown in Figure 5.8, a total of 13 curves were generated and drawn in three sets based on the following relationship:

Table 5.4 Parameter normalization for correction factor –thermoplastic system

W mm (in)	F_r mm (in)	F_s mm (in)	C_f	$\frac{F_r}{F_s}$	$\frac{W}{F_s}$	$\frac{W}{F_r}$
1086 (43)	1220 (48)	610 (24)	4.02	2	1.8	0.9
1390 (55)	1220 (48)	610 (24)	2.40	2	2.3	1.1
1695 (67)	1220 (48)	610 (24)	1.70	2	2.8	1.4
2000 (79)	1220 (48)	610 (24)	1.35	2	3.3	1.6
2305 (91)	1220 (48)	610 (24)	1.16	2	3.8	1.9
2610 (103)	1220 (48)	610 (24)	1.06	2	4.3	2.1
2914 (115)	1220 (48)	610 (24)	1	2	4.8	2.4
....	....	....	....	....	....	....
....	....	....	....	....	....	....
781 (31)	1700 (67)	305 (12)	3.68	5.6	2.6	0.5
1086 (43)	1700 (67)	305 (12)	2.46	5.6	3.6	0.6
1390 (55)	1700 (67)	305 (12)	1.87	5.6	4.6	0.8
1695 (67)	1700 (67)	305 (12)	1.50	5.6	5.6	1
2000 (79)	1700 (67)	305 (12)	1.28	5.6	6.6	1.2
2305 (91)	1700 (67)	305 (12)	1.14	5.6	7.6	1.4
2610 (103)	1700 (67)	305 (12)	1.05	5.6	8.6	1.5
2914 (115)	1700 (67)	305 (12)	1	5.6	9.6	1.7
....	....	....	....		....	....
....	....	....	....	....	....	....
781 (31)	1830 (72)	152 (6)	2.92	12	5.2	0.4
1086 (43)	1830 (72)	152 (6)	2.12	12	7.2	0.6
1390 (55)	1830 (72)	152 (6)	1.63	12	9.2	0.8
1695 (67)	1830 (72)	152 (6)	1.34	12	11.2	0.9
2000 (79)	1830 (72)	152 (6)	1.17	12	13.2	1.1
2305 (91)	1830 (72)	152 (6)	1.06	12	15.2	1.3
2610 (103)	1830 (72)	152 (6)	1	12	17.2	1.4

- Set 1 : $\frac{F_r}{F_s} \leq 5$
- Set 2 : $5 < \frac{F_r}{F_s} \leq 7$
- Set 3 : $\frac{F_r}{F_s} > 7$ (5.1)

The comparison of these three sets revealed the following points:

1. The computed data has the width over fastener spacing ratio (W/F_s) ranged from 1.8 to 17.2, which has the corresponding correction factor of 4.0 and 1.0 respectively.

2. Increasing the width over fastener spacing reduces the correction factor if F_r/F_s is kept constant. It also reveals that, the ratio of W/F_s increases while the table width increases and causing the correction factor reduce when a roofing system tested on a wider table.

3. For a constant value of W/F_s, the correction factor has a direct relation with F_r/F_s. In other words, the correction factor increases while F_r/F_s increases, when the W/Fs remains constant. For instance, for a value of W/F_s of four, the values of the correction factor change from 1.1 to 1.6 while F_r/F_s increases from two to three.

4. Increasing F_r increases the correction factor if the other parameters remain constant. This is another interpretation of the last conclusion since by increasing the fastener row spacing the F_r/F_s ratio increases. Therefore when W/F_s remains constant, F_r/F_s increases, and as a result the correction factor increases.

Based on the above analysis, it can be concluded that no correction factor is needed or correction factor is equal 1.0, for:

- Set 1 when $\frac{W}{F_s} > 7$
- Set 2 when $\frac{W}{F_s} > 10$
- Set 3 when $\frac{W}{F_s} > 17$ (5.2)

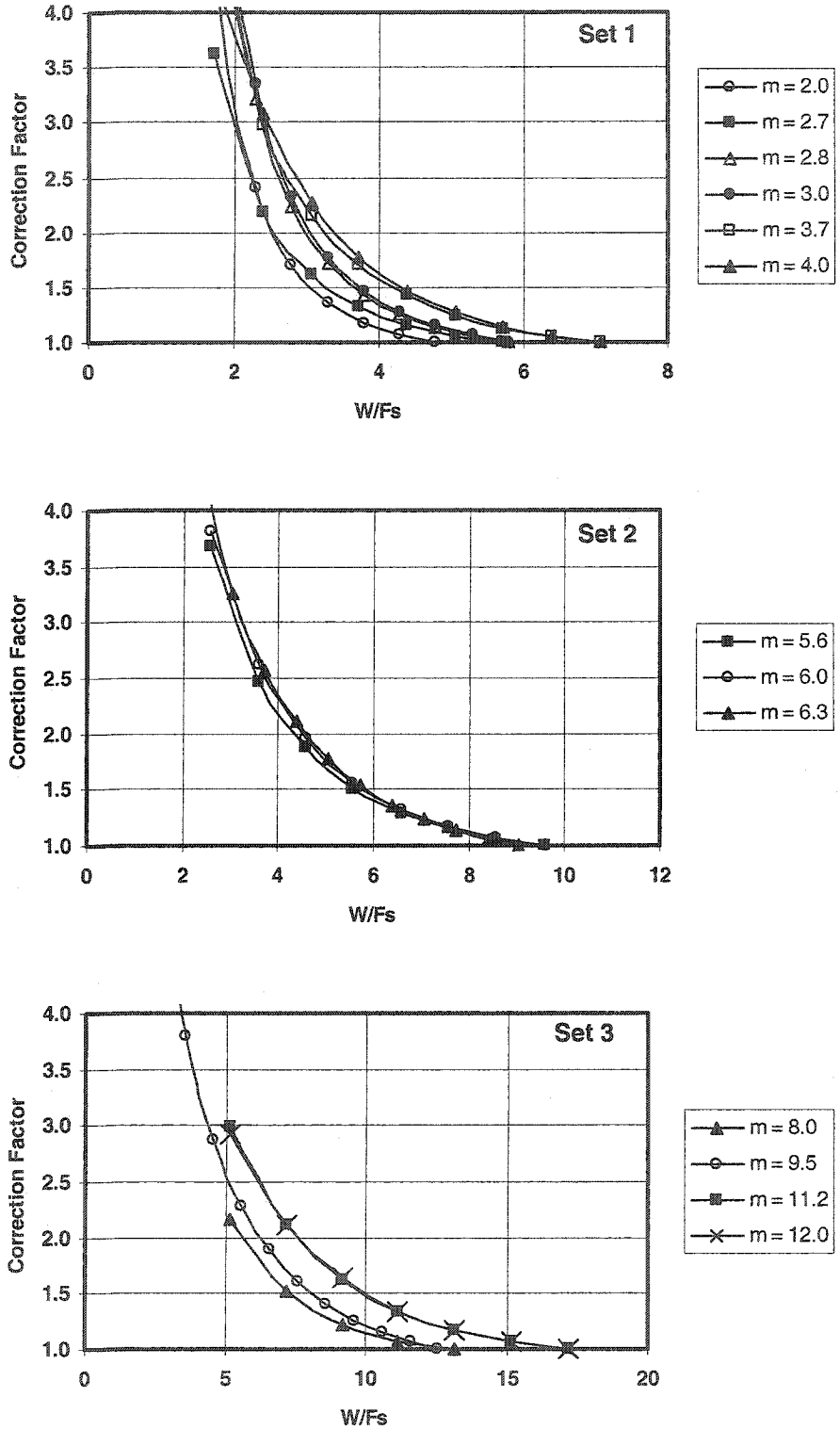

Figure 5.8 Grouping of correction factors for thermoplastic system

Although the correction factors shown in Figure 5.8 cover a wide range of table width, the factors may not be practical for some cases. For example, when the width of the table decreases to 781 mm (31"), the table cannot be used for the evaluation of a system with a fastener spacing of the 610 mm (24"). Also, the higher correction factors create accumulative errors for the measured fastener force. Therefore, it was decided to set a maximum of 1.5 for the correction factor. Based on this extensive data analysis, Figure 5.9 shows the developed correction factor for the thermoplastic system when correction factors vary from 1.0 and 1.5.

5.4.2 Thermoset System

To develop correction factor for themoset systems similar methodology was followed. Three most commonly used thermoset system configurations 78/6, 78/12, 78/18 were considered for this study. The configurations were simulated by finite element numerical models explained on last chapter. Then, the effect of fastener row spacing (F_r) and fastener spacing (F_s) were investigated by varying the table using the developed model. Since the maximum correction factor was set as 1.5, instead of investigating the full range of table size, only table widths studied to cover that range.

Table 5.5 shows the normalized parameters and calculated correction factors. The fastener force results are given in tabular format in the Appendix D. Using the data, the F_r/F_s and W/F_s values were calculated for each configuration. It was observed for a fixed value of F_r/F_s, as W/F_s increases, the correction factor decreases. This trend was similar to that observed for thermoplastic system.

The relations of W/F_s and C_f for three computed configurations of F_r/F_s (4.3, 6 and 13) are shown in Figure 5.10. The W/F_s varies from 4 to 18 while the correction factor changes from 1 to 1.5.

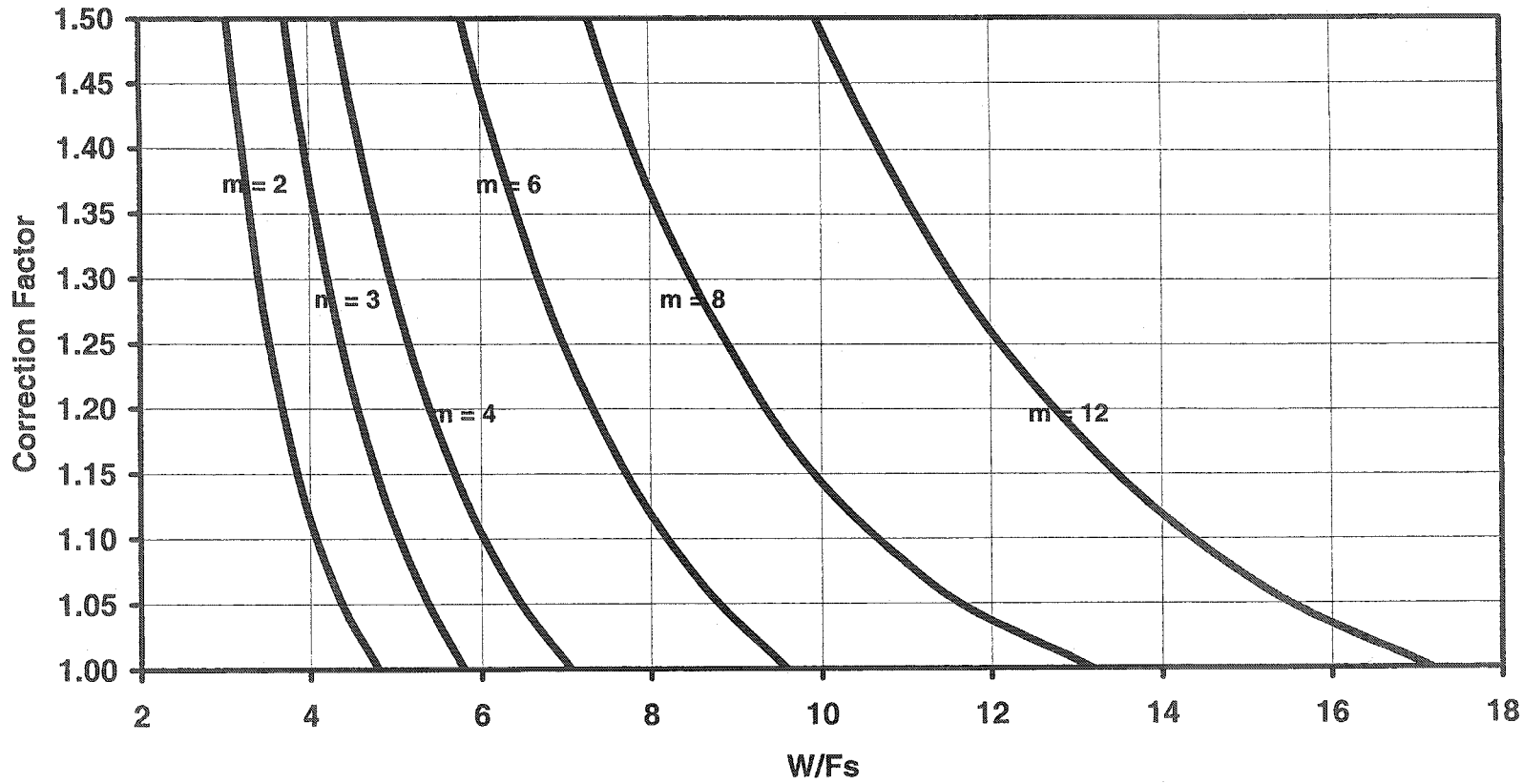

Figure 5.9 Developed correction factors for thermoplastic system

Table 5.5 Parameter normalization for correction factor –Thermoset system

W mm (in)	F_r mm (in)	F_s mm (in)	C_f	$\frac{F_r}{F_s}$	$\frac{W}{F_s}$
2000 (79)	1980 (78)	460 (18)	1.31	4.3	4.4
2305 (91)	1980 (78)	460 (18)	1.15	4.3	5.1
2610 (103)	1980 (78)	460 (18)	1.06	4.3	5.7
2914 (115)	1980 (78)	460 (18)	1.00	4.3	6.4
1695 (67)	1980 (78)	305 (12)	1.41	6.5	5.6
2000 (79)	1980 (78)	305 (12)	1.21	6.5	6.6
2305 (91)	1980 (78)	305 (12)	1.08	6.5	7.6
2610 (103)	1980 (78)	305 (12)	1.00	6.5	8.6
1695 (67)	1980 (78)	152 (6)	1.36	13	11.2
2000 (79)	1980 (78)	152 (6)	1.17	13	13.2
2305 (91)	1980 (78)	152 (6)	1.07	13	15.2
2610 (103)	1980 (78)	152 (6)	1.00	13	17.2

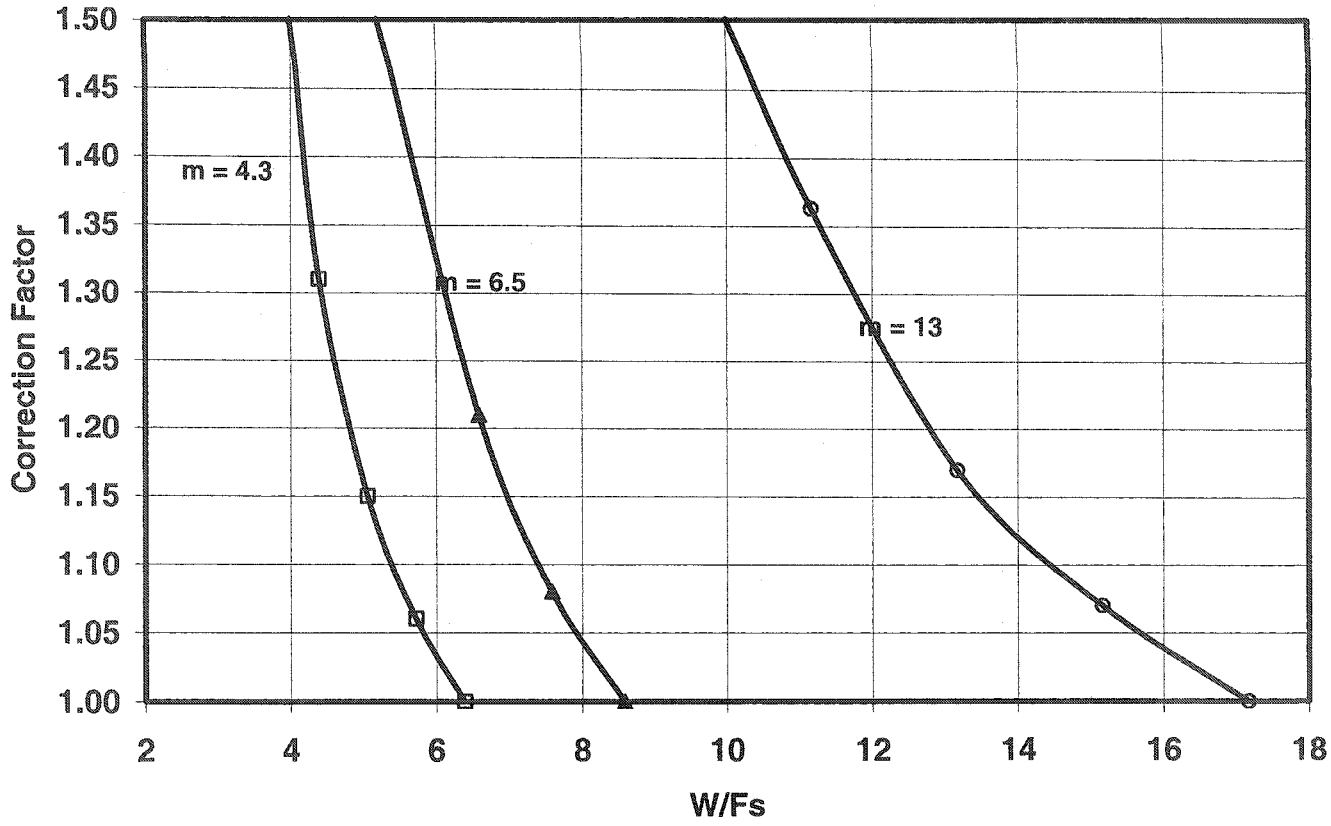

Figure 5.10 Developed correction factors for thermoset system

5.5 Correction Factor Curves for Roofing Design

Figures 5.9 and 5.10 propose the independently developed correction factors for thermoplastic and thermoset systems respectively. Such that the measured fastener force attained by the experimental results can be multiplied by the correction factor to adjust for the influence of edge effect. It would be ideal for roof designers to have a single correction factor graph for both thermoplastic and thermoset systems. In other words, it is preferable to have a single set of correction factor for polymer-based systems (ref. Fig. 3.1).

To address the issue, the calculated correction factors of thermoplastic and thermoset systems were compared. First, the value of W/F_s and F_r/F_s ratios are calculated for various system configurations. Then, the correction factors were identified using the Figures 5.9 and 5.10. For instance, a 48/12 configuration test using table width of 1524 mm (60") is selected. The W/F_s and F_r/F_s ratios for this configuration are 5 and 4 respectively. Using the Figures 5.9 and 5.10, the correction factor for thermoplastic and thermoset systems were 1.29 and 1.13 respectively. Such calculated data are shown in Table 5.6.

The analysis reveals that the thermoset system always has the lower correction factor compared to the thermoplastic system. As discussed in the Section 4.5.2, the membrane properties and seam details vary between the thermoplastic and thermoset systems. This causes differences in the correction factors. The ratio of the thermoset system correction factor over the thermoplastic system correction factor is also shown in the last column of the Table 5.6. It reveals that the ratio changes from 0.85 to 0.96 considering all the configurations. Comparing the correction factor ratios shows that the values remain constant in each set. If the average values for each set are considered, the ratio for three sets are 0.88, 0.88 and 0.96.

Based on the above comparison a single set of correction factor curves for the polymer-based systems are shown in Figure 5.11. For the thermoplastic system the correction factor can be applied directly to calculate the design fastener forces. It is suggested for the case of thermoset system the following procedure could amend the calculated correction factor:

- When $m \leq 7$, then correction factors are multiplied by 0.88 and;
- When $m > 7$, then correction factor are multiplied by 0.96

Table 5.6 Comparison of correction factor for various TP and TS systems

Set	$\frac{W}{F_s}$	$\frac{F_r}{F_s}$	Correction Factor		Ratio (TS/TP)
			TP	TS	
Set #1 $m \leq 5$	4.5	4	1.43	1.24	0.87
	5.0	4	1.29	1.13	0.88
	5.5	4	1.18	1.06	0.90
Set # 2 $5 < m \leq 7$	6.5	6.5	1.45	1.23	0.85
	7.0	6.5	1.30	1.14	0.88
	8.0	6.5	1.18	1.05	0.89
Set # 3 $m > 7$	10.0	12	1.49	1.43	0.96
	12.0	12	1.26	1.21	0.96
	14.0	12	1.12	1.06	0.95

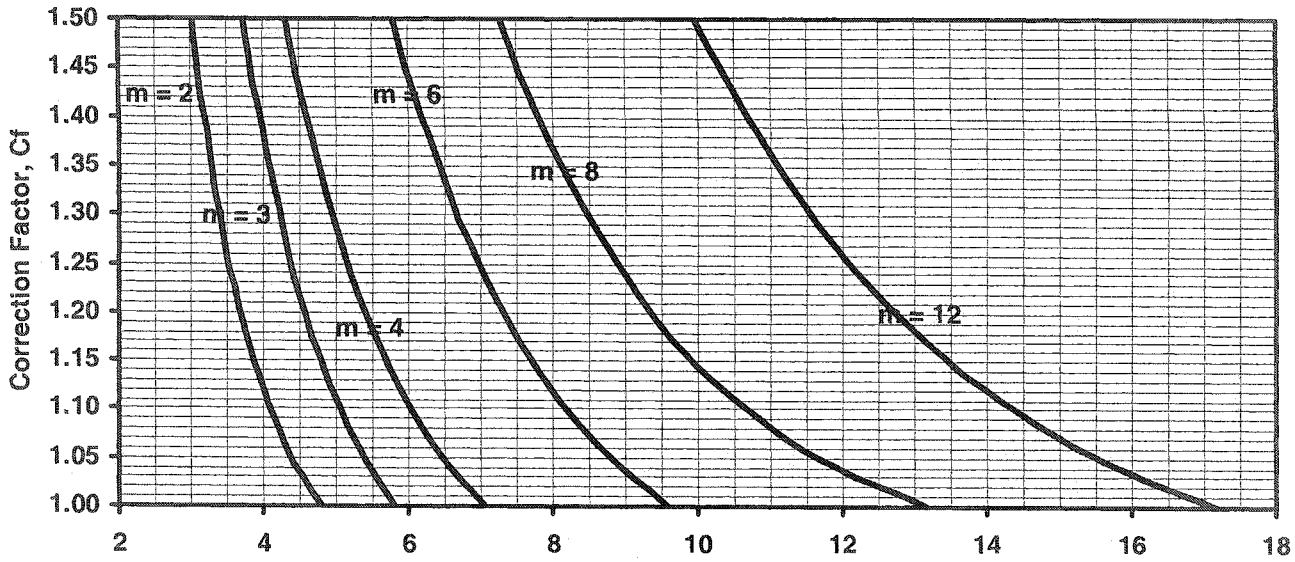

Note:
For thermoset systems when:
m ≤ 7 multiply C_f by 0.88 and
m > 7 multiply C_f by 0.96

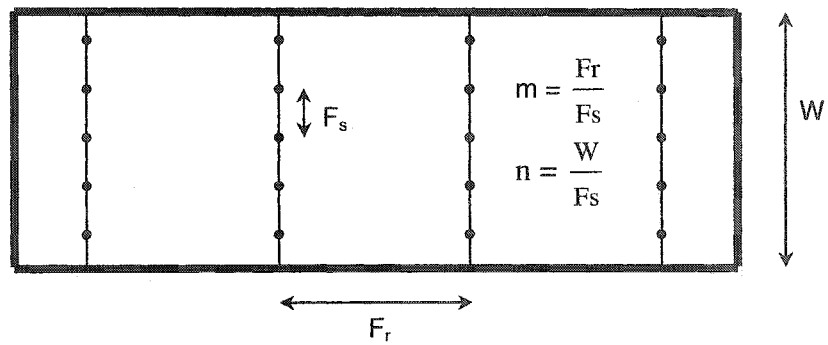

Figure 5.11 Correction factor curves for roofing design

The practical application of the Figure 5.11 is illustrated with a case study. A manufacturer obtained a fastener force of 1420 N (319 lbf) by testing a 78/12 thermoset system in a 2135 mm (84") table width. The use of correction factor is as follows:

Case study:

- Membrane used: Thermoset
- Fastener row spacing (F_r) = 1980 mm (78")
- Fastener spacing (F_s) = 300 mm (12")
- Tested table width (W) = 2135 mm (84")
- Measured fastener force = 1420 N (319 lbf)

Step 1:

- Calculate; $m = \frac{F_r}{F_s}$, which is 6.5
- Calculate; $n = \frac{W}{F_s}$, which is 7.0

Step 2:

- Identify correction factor from the Figure 5.10, $C_f = 1.30$

Step 3:

- Since the selected system is thermoset and $m \leq 7$, the above correction factor should be multiplied by 0.88. Therefore, the correction factor to calculate the design fastener force is 1.14.

Step 4:

- Design fastener force = $1420 \times 1.14 = 1619$ N (412 lbf)

6 Conclusions and Recommendations

The dissertation focused on the application of the existing computer software and numerical techniques for both wind load estimation and wind uplift resistance evaluation of single-ply roofing systems. Present study contribution not only helps the roof designers for the estimation of wind load, but also complements the interpretation of standard testing procedures for the evaluation of single-ply roofing systems.

6.1 Concluding Remarks

The present study developed a knowledge-based module for the estimation of wind load distribution on roofs. Extensive pressure data were collected from various sources in the open literature. Concentration has been focused on data containing roof wind uplift pressure coefficients (mean/peak). Studies carried out in using boundary layer wind tunnels after 1970 and full-scale measurements were used. All the data were presented in a common format by converting to full-scale building representation and wind speed at roof height. In total, more than 200 design figure data were extracted. A database management program, Microsoft Access, was used to manage the collected data. A user-friendly interface has been developed to search data conveniently. Based on input, user can obtained the wind uplift pressure coefficients that are applicable to compute design wind load.

Various mechanically attached single-ply roofing systems were numerically modeled based on the Finite Element program with the capability of non-linear analysis. Experimental data obtained from the Dynamic Roofing Facility was used for benchmarking the developed model. Numerical results for various system configurations compared well with those obtained from the experimental studies.

The validated model was further used to investigate the effect of table size on the roofing system performance. Attempts were made to identify the required table width. It was found that an increase in the table width beyond a certain level did not significantly change the system response and found that the specific limit depends mainly on two system parameters, namely, fastener row spacing and fastener spacing. Influences of these two parameters on the required table width were also investigated.

Based on such modeling efforts, correction factors were established for thermoplastic and thermoset systems. Generalized correction factor curves were developed for the evaluation of mechanically attached single-ply roofing systems. These correction factor curves are applicable, where the test table is less than the required table width.

6.2 Recommendations for Future Work

World Wide Web-based design tools have the advantage of providing out of office accessibility. It is preferable to have the developed knowledge-based wind load module on the World Wide Web such that it can easily accessible from anywhere and anytime. In addition, as new design data become available the database can be updated on the web server. The database developed by the present study is based on existing data up to the year 1999. Therefore, one can collect any new data and integrate it into the database so that the database remain current.

The existing numerical model can be enhanced for the simulation of various type of roofing systems. The following enhancements on numerical model are suggested:

- Simulation of non-polymer based roofing membrane
- Simulation of adhered and ballasted attachments for single-ply roofing systems
- Dynamic wind load simulation using the numerical model

Appendix A: List of resources used for wind load database

To develop a knowledge-based database for the estimation of wind load distribution on roofs, all data of wind uplift pressure from the open literature are collected. Table A.1 lists the sources from which data are extracted for the present study.

Table A.1 List of resources used for wind load database

ID	Title	Authors	Year	Source
1	A study of wind pressures on a single-family dwelling in model and full scale	Marshall Richard D.	1975	*Journal of Wind Engineering and Industrial Aerodynamics, Volume 1, pp. 177-199*
2	Tests to determine wind speeds for scouring and blowoff of rooftop gravel	Kind R J	1975	*Proceedings of the fourth International Conference on Wind Engineering*
3	The measurement of wind pressures on two-storey houses at Aylesbury	Eaton K. J., Mayne J. R.	1975	*Journal of Wind Engineering and Industrial Aerodynamics, Volume 1, pp. 67-109*
4	Wind loads on low-rise buildings - effect of roof geometry	Eaton Keith J, Mayne John R, Cook Nicholas J	1975	*Proceedings of the fourth International Conference on Wind Engineering*
5	Comparative measurements of wind pressure on a model of the full-scale experimental house at Aylesbury, England	Apperley L., Surry D., Stathopoulos T., Davenport A. G.	1979	*Journal of Wind Engineering and Industrial Aerodynamics, Volume 4, pp. 207-228*
6	Measurements of wind loads on full-scale glasshouses	Wells D. A., Hoxey R. P.	1980	*Journal of Wind Engineering and Industrial Aerodynamics, Volume 6, pp. 139-167*
7	An approach to the determination of wind load effects on low-rise buildings	Holmes J. D., Best R. J.	1981	*Journal of Wind Engineering and Industrial Aerodynamics, Volume 7, pp. 273-287*
8	Effective wind loads on flat roofs	Stathopoulos T., Surry D., Davenport A. G.	1981	*Journal of the structural division, Volume 107, pp. 281-298*
9	Failure mechanisms of loose-laid roof-insulation systems	Kind R. J., Wardlaw R. L.	1982	*Journal of Wind Engineering and Industrial Aerodynamics, Volume 9, pp. 325-341*
10	A full-scale study of the geometric parameters that influence wind loads on low rise buildings	Hoxey R. P., Moran P.	1983	*Journal of Wind Engineering and Industrial Aerodynamics, Volume 13, pp. 277-288*
11	Comparison of wind pressures on a mobile home in model and full scale	Macha J. M., Sevier J. A., Bertin J. J.	1983	*Journal of Wind Engineering and Industrial Aerodynamics, Volume 12, pp. 109-124*

12	Large models of low rise buildings loaded by the natural wind	Leicester K. H., Hawkins B. T.	1983	*Journal of Wind Engineering and Industrial Aerodynamics, Volume 13, pp. 289-300*
13	Scale effects in wind tunnel testing on low buildings	Stathopoulos T.	1983	*Journal of Wind Engineering and Industrial Aerodynamics, Volume 13, pp. 313-326*
14	Use of eigenvalues in the covariance integration method for determination of wind load effects	Best R. J., Holmes J. D.	1983	*Journal of Wind Engineering and Industrial Aerodynamics, Volume 13, pp. 359-370*
15	Wind loading of flat roofs with and without parapets	Lythe G., Surry D.	1983	*Journal of Wind Engineering and Industrial Aerodynamics, Volume 11, pp. 75-94*
16	A full-scale study of wind loads on agricultural ridged canopy roof structures and proposals for design	Robertson A. P., Hoxey R. P., Moran P.	1985	*Journal of Wind Engineering and Industrial Aerodynamics, Volume 21, pp. 167-205*
17	Comparisons between wind tunnel and full scale estimates of wind loads on a mobile home	Surry D., Johnson G. L.	1986	*Journal of Wind Engineering and Industrial Aerodynamics, Volume 23, pp. 165-180*
18	Comparisons of full-scale and wind-tunnel measurements for wind loads on a free-standing canopy roof structure	Robertson A. P., Moran P.	1986	*Journal of Wind Engineering and Industrial Aerodynamics, Volume 23, pp. 113-125*
19	Wind loads on low buildings with mono-sloped roofs	Stathopoulos T., Mohammadian A. R.	1986	*Journal of Wind Engineering and Industrial Aerodynamics, Volume 23, pp. 81-97*
20	Wind pressure load on an industrial building	Szalay Zoltan	1986	*Journal of Wind Engineering and Industrial Aerodynamics, Volume 23, pp. 73-79*
21	Design pressure distribution on circular silos with conical roofs	Sabransky I. J., Melbourne W. H.	1987	*Journal of Wind Engineering and Industrial Aerodynamics, Volume 26, pp. 65-84*
22	Wind pressures on flat roofs with parapets	Stathopoulos T., Baskaran A.	1987	*Journal of Structural Engineering, Vol. 113, No. 11, pp. 2166-2180*
23	Codification of local pressure coefficients for low-rise structures	Robertson A. P.	1988	*Journal of Wind Engineering and Industrial Aerodynamics, Volume 30, pp. 143-152*
24	Distribution of peak wind loads on a low-rise building	Holmes J. D.	1988	*Journal of Wind Engineering and Industrial Aerodynamics, Volume 29, pp. 59-67*
25	Prediction of wind-induced failure of loose laid roof cladding systems	Kind R. J., Savage M. G., Wardlaw R. L.	1988	*Journal of Wind Engineering and Industrial Aerodynamics, Volume 29, pp. 29-37*
26	Reducing the wind loading on large cantilevered roofs	Melbourne W. H., Cheung J. C. K.	1988	*Journal of Wind Engineering and Industrial Aerodynamics, Volume 28, pp. 401-410*

27	Design Recommendation for wind loadings of intermediate height	Stathopoulos T., Dumitrescu-Brulotte M.	1989	*Canadian Journal of Civil Engineering, Vol. 16, No. 6, pp. 910-916*
28	Full-scale, model-scale and computational comparisons of wind loads on the silsoe structures building	Hoxey R. P., Robertson A. P., Richards P. J.	1989	*Proceedings of the second Asia-Pacific Symposium on Wind Engineering*
29	Wind effect on roofs and roofing	Kramer C., Gerhardt H. J.	1989	*Proceedings of the sixth U.S. National Conference on Wind Engineering*
30	Wind pressure on buildings with multi-level roofs	Stathopoulos T., Lucnian H. D.	1989	*Proceedings of the sixth U.S. National Conference on Wind Engineering*
31	Wind tunnel simulation of the Texas Tech research buildings: Effect of terrain features and building orientation	Lakas B. D., Mehta K. C., Kiesling E. W., Dunn J. R.	1989	*Proceedings of the sixth U.S. National Conference on Wind Engineering*
32	Full-scale and model investigations of pressures on an industrial/agricultural building	Richardson G. M., Robertson A. P., Hoxey R. P., Surry D.	1990	*Journal of Wind Engineering and Industrial Aerodynamics, Volume 36, pp. 1053-1062*
33	The magnitude and distribution of wind-induced pressures on hip and gable roofs	Meecham D., Surry D., Davenport A. G.	1991	*Journal of Wind Engineering and Industrial Aerodynamics, Volume 38, pp. 257-272*
34	Wind pressure on roofs of various geometries	Stathopoulos T., Saathoff P.	1991	*Journal of Wind Engineering and Industrial Aerodynamics, Volume 38, pp. 273-284*
35	Codification of wind pressure coefficients for sawtooth roofs	Stathopoulos T., Saathoff P.	1992	*Journal of Wind Engineering and Industrial Aerodynamics, Volume 41-44, pp. 1727-1738*
36	Computation of wind pressures on low-rise structures	Paterson D. A., Holmes J. D.	1992	*Journal of Wind Engineering and Industrial Aerodynamics, Volume 41-44, pp. 1629-1640*
37	Computational and wind tunnel modeling of mean wind loads on the silsoe structures building	Richards P. J., Hoxey R. P.	1992	*Journal of Wind Engineering and Industrial Aerodynamics, Volume 41-44, pp. 1641-1652*
38	Jan Smuts experiment: Details of full-scale experiment	Milford R V, Waldeck J. L., Goliger A. M.	1992	*Journal of Wind Engineering and Industrial Aerodynamics, Volume 41-44, pp. 1693-1704*
39	Peak wind loads under delta wing vortices on canopy roofs	Ginger J. D., Letchford C. W.	1992	*Journal of Wind Engineering and Industrial Aerodynamics, Volume 41-44, pp. 1739-1750*
40	Pressure fluctuation on flat roofs with parapets	Kareem Ahsan, Lu P. C.	1992	*Journal of Wind Engineering and Industrial Aerodynamics, Volume 41-44, pp. 1775-1786*
41	The effects of eaves geometry, model scale and approach flow conditions on portal frame building wind loads	Savory E., Dalley S., Toy N.	1992	*Journal of Wind Engineering and Industrial Aerodynamics, Volume 41-44, pp. 1665-1676*

42	The improved performance of hip roofs in extreme winds - A case study	Meecham D.	1992	*Journal of Wind Engineering and Industrial Aerodynamics, Volume 41-44, pp. 1717-1726*
43	The silsoe building: a comparison of pressure coefficients and spectra at model and full-scale	Richardson G. M., Surry D.	1992	*Journal of Wind Engineering and Industrial Aerodynamics, Volume 41-44, pp. 1653-1664*
44	Wind tunnel study of wind loading on loose-laid roofing systems	Bienkiewicz B., Sun Y.	1992	*Journal of Wind Engineering and Industrial Aerodynamics, Volume 41-44, pp. 1817-1828*
45	Characteristics of fluctuating wind pressure on long low-rise buildings with gable roofs	Kanda M., Maruta E.	1993	*Journal of Wind Engineering and Industrial Aerodynamics, Volume 50, pp. 173-182*
46	Predicting pressure distribution underneath loose laid roof cladding systems	Kind R. J.	1994	*Journal of Wind Engineering and Industrial Aerodynamics, Volume 51, pp. 371-379*
47	Pressure coefficients for low-rise building envelopes derived from full-scale experiments	Hoxey R. P., Robertson A. P.	1994	*Journal of Wind Engineering and Industrial Aerodynamics, Volume 53, pp. 283-297*
48	Wind loads on planar canopy roofs, Part 2: fluctuating pressure distributions and correlations	Ginger J. D., Letchford C. W.	1994	*Journal of Wind Engineering and Industrial Aerodynamics, Volume 51*
49	Wind-induced forces on eaves of low buildings	Stathopoulos T., Luchian Horia	1994	*Journal of Wind Engineering and Industrial Aerodynamics, Volume 52, pp. 249-261*
50	parametric CFD studies of external building aerodynamics	Osmond S. D.	1995	*Proceedings of the ninth International Conference on Wind Engineering*
51	The effect of surroundings and roof corner geometric modifications on roof pressures on low-rise buildings	Surry D., Lin J. X.	1995	*Journal of Wind Engineering and Industrial Aerodynamics, Volume 58, pp. 113-138*
52	The silsoe structures building: the completed experiment Part 1	Richardson G. M., Hoxey R. P., Robertson A. P., Short J. L.	1995	*Proceedings of the ninth International Conference on Wind Engineering*
53	Characteristics of fluctuating suction and vortices on a flat roof in oblique flow	Kawai H., Nishimura G.	1996	*Journal of Wind Engineering and Industrial Aerodynamics, Volume 60, pp. 147-173*
54	Design wind loads for low-rise buildings: A critical review of wind load specifications for industrial buildings	Kasperski Michael	1996	*Journal of Wind Engineering and Industrial Aerodynamics, Volume 61, pp. 169-179*
55	Wind-induced dynamic response and resultant load estimation for a flat long-span roof	Uematsu Y., Yamada M., Sasaki A.	1996	*Journal of Wind Engineering and Industrial Aerodynamics, Volume 65*
56	Wind-induced fatigue loading and damage to hip and gable roof claddings	Xu Y. L.	1996	*Journal of Structural Engineering, Volume 122*

57	Correction of wind-tunnel pressure coefficients for Reynolds number effect	Hoxey R. P., Robertson A. P., Richardson G. M., Short J. L.	1997	*Journal of Wind Engineering and Industrial Aerodynamics, Volume 69-71, pp. 547-555*
58	The assessment of wind loads on roof overhang of low-rise buildings	Wiik Tore, Hansen Ernst W. M.	1997	*Journal of Wind Engineering and Industrial Aerodynamics, Volume 67-68, pp. 687-696*
59	Peak gust pressures acting on the roof and wall edges of a low-rise building	Uematsu Yasushi, Isyumov Nicholas	1998	*Journal of Wind Engineering and Industrial Aerodynamics, Volume 77& 78, pp.-217-231*
60	The aerodynamics of a hanger membrane roof	Kazakevitch M.	1998	*Journal of Wind Engineering and Industrial Aerodynamics, Volume 77&78, pp.157-169*
61	Variations of wind pressure on hip roofs with roof pitch	Xu Y. L., Reardon G. F.	1998	*Journal of Wind Engineering and Industrial Aerodynamics, Volume 73, Issue 3*
62	Wind loads on low buildings with 4:12 gable roofs in open country and suburban exposures	Case P. C., Isyumov N.	1998	*Journal of Wind Engineering and Industrial Aerodynamics, Volume 77&78, pp. 107-118*
63	Wind tunnel simulation of TTU flow and building roof pressure	Ham Hee J., Bienkiewicz Bogusz	1998	*Journal of Wind Engineering and Industrial Aerodynamics, Volume 77&78 pp. 119-133*
64	Net pressure on a low-rise full-scale building	Ginger J. D., Letchford C. W.	1999	*Journal of Wind Engineering and Industrial Aerodynamics, Volume 83, pp. 239-250*
65	Wind standard provisions for low building gable roofs revisited	Stathopoulos T., Wu H.	1999	*Proceedings of the tenth International conference on Wind Engineering, Volume 1, pp. 155-162*

Appendix B: Typical ABAQUS input file for the simulation of thermoplastic system

The numerical models have been used for the performance evaluation of single-ply roofing system. A typical ABAQUS input file for the simulation of 67/12 thermoplastic system configuration subjected to 1.44 kPa (30 psf) pressure is presented below. Critical explanations are highlighted in bold.

```
*HEADING
W=2 m, L=6m., Fastener spacing = 12", Fastener row spacing = 67"
** Node definition and generation
*NODE,NSET=L1
1,0.0,0.0,0.0
*NODE,NSET=P2
2,0.0,0.0856,0.0
*NODE,NSET=P3
26,0.0,1.9144,0.0
*NFILL,NSET=L1
P2,P3,24,1
*NODE,NSET=L1
27,0.0,2.0000,0.0
*NCOPY,CHANGE NUMBER=100,OLD SET=L1,SHIFT,NEW SET=DUMMY1
0.33,0.0,0.0
0.0,
*NCOPY,CHANGE NUMBER=200,OLD SET=L1,SHIFT,NEW SET=L2
0.4473,0.0,0.0
0.0,
*NCOPY,CHANGE NUMBER=700,OLD SET=L2,SHIFT,NEW SET=L23
0.8509,0.0,0.0
0.0,
*NCOPY,CHANGE NUMBER=700,OLD SET=L23,SHIFT,NEW SET=L3
0.8509,0.0,0.0
0.0,
*NCOPY,CHANGE NUMBER=700,OLD SET=L3,SHIFT,NEW SET=L34
0.8509,0.0,0.0
0.0,
*NCOPY,CHANGE NUMBER=700,OLD SET=L34,SHIFT,NEW SET=L4
0.8509,0.0,0.0
0.0,
*NCOPY,CHANGE NUMBER=700,OLD SET=L4,SHIFT,NEW SET=L45
0.8509,0.0,0.0
0.0,
*NCOPY,CHANGE NUMBER=700,OLD SET=L45,SHIFT,NEW SET=L5
0.8509,0.0,0.0
0.0,
*NCOPY,CHANGE NUMBER=100,OLD SET=L5,SHIFT,NEW SET=DUMMY2
0.1173,0.0,0.0
0.0,
*NCOPY,CHANGE NUMBER=100,OLD SET=DUMMY2,SHIFT,NEW SET=L6
0.33,0.0,0.0
0.0,
*NFILL,BIAS=0.9
```

L2,L23,7,100
L3,L34,7,100
L4,L45,7,100
*NFILL,BIAS=1.03
L23,L3,7,100
L34,L4,7,100
L45,L5,7,100
*NSET,NSET=BC,GENERATE1
1,4601,100
27,4627,100
**** Shell element definition and generation**
*ELEMENT,TYPE=S4,ELSET=SHELL
1,1,101,102,2
*ELGEN,ELSET=SHELL
1,26,1,1,46,100,100
**** Definition of spring elements**
*ELEMENT,TYPE=SPRING1,ELSET=SPRING
6001,202
6002,206
6003,210
6004,214
6005,218
6006,222
6007,226
6101,1602
6102,1606
6103,1610
6104,1614
6105,1618
6106,1622
6107,1626
6201,3002
6202,3006
6203,3010
6204,3014
6205,3018
6206,3022
6207,3026
6301,4402
6302,4406
6303,4410
6304,4414
6305,4418
6306,4422
6307,4426
**** Definition of seam elements**
*ELSET,ELSET=SEAM,GENERATE
101,126,1
201,226,1
1501,1526,1
1601,1626,1
2901,2926,1
3001,3026,1
4301,4326,1
4401,4426,1
**** Definition of plate elements**

```
*ELSET,ELSET=DISK,GENERATE
101,125,4
102,126,4
201,225,4
202,226,4
1501,1525,4
1502,1526,4
1601,1625,4
1602,1626,4
2901,2925,4
2902,2926,4
3001,3025,4
3002,3026,4
4301,4325,4
4302,4326,4
4401,4425,4
4402,4426,4
** Material definition
*SPRING,ELSET=SPRING
3
20000
*MATERIAL,NAME=TPO
*ELASTIC
3.0E08,.40
*MATERIAL,NAME=PLASTIC
*ELASTIC
5.00E08,.40
*SHELL SECTION,ELSET=SHELL,MATERIAL=TPO
0.00104
*SHELL SECTION,ELSET=SEAM,MATERIAL=TPO
0.00208
*SHELL SECTION,ELSET=DISK,MATERIAL=PLASTIC
0.003
** Applied load and boundary condition
*STEP,NLGEOM,INC=550
*STATIC
0.00001,1.0,1.0E-07,0.51
*BOUNDARY
L1,1,3
L6,1,3
BC,1,3
*DLOAD
SHELL,P,1436.4
** Output format
*RESTART,WRITE,FREQUENCY=50
*NODE PRINT
U
*NODE FILE
U
RF
*EL PRINT,ELSET=SPRING
S11
*EL FILE,ELSET=SPRING
S
*END STEP
```

Appendix C: Typical ABAQUS input file for the simulation of thermoset system

The numerical models have been used for the performance evaluation of single-ply roofing system. A typical ABAQUS input file for the simulation of 78/6 thermoset system configuration subjected to 1.44 kPa (30 psf) pressure is presented below.

```
*HEADING
EPDM,W=2 m, L=6m,fastener spacing=6", fastener row spacing = 78"
** Node definition and generation
*NODE,NSET=L1
1,0.0,0.0,0.0
*NODE,NSET=P2
2,0.0,0.0856,0.0
*NODE,NSET=P3
50,0.0,1.9144,0.0
*NFILL,NSET=L1
P2,P3,48,1
*NODE,NSET=L1
51,0.0,2.0000,0.0
*NCOPY,CHANGE NUMBER=1000,OLD SET=L1,SHIFT,NEW SET=L12
0.7874,0.0,0.0
0.0,
*NCOPY,CHANGE NUMBER=1000,OLD SET=L12,SHIFT,NEW SET=L2
0.7874,0.0,0.0
0.0,
*NCOPY,CHANGE NUMBER=1000,OLD SET=L2,SHIFT,NEW SET=L23
0.9906,0.0,0.0
0.0,
*NCOPY,CHANGE NUMBER=1000,OLD SET=L23,SHIFT,NEW SET=L3
0.9906,0.0,0.0
0.0,
*NCOPY,CHANGE NUMBER=1000,OLD SET=L3,SHIFT,NEW SET=L34
0.9906,0.0,0.0
0.0,
*NCOPY,CHANGE NUMBER=1000,OLD SET=L34,SHIFT,NEW SET=L4
0.9906,0.0,0.0
0.0,
*NCOPY,CHANGE NUMBER=500,OLD SET=L4,SHIFT,NEW SET=L5
0.4628,0.0,0.0
0.0,
*NFILL,BIAS=0.8
L1,L12,10,100
L2,L23,10,100
L3,L34,10,100
L4,L5,5,100
*NFILL,BIAS=1.25
L12,L2,10,100
L23,L3,10,100
L34,L4,10,100
*NSET,NSET=BC,GENERATE1
```

```
1,6501,100
51,6551,100
** Shell element definition and generation
*ELEMENT,TYPE=S4,ELSET=SHELL
1,1,101,102,2
*ELGEN,ELSET=SHELL
1,50,1,1,65,100,100
** Definition of spring elements
*ELEMENT,TYPE=SPRING1,ELSET=SPRING
7001,2002
7002,2006
7003,2010
7004,2014
7005,2018
7006,2022
7007,2026
7008,2030
7009,2034
7010,2038
7011,2042
7012,2046
7013,2050
7101,4002
7102,4006
7103,4010
7104,4014
7105,4018
7106,4022
7107,4026
7108,4030
7109,4034
7110,4038
7111,4042
7112,4046
7113,4050
7201,6002
7202,6006
7203,6010
7204,6014
7205,6018
7206,6022
7207,6026
7208,6030
7209,6034
7210,6038
7211,6042
7212,6046
7213,6050
** Definition of seam  and plate elements
*ELSET,ELSET=SEAM,GENERATE
1801,1850,1
1901,1950,1
2001,2050,1
2101,2150,1
3801,3850,1
3901,3950,1
```

```
4001,4050,1
4101,4150,1
5801,5850,1
5901,5950,1
6001,6050,1
*ELSET,ELSET=DISK,GENERATE
1901,1949,4
1902,1950,4
2001,2049,4
2002,2050,4
3901,3949,4
3902,3950,4
4001,4049,4
4002,4050,4
5901,5949,4
5902,5950,4
6001,6049,4
6002,6050,4
** Definition of spring elements and materials
*SPRING,ELSET=SPRING
3
60000
*MATERIAL,NAME=EPDM
*ELASTIC
1.5E08,0.22
*MATERIAL,NAME=METAL
*ELASTIC
2.00E11,.20
*SHELL SECTION,ELSET=SHELL,MATERIAL=EPDM
0.0011
*SHELL SECTION,ELSET=SEAM,MATERIAL=EPDM
0.0022
*SHELL SECTION,ELSET=DISK,MATERIAL=METAL
0.002
** Applied load and boundary condition
*STEP,NLGEOM,INC=550
*STATIC
1.0E-6,1.0,1.0E-11,0.2
*BOUNDARY
L1,1,3
L5,1,3
BC,1,3
*DLOAD
SHELL,P,1436.4
** Output format
*RESTART,WRITE,FREQUENCY=10
*NODE PRINT
U
*NODE FILE
U
RF
*EL PRINT,ELSET=SPRING
S11
*EL FILE,ELSET=SPRING
S
*END STEP
```

Appendix D: Computed fastener forces from the numerical experiments

By taking advantage of the validated model, an extensive parametric investigation has been completed. This appendix tabulates the computed fastener forces of 225 numerical experiments.

Table D.1 Computed fastener forces for thermoplastic system with F_r = 1220 mm (48")

Simulation No.	Table Width mm (in)	48/6		48/12		48/18		48/24	
		Fastener Force		Fastener Force		Fastener Force		Fastener Force	
		N	lbf	N	lbf	N	lbf	N	lbf
1 to 4	5048 (199)	267	60	534	120	801	180	1066	240
5 to 8	4743 (187)	267	60	534	120	801	180	1062	239
9 to 12	4438 (175)	267	60	534	120	800	180	1058	238
13 to 16	4134 (163)	267	60	534	120	800	180	1054	237
17 to 20	3829 (151)	267	60	534	120	799	180	1045	235
21 to 24	3524 (139)	267	60	533	120	796	179	1028	231
25 to 28	3219 (127)	267	60	532	120	789	177	1000	225
29 to 32	2914 (115)	267	60	529	119	774	174	962	216
33 to 36	2610 (103)	266	60	522	117	751	169	906	204
37 to 40	2305 (91)	264	59	507	114	713	160	825	185
41 to 44	2000 (79)	255	57	476	107	650	146	711	160
45 to 48	1695 (67)	238	54	430	97	569	128	564	127
49 to 52	1390 (55)	209	47	361	81	466	105	400	90
53 to 56	1086 (43)	167	38	280	63	343	77	239	54
57 to 60	781 (31)	118	27	188	42	207	47	92	21

Table D.2 Computed fastener forces for thermoplastic system with F_r = 1700 mm (67")

Simulation No.	Table Width mm (in)	67/6		67/12		67/18		67/24	
		Fastener Force		Fastener Force		Fastener Force		Fastener Force	
		N	lbf	N	lbf	N	lbf	N	lbf
61 to 64	5048 (199)	372	84	745	167	1101	248	1435	323
65 to 68	4743 (187)	372	84	745	167	1097	247	1420	319
69 to 72	4438 (175)	372	84	740	166	1092	245	1403	315
73 to 76	4134 (163)	372	84	730	164	1080	243	1377	310
77 to 80	3829 (151)	372	84	725	163	1056	237	1343	302
81 to 84	3524 (139)	371	83	723	163	1037	233	1293	291
85 to 88	3219 (127)	368	83	708	159	1009	227	1224	275
89 to 92	2914 (115)	361	81	685	154	958	215	1140	256
93 to 96	2610 (103)	349	78	648	146	895	201	1034	232
97 to 100	2305 (91)	329	74	599	135	811	182	905	203
100 to 104	2000 (79)	299	67	533	120	706	159	752	169
105 to 108	1695 (67)	260	58	455	102	591	133	578	130
109 to 112	1390 (55)	214	48	365	82	470	106	402	90
113 to 116	1086 (43)	165	37	278	62	340	76	237	53
117 to 120	781 (31)	117	26	186	42	205	46	90	20

Table D.3 Computed fastener forces for thermoplastic system with F_r = 1830 mm (72")

Simulation No.	Table Width mm (in)	72/6		72/12		72/18		72/24	
		Fastener Force		Fastener Force		Fastener Force		Fastener Force	
		N	lbf	N	lbf	N	lbf	N	lbf
121 to 124	5048 (199)	400	90	797	179	1162	261	1514	340
125 to 128	4743 (187)	400	90	793	178	1159	261	1493	336
129 to 132	4438 (175)	400	90	787	177	1150	259	1469	330
133 to 136	4134 (163)	400	90	782	176	1136	255	1439	324
137 to 140	3829 (151)	399	90	774	174	1116	251	1396	314
141 to 144	3524 (139)	397	89	762	171	1086	244	1337	301
145 to 148	3219 (127)	393	88	741	167	1044	235	1259	283
149 to 152	2914 (115)	385	87	711	160	987	222	1165	262
153 to 156	2610 (103)	371	83	667	150	912	205	1049	236
156 to 160	2305 (91)	349	78	610	137	820	184	913	205
161 to 164	2000 (79)	317	71	539	121	710	160	754	170
165 to 168	1695 (67)	276	62	456	103	588	132	577	130
169 to 172	1390 (55)	227	51	364	82	461	104	400	90
173 to 176	1086 (43)	175	39	271	61	339	76	237	53
177 to 180	781 (31)	127	29	186	42	240	54	91	20

Table D.4 Computed fastener forces for thermoplastic system with F_r = 2900 mm (114")

Simulation No.	Table Width mm (in)	114/12		114/18	
		Fastener Force		Fastener Force	
		N	lbf	N	lbf
181 to182	5048 (199)	1157	260	1635	368
183 to 184	4743 (187)	1134	255	1592	358
185 to 186	4438 (175)	1102	248	1540	346
187 to 188	4134 (163)	1063	239	1475	332
189 to 190	3829 (151)	1014	228	1396	314
191 to 192	3524 (139)	955	215	1306	294
193 to 194	3219 (127)	885	199	1201	270
195 to 196	2914 (115)	806	181	1083	243
197 to 198	2610 (103)	719	162	960	216
199 to 200	2305 (91)	628	141	832	187
201 to 202	2000 (79)	535	120	700	157
203 to 204	1695 (67)	444	100	574	129
205 to 206	1390 (55)	353	79	453	102
207 to 208	1086 (43)	267	60	330	74
209 to 210	781 (31)	181	41	202	45

Table D.5 Computed fastener forces for thermoset system with F_r = 1980 mm (78")

Simulation No.	Table Width mm (in)	78/6		78/12		78/18	
		Fastener Force		Fastener Force		Fastener Force	
		N	lbf	N	lbf	N	lbf
	5048 (199)						
	4743 (187)						
	4438 (175)						
	4134 (163)						
	3829 (151)						
	3524 (139)						
211 to 213	3219 (127)	445	100	876	197	1292	290
214 to 216	2914 (115)	437	98	853	192	1245	280
217 to 219	2610 (103)	422	95	816	183	1178	265
220 to 222	2305 (91)	396	89	757	170	1081	243
223 to 225	2000 (79)	359	81	676	152	947	213
	1695 (67)						
	1390 (55)						
	1086 (43)						
	781 (31)						

References

ABAQUS user's manual, version 5.8, 1998. Hibbitt, Karlsson and Sorensen, Inc., Pawtucket, RI.

American Society of Civil Engineering (2002), *Minimum Design Loads for Building and Other Structures*, SEI/ASCE 7-02, New York, USA 10017-2398.

American Society for Testing and Materials (1998), "Standard Test Methods for Coated Fabrics," D 751-98", ASTM, Philadelphia, USA.

American Society for Testing and Materials (2003), "Standard Specification for Thermoplastic Polyolefin Based Sheet Roofing" D 6878-03, West Conshohocken, PA, USA 19428-2959

American Society for Testing and Materials (1996), "Standard Specification for EPDM Sheet Used in Single-Ply Roof Membrane" D4637-96, West Conshohocken, PA, USA 19428-2959

Baskaran, A. and Borujerdi, J. (2001), "Application of Numerical Models to Determine Wind Uplift Ratings of Roofs," *Journal of Wind and Structures*, 4, (3), June, pp. 213-226.

Baskaran, A., Molleti S. and Borujerdi, J. (2003), "Application of Numerical Models to Determine Wind Uplift Ratings of Roofs – Part II," Submitted for *Journal of Wind and Structures*.

Baskaran, A., Chen Y. and Vilaipornsawai U. (1999), "A new dynamic wind load cycle to evaluate flexible membrane roofs," *Journal of Testing & Evaluation*, 27, (4), July, pp. 249-265.

Baskaran, A., Chen, Yin (1998), "Wind Load Cycle Development for Evaluating Mechanically Attached Single-ply Roofs," *Journal of Wind Engineering and Industrial Aerodynamics*, Vol. 77-78, pp. 83-96.

Baskaran, A. and Dutt, O. (1995), "Application of Lab Procedures for the Dynamic Evaluation of Roofing Systems. Part 1: Review of Existing Standards," IRC Internal Report No. 692, National Research Council, Ottawa, Ontario.

Baskaran, A. and Kashef, A. (1995), "Application of Numerical Models for the Dynamic Evaluation of Roofing Systems, Part 1: Review of the state-of-the-art," Internal report No. 690, National Research Council Canada, Ottawa, Ontario, Canada.

Baskaran, A., Lei, W. and Richardson C. (1999), "Dynamic Evaluation of Thermoplastic Roofing Systems for Wind Performance," *Journal of Architectural Engineering,* ASCE, vol. 5, No 5, pp. 16-24.

Baskaran, A. and Lei, W. (1997), "A New Facility for Dynamic Wind Performance Evaluation of Roofing Systems," *Proceedings of the Fourth International Symposium on Roofing Technology,* NRCA/NIST, Washington, D.C., U.S.A., pp. 168-179.

Baskaran, B. A., Paroli R. M. and Booth R. J. (1997), "Wind performance evaluation procedures for roofing systems current status and future trends," *Fifth International Conference on Building Envelope Systems and Technology*, BATH, U.K., pp. 37-52.

Baskaran, A., Zahrai, S.M. and Chen, Y. (1999), "Numerical evaluation of roofing systems for wind uplift pressures," *Proceedings of the tenth ICWE*, Copenhagen, Denmark, June, Vol. 3, pp. 1747-1754.

Bienkiewicz, B. and Sun Y. (1993), " Numerical and Experimental Studies of Wind Loading on Loose-Laid Roofing Systems," Colorado State University, Civil Engineering Department, Fort Collins, Colorado, USA.

Borujerdi, J. and Baskaran, A. (2000), "Application of Information Technology for the Development of Wind Uplift Pressure Database," *Proceedings of the third Structural Specialty Conference of Canadian Society of Civil Engineering*, London, ON, pp. 225-282.

Byrne, S.M. (1976), "Dynamic-Load Testing of Sheet Metal Roofing," Metal Structures Conference, Adelaide, Australia, November 25-26, pp. 46-50.

Cook, N.J., Keevil, A.P. and Stobart, R.K. (1988), "BRERWULF- The Big Bad Wolf," *Journal of Wind Engineering and Industrial Aerodynamics*, Vol. 29, pp. 99-107.

Cook, N. J. (1992), "Dynamic Response of Single-Ply membrane Roofing Systems", *Journal of Wind Engineering and Industrial Aerodynamics*, Vol. 41-44, pp. 1525-1536.

Corel Draw User Manual – Version 8.0 (1997) Corel Corporation and Corel Corporation Limited, Ottawa, Ontario, Canada, 10017-2398.

Easter, M.R. (1990), "Finite Element Analysis of Roofing Systems," Roofing Research and Standards Development: American Society for Testing and Materials, Philadelphia, Vol. 2, STP 1088, pp. 138-151.

Factory Mutual Research, (1986), Approval Standard: Class I Roof Covers (4470), Norwood, Massachusetts, USA.

Factory Mutual Research, (1992), Approval Standard: Class I Roof Covers (4470), Norwood, Massachusetts, USA.

Factory Mutual Research (1992), "In Search of Excellence...FMRC Improves Roof Tests", The Roofing Industry Educational Institute Information Letter, pp. 5-7

Gerhardt, H.J. and Kramer, C. (1986), "Wind Induced Loading Cycle and Fatigue Testing of Lightweight Roofing Fixations," *Journal of Wind Engineering and Industrial Aerodynamics*, Vol. 23, pp. 237-247.

Gerhardt, H.J. and Gerbatsch, R.W. (1989), "Wind Loads on Single-Ply Membranes," The Construction Specifier, November, pp. 60-71.

Haddock (1992), "UL test procedure"

Hoxey, R. P. and Moran, P. (1983)," A full scale of the geometric parameters that influence wind loads on low ride buildings," *Journal of Wind Engineering and Industrial Aerodynamics*, 13: 277-288.

Jennings, Roger (1997), *Special edition using Access 97*, Que Corporation, Indianapolis, IN, USA 46290-1097.

Letchford, C.W. and Norville, H.S. (1993), "Wind Induced Pressure Loading Cycles for Wall Cladding During Hurricanes," Glass Research and Testing Laboratory, Texas Tech University, Lubbock, Texas, USA.

Lewis, J.E. (1980), "Preliminary Stress evaluation of the Effects of Gaps Between Roof Insulation Panels," Journal of Thermal Insulation, Vol. 4, pp. 3-36.

Low-slope roofing materials guide (1999), National Roofing Contractors Association, 10255 West Higgins Road, Suite 600, Rosemont, IL 60018-5607 – 847/299-9070.

Mahendran, M. (1990), "Fatigue Behavior of Corrugated Roofing under Cyclic Wind Loading," Transaction of the Institution of Engineers, Australia, Civil Engineering, Vol. CE 32, No. 4, pp. 219-226.

Mahendran, M. (1994), "Effect of Overload Cycles on Thin Steel Roof Claddings during Cyclone Winds," *Journal of Testing and Evaluation*, ASTM, Vol. 22, No. 5, pp. 453-459.

Malpezzi, Joseph A. and Gillenwater, Richard J. (1993), "Static Vs. Dynamic: A wind uplift testing study," *Proceedings of the 10th conference on Roofing Technology*, Gaithersburg, MD; NRCA Rosemont, IL, pp. 123-129.

Morgan, J.W. and Beck, V.R. (1997), "Failure of Sheet Metal Roofing Under Repeated Wind Loading," Civil Engineering Transactions, The Institution of Engineers, Australia, Vol. CB19, pp. 1-5.

National Research Council Canada (1995), National Building Code of Canada User's Guide – Structural commentaries (Part 4), Ottawa, Ontario, Canada, K1A 0R6.

Paulsen, E.M., (1989), "NBI Roof Wind Uplift Strength Test Facility and Load Programs," *Proceedings of the Roof Wind Uplift Testing Workshop*, Oak Ridge, Tennessee, pp. 46-51.

Prevatt, David. O., Schiff, D. Schiff and Malpezzi, Joseph A., (1997) "Investigation of Chamber Size for Uplift Performance Testing of Single-Ply Roof Systems," *Proceedings of the Fourth International Symposium on Roofing Technology*, NRCA/NIST, Washington, D.C., U.S.A., pp. 163-167.

Rossiter, W.J., Jr. and Batts, M.E. (1985), "Finite-Element Analysis of Temperature Induced Stresses in Single-Ply Roofing Membranes," Durability of Building Materials, Vol. 2, pp. 195-208.

SBCCI (1994), "SSTD 12 - Test Standard for Determining Impact Resistance from Wind-borne Debries," pp. 12-94

Savage, M. G.; Baskaran, A.; Cooper, K. R. and Lei, W. (1996), "Pressure distribution data measured during the November 1994 wind tunnel tests on a mechanically-attached, PVC single-ply roofing systems," Internal Report of National Research Council Canada, Institute for Aerospace Research, LTR-A-003, Ottawa, Ontario, Canada.

Smith, G.A. (1989), "How sample size affects Factory Mutual results," *Proceedings Roof Wind Uplift Testing Workshop*, Oak Ridge National Laboratory, Oak Ridge TN, Nov.

Smith, P.J. (1992), "Testing Methods for Roof Systems," ASCE symposium on the Hurricances, pp. 46-51.

Stathopoulos, T. and Saathoff P. (1991), "Wind pressure on roofs of various geometrics," *Journal of Wind Engineering and Industrial Aerodynamics*, 38:273-284.

TR 440 (1978), Guidelines for Testing and Evaluation of products for Cyclone prone areas, Experimental Building Station (EBS), Sydney, Australia.

Uematsu Y. and Isyumov N. (1999), "Review wind pressure acting on low-rise buildings," *Journal of Wind Engineering and Industrial Aerodynamics*, 82:1-25.

Underwriters Laboratories Inc. (1991), "Standard for Wind Uplift Pressure of Roof Assemblies (UL 580)," third edition, Nov.

Zahrai, S. M. and Baskaran, A. (1999), "Numerical evaluation for the effect of table size on roof wind uplift resistance, Part 1: Thermoplastic roofing system," Internal report No. (IRC-IR 709), National Research Council Canada, Ottawa, Ontario, Canada.

Zarghamee, M. S. (1990), "*Wind Effects on Single-Ply Roofing Systems,*" Journal of Structural Engineering, Vol. 116, No. 1, January, pp. 177-187, Paper No. 24277.